Small Molecule Organic Optoelectronic Devices

by

Nathan Bakken

A Dissertation Presented in Partial Fulfillment
of the Requirements for the Degree
Doctor of Philosophy

Approved January 2017 by the
Graduate Supervisory Committee:

Lenore Dai, Co-Chair
Jian Li, Co-Chair
James Adams
Terry Alford
Mary Lind

ARIZONA STATE UNIVERSITY

May 2017

ABSTRACT

Organic optoelectronics include a class of devices synthesized from carbon containing ‘small molecule’ thin films without long range order crystalline or polymer structure. Novel properties such as low modulus and flexibility as well as excellent device performance such as photon emission approaching 100% internal quantum efficiency have accelerated research in this area substantially. While optoelectronic organic light emitting devices have already realized commercial application, challenges to obtain extended lifetime for the high energy visible spectrum and the ability to reproduce natural white light with a simple architecture have limited the value of this technology for some display and lighting applications. In this research, novel materials discovered from a systematic analysis of empirical device data are shown to produce high quality white light through combination of monomer and excimer emission from a single molecule: platinum(II) bis(methyl-imidazolyl)toluene chloride (Pt-17). Illumination quality achieved Commission Internationale de L’Éclairage (CIE) chromaticity coordinates (x = 0.31, y = 0.38) and color rendering index (CRI) > 75. Further optimization of a device containing Pt-17 resulted in a maximum forward viewing power efficiency of 37.8 lm/W on a plain glass substrate. In addition, accelerated aging tests suggest high energy blue emission from a halogen-free cyclometalated platinum complex could demonstrate degradation rates comparable to known stable emitters. Finally, a buckling based metrology is applied to characterize the mechanical properties of small molecule organic thin films towards understanding the deposition kinetics responsible for an elastic modulus that is both temperature and thickness dependent. These results could contribute to the viability of organic electronic technology in potentially flexible display and lighting applications. The

results also provide insight to organic film growth kinetics responsible for optical, mechanical, and water uptake properties relevant to engineering the next generation of optoelectronic devices.

ACKNOWLEDGMENTS

I would like to thank Dr. Jian Li and all from the Advanced Applied Materials Lab who have contributed to this work. Our efforts are distinctively collaborative and I must thank Tyler Fleetham and Miguel Reyes for operating our organic device fabrication and testing line. Within Dr. Li's group, Eric Turner and Dr. Zixing Wang should be commended for their tireless hours spent to synthesize many of the materials that I have so carefully spread across the walls of the growth chamber. I appreciate the support from Dr. Bryan Vogt and his students Jessica Torres and Xinxin Wang. Our collaboration has not only granted me the equipment necessary for investigations, it has also enabled my transition into PhD study in Chemical Engineering. Dr. Lenore Dai has also been extremely accommodating and a pleasure to work with. Her genuine interest in the wellbeing of students continues to be a blessing. Dr. Terry Alford has been very supportive throughout my study at ASU and has been an enabler toward a successful career within industry. It was his teaching that earned my employment in the technology sector. Dr. Jim Adams played a key role to direct my ambition at an early and malleable age and I credit him for my interest in Chemical and Materials Engineering. ASU's Flexible Display Center has also been extremely generous to grant access to facilities, equipment, and expertise that has fueled critical components of my research. Finally, I must recognize my advisor for undergraduate research, Dr. Jeff Drucker, who acted as a catalyst to motivate graduate research. His selfless investment as a mentor and friend provided the confidence necessary to navigate the perils and frustrations tied to the pursuit of academic award. Thank you to all who have supported my endeavors.

TABLE OF CONTENTS

Page

CHAPTER Page

CHAPTER Page

LIST OF TABLES

LIST OF FIGURES

Figure Page

Figure Page

Figure Page

Figure Page

Figure Page

LIST OF SYMBOLS

2,6mCPy: 2,6-di(9H-carbazol-9-yl)pyridine

AFM: atomic force microscopy

Alq_3: tris-(8-hydroxyquinoline)aluminum

AMOLED: active matrix organic light emitting device

BCP: bathocuproine

BLS: Brillouin light scattering

CBP: 4,4′-Bis(*N*-carbazolyl)-1,1′-biphenyl

CIE: International Commission on illumination color space coordinates

CsF: cesium flouride

CRI: color Rendering Index

ε: strain applied for buckling based metrology

ε_c: critical strain that defines the minimum amount of deformation required to achieve a stable sinusoidal structure useful for buckling based metrology

EBL: electron blocking layer

EL: electroluminescence layer

E_f: thin film elastic modulus or modulus of a specified film if a substitution is made for subscript '$_f$'

E_s: substrate elastic modulus or modulus of a specified substrate if a substitution is made for subscript '$_s$'

$\bar{E}_x$: reduced modulus defined as $\bar{E} = E/(1-\nu^2)$ where subscript '$_x$' will be substituted with description of a specific layer

EMF: electromotive force

EML: emissive layer

EQE: external quantum efficiency

Excimer: special case exciplex where both molecules are of the same species

Exciplexes: excited state involving more than one molecule

Exciton: excited state molecule

FFT: Fast Fourier Transform

FPt: platinum(II) [2-(4',6'-difluorophenyl) pyridinato-N, $C^{2'}$)](2,4-pentanedionato)

h_f: film thickness or thickness of a specified film if a substitution is made for subscript '$_f$'

h_s: film thickness or thickness of a specified film if a substitution is made for subscript '$_f$'

HOMO: highest occupied molecular orbital

HTL: hole transport layer

ILC: injection limited current

IMC: indomethacin

IPA: isopropyl alcohol

IQE: internal quantum efficiency

$Ir(ppy)_3$: (fac-tris(2-phenyl-pyridinato)iridium(III)

ISC: intersystem crossing

ITO: indium tin oxide

J-V: current density vs. voltage

LiF: lithium fluoride

LUMO: lowest unoccupied molecular orbital

λ: wavelength of light or wavelength observed in buckling based metrology

ν_f: Poisson's ratio of a film or of a specified film if a substitution is made for subscript '$_f$'

ν_s: Poisson's ratio of a substrate or of a specified substrate if a substitution is made for subscript '$_s$'

MLCT: metal ligand charge transfer

MMLCT:

NI: nano indentation

NIR: near infrared

NMR: nuclear magnetic resonance spectroscopy

NPD: *N*,*N*′-Di-[(1-naphthyl)-*N*,*N*′-diphenyl]-1,1′-biphenyl)-4,4′-diamine

NTSC: National Television System Committee

OLED: organic light emitting device

OM: optical microscope

OPV: organic photovoltaic

OVPD: organic vapor phase deposition

PDMS: polydimethylsiloxane

Pedot:PSS: Poly(3,4-ethylenedioxythiophene)-poly(styrenesulfonate)

PL: photoluminescence

PO15: 2,8-bis(diphenylphosphoryl)dibenzothiophene

PS: polystyrene

Pt-4: platinum(II) 1,3-difluoro-4,6-di(2-pyridinyl)benzene chloride

Pt-17: platinum(II) bis(methyl-imidazolyl)toluene chloride

PVD: physical vapor deposition

QCM: quartz crystal microbalance

S1: singlet exciton

SCLC: space charge limited current

SIEBIMM: strain-induced elastic buckling instability for mechanical measurements

T1: triplet exciton

TA: texture analyzer

TAPC: 1,1-bis_di-4-tolylamino_phenyl_cyclohexane

T_g: glass transition temperature

TCLC: trap charge limited current

TCTA: Tris(4-carbazoyl-9-ylphenyl)amine

UV: ultraviolet

VASE: variable angle spectroscopic elipsometry

VIS: Visible electromagnetic spectrum

WOLED: White organic light emitting diodes

QCM: quartz crystal microbalance

CHAPTER 1

INTRODUCTION

1.1 Motivation

Organic electronics have continued to develop scientific and commercial interests based on a rich array of potentially useful electronic and optical characteristics. As early as the 1952 novel properties including, relatively high conductivity,[1] photoluminescence (PL),[2] electroluminescence (EL),[3] and the photovoltaic effect (PV)[4] have all been properties of interest for applications to organic photovoltaics (OPV) and organic light emitting devices (OLEDs). Although renewable energy has become insistently popular in recent years, it is OLED rather than OPV technology that has currently reached a state of technical maturity that enables it to reach the marketplace.[5] Numerous products including full color large format displays,[6] high resolution mobile devices, and paradigm shifting OLED lighting[7] are already available to the consumer. Selected examples are shown in Figure 1.

[a] 

[b] 

Figure 1. [a] Samsung Galaxy S7 with 2560 x 1440 curved AMOLED display.[8] [b] General Electric lighting concepts enabled by white OLED technology.[7]

Organics, as compared to their inorganic analogs, have the potential to be easily processed without the need for high vacuum, ultra clean, and high temperature environments. This class of materials is inherently soft (modulus of elasticity ~ 1GPa), very adhesive, and very conformal at low thicknesses (organic device stack ~ 100nm). Flexible technology as well as novel processing methods can exploit these properties. Solution based processing, roll-to-roll processing, and even inkjet printing methods have all been proposed as feasible routes to manufacture organic electronics.[9] Figure 2 from 3M Corporation shows an example of a flexible electronics manufacturing line. In addition, organic vapor phase deposition (OVPD) and other more traditional fabrication techniques have been employed and developed to support a growing consumer interest in organic electronics.

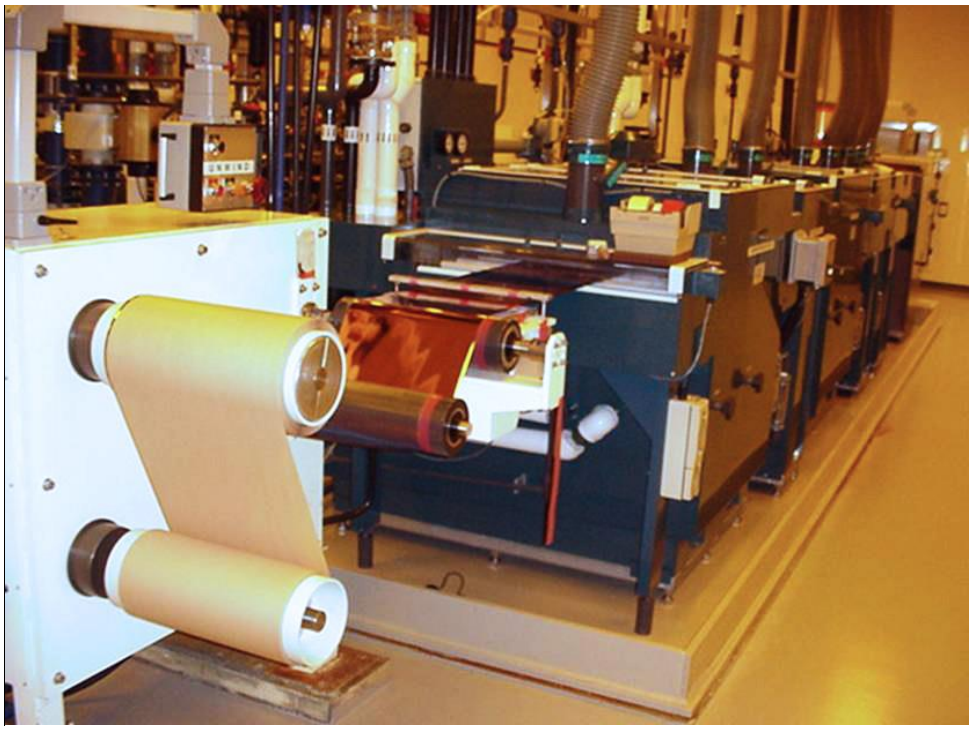

Figure 2. Photograph from 3M Corporation showing roll-to-roll processing to enable high volume and low cost manufacturing techniques for flexible electronics.[10]

OLED technology has gathered specific and recent attention as a useful technology for display and lighting applications.[5] Initial technology has evolved from extremely inefficient devices with high turn-on voltages, low stability, and nondescript color targets.[11,12] In the last twenty years, published successes have shown that internal quantum efficiencies (IQE) approaching 100% and external quantum efficiency (EQE) of over 20%[13] have been achieved (approaching the theoretical EQE limit of ~22% on glass substrates).[14] As an extremely attractive characteristic for growing mobile markets, OLED devices are now also regularly discussed with turn-on voltages below 3 volts.[15] Color tuning to hit broad or narrow emission spectral targets has ample latitude for development due to the freedom of molecular design. Many classes of molecules have been red shifted, blue shifted, and even made to emit over the entire visual spectrum with small adjustments to their chemical structure.[16] Degradation mechanisms remain a poorly understood segment of the field as it has been shown that undetectably small number of degraded molecules can significantly taint performance.[17,18] Still, operational lifetimes exceeding 35,000 hours have been reported on numerous accounts in the last several years. The future for OLED and organic optoelectronic technology is promising as rapid advances in the understanding and performance of organic electronics are being achieved.[19]

1.2 Molecular States in OLED

Transport phenomena in organic semiconductor devices are fundamentally different than inorganic semiconductors. Some mechanistic parallels to traditional inorganic materials exist; however, organics are markedly unique in many ways. In both of organic and inorganic devices, a thorough understanding of charge and energy transport through an operational device is required to draw conclusions from macroscopic

performance metrics. In this way, the relationships between optical power, current, and voltage can be correlated to material properties and device architecture variables towards improving particular materials or structures. For example, a device with an undesirable low power efficiency because of a relatively high resistance has electrical characteristics that result from the bulk and interface properties of all layers of the device stack. Models can then be formulated and fit to observed phenomena towards understanding and improving device performance through application of novel materials or architecture optimization. In the example of a high resistance device, the mobility of individual films as well as the relative energy of charge carriers through the device layers would be useful to predict methods to increase current at lower voltages. To begin discussion on the mechanics of organic semiconductors, one can consider that an operating optoelectronic device will contain several molecular species as shown in Figure 3. This figure also demonstrates electronic states of interest where the neutral molecule has its highest occupied molecular orbital (HOMO) energy level below the energy gap. The lowest unoccupied molecular orbital (LUMO) is just above the energy gap.

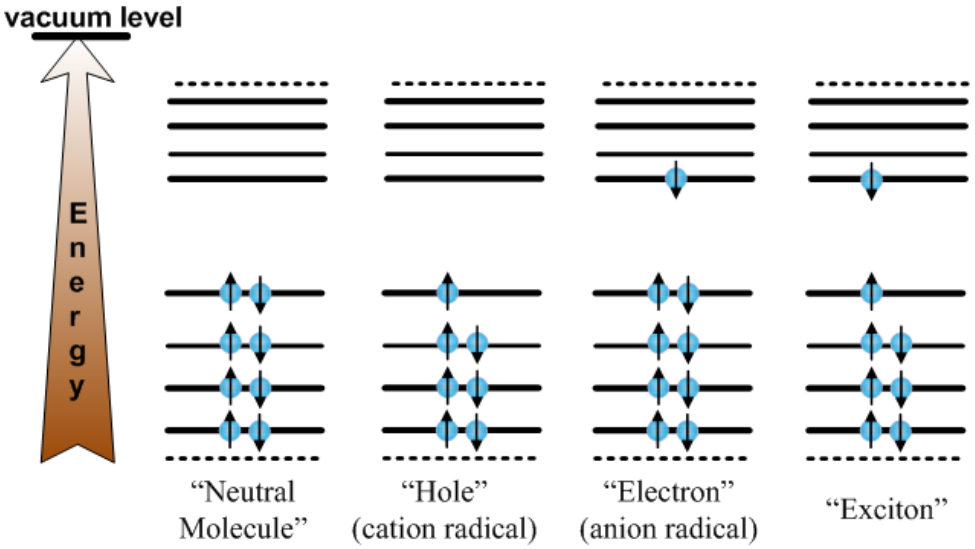

Figure 3. Schematic presentation of neutral molecules, hole, electron, and excitons of organic semiconductors.

In 1987 Tang and Vanslyk inspired a revolution in organic electronics research with the first thin film OLED.[20] This was a simple single heterojunction device that made use of Tris-(8-hydroxyquinoline)aluminum (Alq_3) as both an emitter and electron transporting layer as shown in figure 4. *N*,*N*′-Di-[(1-naphthyl)-*N*,*N*′-diphenyl]-1,1′-biphenyl)-4,4′-diamine (NPD) acts as the hole transport material from the anode to emissive region with a transparent anode being constructed from indium tin oxide (ITO) opposite of an Aluminum metallic cathode. The device emits a green light as a result of radiative decay of excited state Alq_3 molecules.

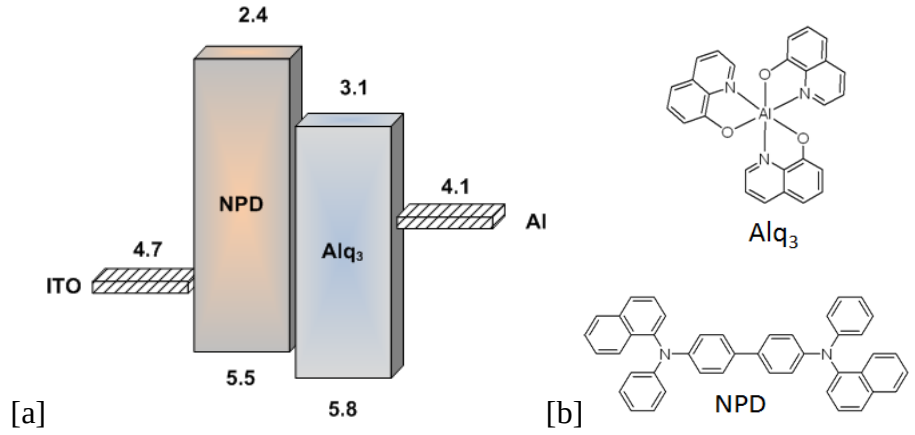

Figure 4. [a] Energy diagram (w.r.t. vacuum) for NPD/Alq_3 devices [b] chemical structures of Alq_3 and NPD [21]

The operation of an NPD/Alq_3 device can be separated into component steps shown in Figure 5. Contemporary small molecule OLEDs may have substantially more complicated structure as compared to the NPD/Alq_3 example, but at a high level the principles of operation remain the same. Following an electron from the Al cathode towards the organic interface, we see that an energy barrier exists for injection into the lowest unoccupied molecular orbital from the Fermi level of the metal cathode. Note that low work function cathodes are ideal to minimize this barrier and metals such as Al and Mg/Ag are chosen based on their low work functions simultaneous with relatively good electrochemical stability. Similarly, holes are most readily injected into the organic layer by a high work function anode that is commonly constructed from ITO because of its transparency in the visible spectrum. The details of the injection process and materials parameters for functional layers including the cathode will be discussed in more detail in later sections. Continuing with the path of an electron after injection into the LUMO, the charge is driven

away from the metal cathode in response (primarily) to the applied electric field as shown in Figure 5b.

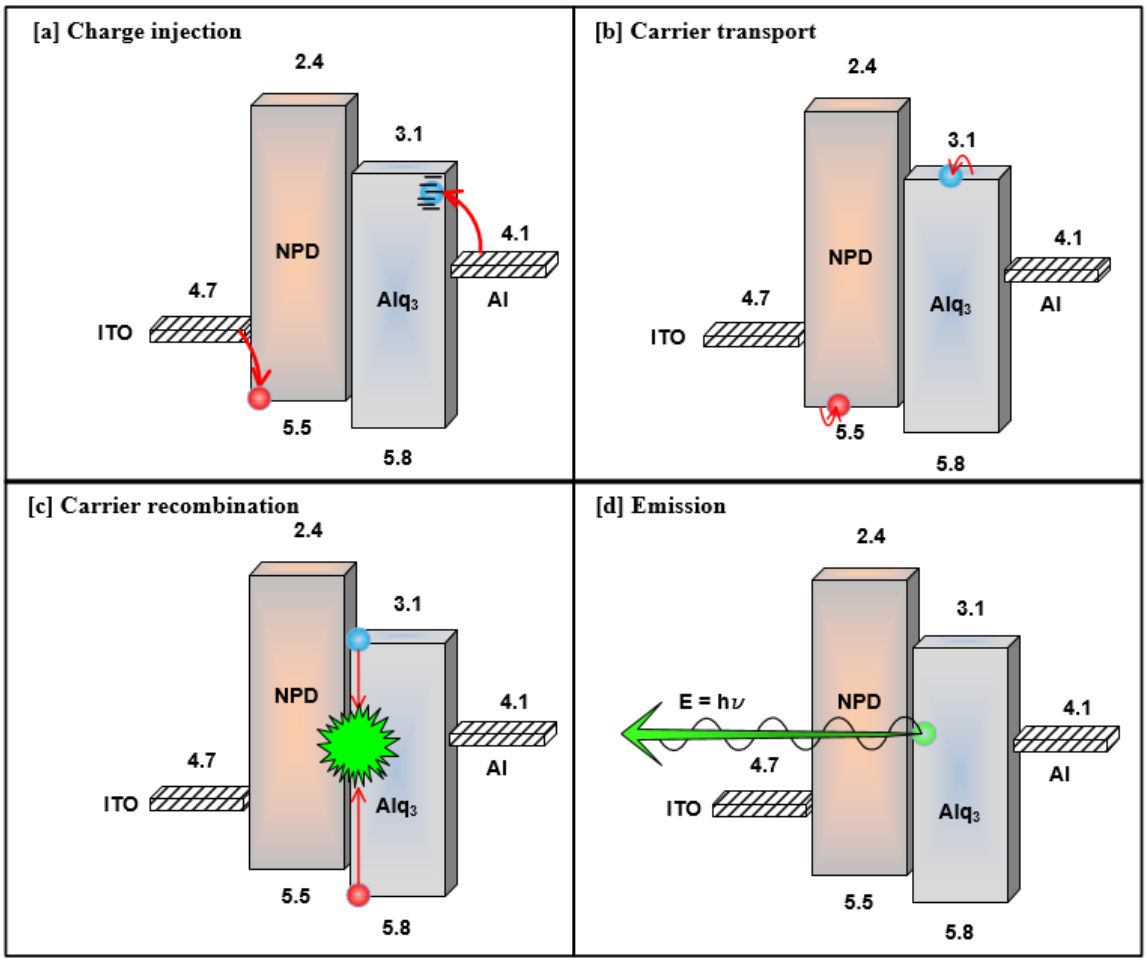

Figure 5. Steps to electroluminescence in OLED [a] charge injection by oxidation and reduction of molecules at the anode and cathode [b] charge transport by 'hoping' mechanisms [c] carrier recombination in the emission region [d] Emission from radiative decay processes.

At the Anode, electrons are accepted from oxidized molecules near the organic interface. This is schematically represented by positive "hole" charge carriers being injected from the anode into the organic layers. Similarly, these carriers hop along the HOMO energy level towards the metal cathode also primarily motivated by an applied electric field. The relative positive and negative carrier concentration as a function of distance from the cathode is critical for effective device operation and will also be discussed in later sections. Ideally, no single carrier current conduction exists. That is, electrons never reach the anode and holes never reach the cathode where they would be quickly and nonradiatively quenched to the respective Fermi level. It is preferred in a high efficiency device for electron and hole recombination to generate excited state molecules (excitons) that can have a high probability to decay radiatively with photons emitted. Thus, a mechanism to luminesce at characteristic energies due to applied electric power using organic materials can be realized.

1.3 Charge Injection and Transport

Injection of charge carriers into organic layers occurs as individual molecules are oxidized or reduced. It is at this interface that the delocalized carriers from the cathode or anode become localized to a specific molecule. It is of particular interest to observe that Aluminum is a common and successful cathode material even though the energy diagram shows a ~1eV injection barrier from the Fermi energy of Al to the LUMO of Alq_3. In practice, this interface can be made Ohmic because of defect states formed at the interface. Defects occur as a result of damage from high kinetic energy inorganic materials that are deposited on organic layers to form the cathode structure barrier. Defect concentration can be further enhanced by adding LiF, CsF, or similar compounds to create additional defect

states.[22] Figure 6 provides a schematic of this phenomenon where carriers can bypass the injection barrier by making use of lower energy defect states to generate charge carriers in the organic transport layers.

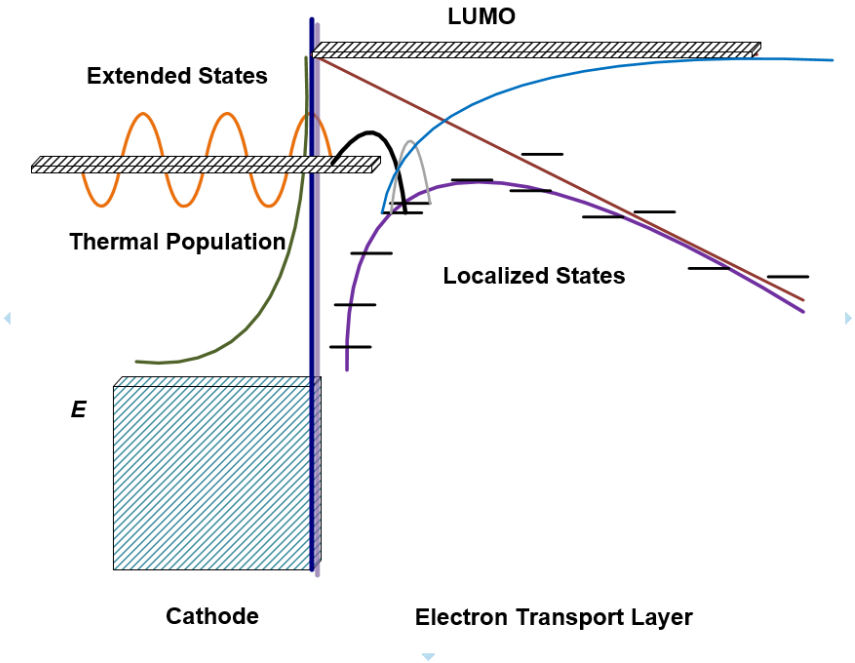

Figure 6. Representation of charge injection across the metal/organic interface showing that defect states in the organic material mitigate the injection barrier.

Amorphous deposited small molecule films are weakly bonded by intermolecular interactions such as Van Der Waals forces. This means that energy bands do not form in the same way that they do in the case of inorganic semiconductors.[23] Instead, cation and anion radicals (that act as holes and electrons) exist within close proximity to other molecules with similar energy levels such that molecule-to-molecule transport is enabled. Figure 7 shows [a] charge carriers sequentially transferred from the anion radical of a molecule to a neutral molecule through the LUMO for electron transport and [b] electrons

sequentially transferred from a neutral molecule to a neighboring cation radical through the HOMO for hole transport.

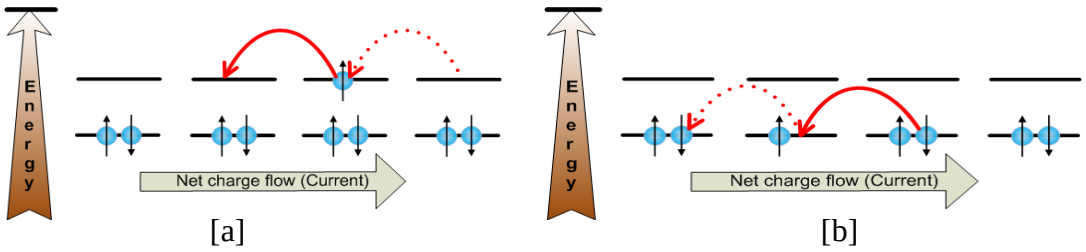

Figure 7. Schematic illustration of the [a] electron transporting process and [b] hole transporting processes.

A study of molecular crystals with long range order has reported mobility values in the range of 10^{-2} to 1 $cm^2V^{-1}s^{-1}$.[24] Small molecule vapor deposited thin films have mobility that is orders of magnitude lower. This reinforces that an amorphous or short range ordered structure is not ideal for the close contact required for hopping mechanisms as well as other transport phenomena related to the film structure.[25] Amorphous structures are chosen for OLEDs because of homogeneous and conformal film properties even though they suffer lower mobility. The mobility of glassy films is field dependent, and generally greatly reduced from crystalline forms; however, device morphology mandates that thin, conformal, and predictable films that cannot be highly crystalline are used for device applications. In contrast to the high mobility observed in crystalline organics, amorphous films are almost always selected for organic optoelectronic applications.

Numerous interactions contribute to the observed electrical behavior in organic semiconductors and more than one charge transport model can be proposed. All models adhere to the fundamental microscopic "hopping" mechanism previously described;

however, models differ to explain observed behavior that can be unique to particular circumstances or materials systems with unique microscopic transport phenomena. Models for transport mechanisms can then be compared to empirical current density vs. voltage (J-V)[22] with the goodness of fit providing one measure of the validity of a proposed transport mechanism. Comparison between macroscopic carrier transport observations and adequate transport models then becomes a useful strategy to elucidate the nature of microscopic behavior in very complex systems. Many authors agree that contemporary OLED devices are well described by space charge limited current (SCLC) transport model and that the J-V response predicted by this theory could represent a theoretical maximum for organic optoelectronic carrier mobility.[22] Figure 8 depicts the effective electromotive force (EMF) as experienced by a single molecule charge carrier (either positive or negative net charge). In Figure 8a the charge carrier will 'hop' in response to the applied EMF from biasing the device, but Figure 8b shows how an increased carrier density can lead to charge build-up. The repulsive force due to close proximity of carriers with like charges aggregates to oppose the applied EMF. The effective EMF as the primary motivation to make it energetically favorable for a carrier to 'hop' is then reduced in comparison to the applied EMF as a function of carrier density.

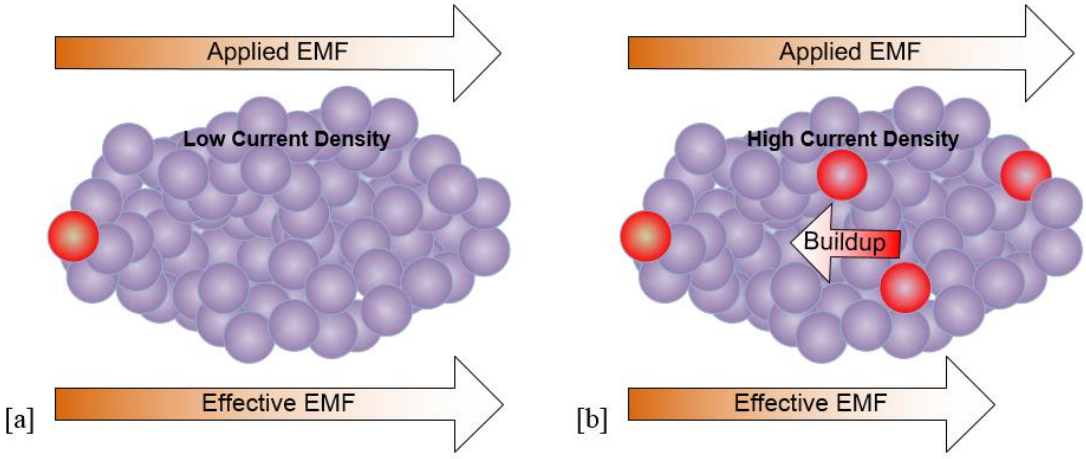

Figure 8. Schematic diagram of thin film charge transport where red molecules represent charge carriers for [a] low current density where the applied EMF equals the effective EMF and [b] high current density where charge buildup contributes to the EMF of individual charge carriers.

The SCLC model can be constructed from a few theories that are grounded by the Mott-Gurney law which has successfully modeled transport in common materials like Alq_3 with a current voltage relationship shown in equation 1.[26]

$$J = \frac{9}{8}\varepsilon_o \varepsilon \mu \frac{V^2}{d^2} \qquad (1)$$

For most cases, the field strength dependence of mobility cannot be ignored so that a correction needs to be made to account for lower observed current. A few models have been proposed to explain the temperature and electric-field dependencies of charge carrier drift mobility observed in organic disordered systems, which include the Poole-Frenkel model, small-polaron model, and disorder formalism.[23,27] The Poole-Frenkel equation can be applied to model the field dependence on mobility according to:

$$\mu(E) = \mu_o \exp(\beta\sqrt{E}) \qquad (2)$$

Then for cases when the injection interface behaves as Ohmic, it is possible to approximate current as SCLC as shown in equation 3. This expression is based on a combination of the models from equations 1 and 2:[28]

$$J_{sclc} = \frac{9}{8}\varepsilon_o \varepsilon \mu_o \exp\left(0.89\beta\sqrt{\frac{V}{d}}\right)\frac{V^2}{d^2} \quad (3)$$

Successful application of SCLC relationship requires that carrier injection is not a limiting component of conduction. In many cases it is inappropriate to assume Ohmic behavior at the metal organic interface such that carrier injection is in fact a limiting process. If the conductivity of a device is constrained by carrier injection, injection limited current (ILC) characteristics are observed and a different J-V relationship shown in equation 4 is obtained:[29]

$$J_{ILC} = 4N_o\psi^2 e\mu E exp\left(\frac{-e^{\phi_B}}{k_B T}\right) exp\left(f^{\frac{1}{2}}\right) \quad (4)$$

The energy barrier at the organic/electrode contact is analogous to a Schottky barrier commonly evaluated in inorganic semiconductor interfaces.[30]

The mechanisms introduced to model current flow in OLEDs are interesting from a theoretical standpoint; however, the predicted current voltage response from these models is often obscured by interrelated effects. In practice, OLEDs at operational brightness should observe current densities in excess of 3mA/cm^2. Mobility within an amorphous film and especially at higher current densities observed during operation is relatively low (10^{-5} to 10^{-3} cm^2 V^{-1} s^{-1}).[23] For most contemporary device structures there is ample injection into the organic layers. This results in a surplus of carriers being added into relatively electrically insulating materials so that charge builds up within the organic layer. Thus, it is a field dependent carrier mobility described by SCLC and less commonly by

ILC that successfully models performance in many contemporary devices with significantly different results than those predicted by Mott-Gurney law.

Another contribution to the resulting carrier mobility seen in recent real devices results from trap states that exist within the energy gap located between the HOMO and LUMO states. Trapped charge limited current (TCLC) models have been successful to explain the J-V curves of many common types of OLEDs.[31] A schematic representation of the trap states involved with charge transport is shown in Figure 9. At room temperature, these traps can provide energy states within proximity of the HOMO and LUMO so that chemical hole-traps and electron-traps are created.[24]

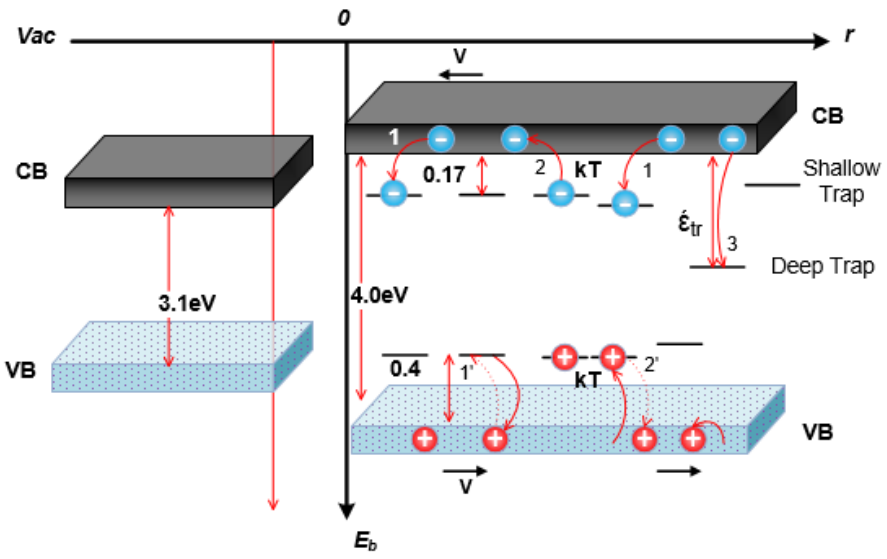

Figure 9. An adapted schematic for TCLC defect states in organic semiconductors.[24]

The exact nature, energy, and description of the traps is highly dependent on the materials system being considered; however, two primary mechanisms will be presented here as

examples. First, the geometry of carrier molecules is different between ground and excited state molecules. A physical relaxation from ground state into carrier state geometry when a molecule is ionized lowers the effective energy of the LUMO by the amount equal to the compliance energy. A rigid molecule and film structure might have higher mobility due to shallower traps associated with low compliance energy. Additionally, this idea predicts some thermal influences on mobility because carriers will interact with phonons in the lattice differently depending on whether they are neutral or charged. A second reason to motivate the existence of shallow traps stems from the similarity in energies for several common defect types found in addition to packing imperfections within an amorphous film. Defects of similar energy might include molecular isomers, irregular morphology, or compositional defects. The similarity in energy for a variety of circumstances is a result of the weak intermolecular interactions in loosely bonded solids without long range order.[32] The conduction mechanism for the organic film does not differ greatly from the conduction into or out of many common types of defects. There is, however, a difference in conduction in the presence of defects due to a thermal activation energy required to release a trapped carrier. The time required for a trapped state to be filled and evacuated contributes directly to the carrier mobility. Decreased temperature should correlate exponentially with detrapping rates so that conductivity related to TCLC should suffer a similar reduction dependent on temperature.[24,33] Effects from TCLC can be significant with low ppm levels of impurities leading to orders of magnitude change in mobility.[34]

Charge transport models for space charge limited current (SCLC) and trapped charge limited current (TCLC) are proposed as good representation of contemporary optoelectronic devices with current density in a range that is relevant to light emitting

devices. Other models do exist to explain less common or poorly understood charge transport behavior in organic electronics;[35,36] however, for devices with adequate cathode materials (not injection limited current) SCLC and TCLC remain the most widely accepted. Devices behavior as an aggregate of numerous transport models can be reviewed carefully so that the shape or particular features of an observed J-V curve can be assigned to the performance of particular material layers and/or transport mechanisms.

1.4 Energy Transfer and Decay Processes

Molecules that are radical cation 'hole' and radical anion 'electron' charge carriers existing within suitable proximity can combine to form excited state molecules as shown in Figure 10. Excitons in organic materials are localized to particular molecules in the same manner as charge carriers. In special cases, excitons can also be localized within small groups of molecules to form exciplexes that will be discussed in a later section for potential application to white OLEDs. It is notable that electroluminescent devices are not spin correlated. Figure 10 depicts the uncertainty of electrically generated charge carriers with the double ended arrows for both of electron and hole carriers. The random distribution of available charge carrier symmetry means that one-of-four (only 25%) of electroluminescent recombination will result in an excited state molecule with asymmetric spin symmetry.

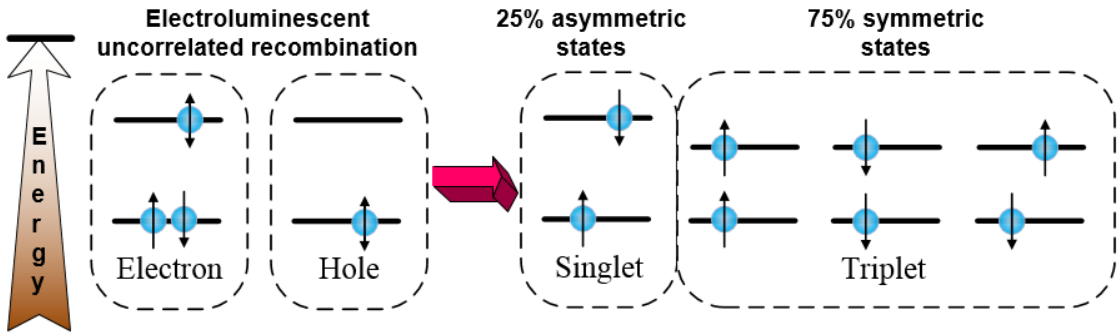

Figure 10. Schematic illustration of formations of electrically generated excitons. Random generation of excitons will result in ~25% spin-symmetric singlet excitons and 75% spin-asymmetric triplet excitons.

One mechanism to reduce an excited molecule to its preferred ground state can be through radiative decay and emission of a photon. The energy of the photon is determined by the energy of transition from excited state to ground state and thus tuning this energy gap enables higher or lower will either blue or red shift the emission spectrum of a device. Other non-radiative decay mechanisms exist and lead to the generation of heat. Methods to mitigate the amount of energy lost to non-radiative mechanisms are also important to maintain high efficiency and potentially stable device structures.

Two models can be applied to the transfer of charge neutral energy. These include Dexter and Förester energy transfer mechanisms. Dexter energy transfer mechanism shown in Figure 11 occurs as a straightforward hoping of an exciton from one molecule to an adjacent one. The activation energy required for the hop can be applied thermally or as the result of interaction with surrounding materials. Some models predict distortions in the film associated with exciton formation that can interact with lattice vibrations and thermally diffuse excitons. Electron transfer does enable both singlet excitons (S1) and

triplet excitons (T1) to be transferred. The interaction is short range (approximately 1nm) reinforcing the semi-classical description where close proximity between molecules is necessary for electron distributions to significantly overlap and transfer the excited state electrons.

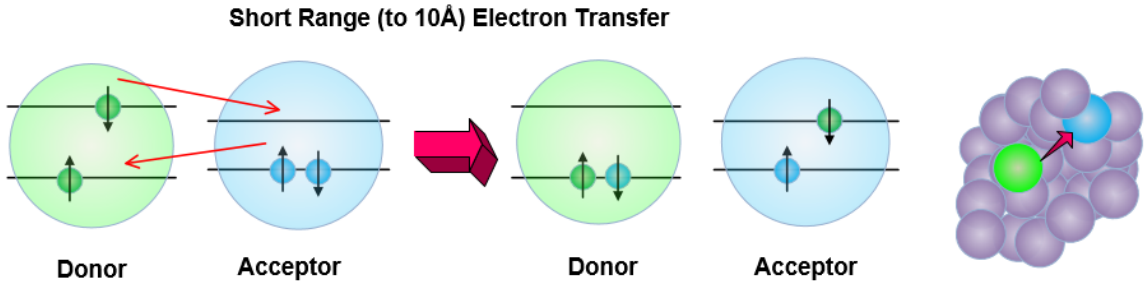

Figure 11. Dexter Energy Transfer. Representation of short range energy transfer from a donor molecule to an acceptor molecule.

Förster energy transfer shown in Figure 12 makes use of dipole-dipole coupling for non-radiative energy transfer over long range (up to 10nm) unlike the Dexter mechanism that requires nearly direct molecule-to-molecule contact. Also unlike the Dexter mechanism, electrons are conserved by the molecule that they were originally associated with in the Förster Method. Förster events can only transfer S1 (spin symmetric) excitons as the electron pair for the recombined exciton donor must not violate exclusion principles.[37]

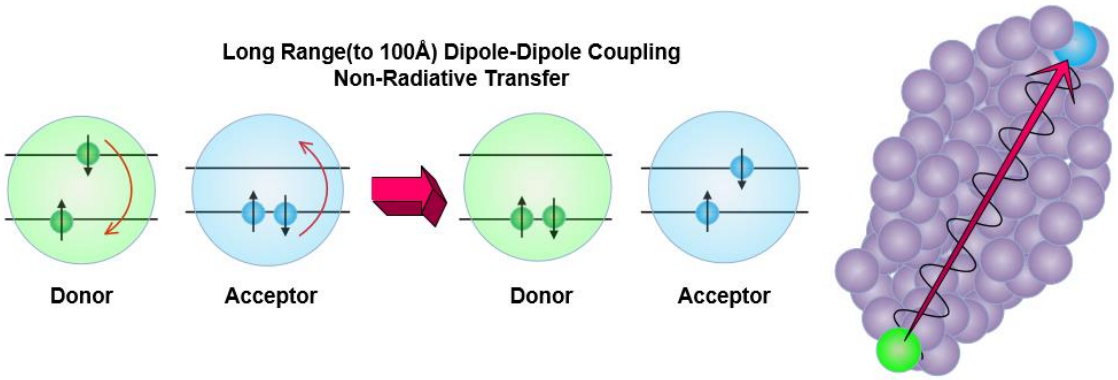

Figure 12. Förster Energy Transfer. Representation of long range energy transfer from a donor molecule located in the host matrix to an acceptor phosphor emitter doped in the emissive layer (EML)

In Förster transfer, it is not possible (as in the Dexter mechanism) for selective electron transfer at the HOMO level to satisfy spin requirements for T1 transfer.[37] Both energy transfer mechanisms have an important role in to enable nearly 100% of emission from molecular species with as little as 1% mass fraction distributed through the emissive layer (EML) in phosphorescent OLEDs.

Photoluminescence and electroluminescence processes differ in terms of the type of exciton and spatial correlation to symmetry that can be formed. Photo generated excitons originate from a single molecule that becomes excited by an incident photon and therefore have correlated electron spin orientations between electrons in the HOMO and LUMO state. In contrast electroluminescent devices inject carriers from independent anodes and cathodes and do not observe spin correlation upon recombination of electron-hole pairs. The resulting uncorrelated carrier recombination will incur an equal number of

each of the four possible exciton species. 25% will be singlet excitons and 75% will be triplets excitons that would require forbidden transition in order to enable decay. Triplet excitons have extended lifetimes because decay is forbidden by the exclusion principle and decay through other non-radiative mechanisms becomes a dominate path.[38]

Phosphorescence emitters are unique because of their ability to achieve 100% internal quantum efficiency (IQE) in for electroluminescent devices containing both singlet and triplet exciton states.[13] Molecules designed for phosphorescence emission may have a heavy metal atom with significant spin-orbit-coupling that can contribute the angular momentum required for electron spin flip. Figure 13 provides a schematic representation of thethe relative excited state energies as well as the intersystem crossing (ISC) mechanism that enables a path to radiative decay through the triplet states that would otherwise (without phosphorescence) be forbidden due to exclusion principles.[39]

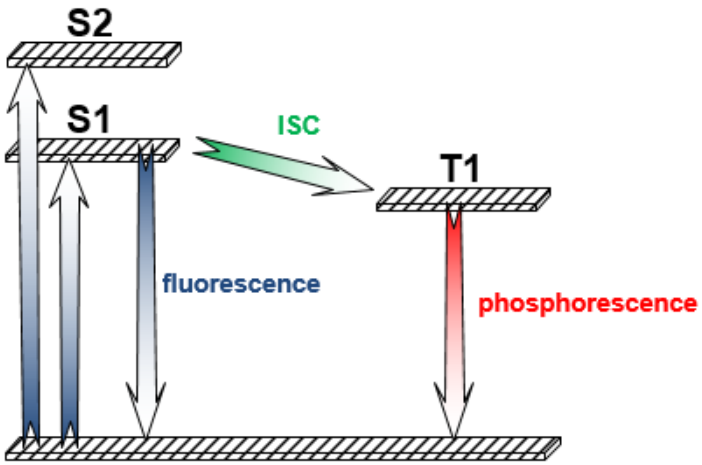

Figure 13. Relative energies and transfer processes including intersystem crossing (ISC) for fluorescence and phosphorescence radiative decay paths[40]

Emitters such as green $Ir(ppy)_3$ fundamentally changed the device emission efficiency achievable by organic optoelectronic light emitters. Addition of the iridium atom positions electrons populated in asymmetric orbitals in proximity to unstable excitons. Intersystem crossing (ISC) then describes the contribution of momentum from iridium to assimilated excitons so that singlet states will rapidly decay to triplet states. ISC and spin-flip mechanisms enable contribute to a radiative decay mechanism for both of singlet and triplet excitons[41] and it has been observed that electroluminescent phosphorescence emission can occur approaching 100% IQE. High efficiency OLEDs making use of phosphorescent molecules will be well suited to portable display technology that can be exceptionally thin, potentially flexible, and exceptionally energy efficient. High quantum efficiency in addition to low turn-on voltages also positions OLED white lighting panels to be among the most efficient and innovative devices on the market.

1.5 Structure and Function of OLED

Device design targets three primary device level objectives that are not specifically dependent on the properties of the individual materials selected.[42] An appropriately designed OLED will maintain all of: efficient charge injection from the electrodes for lower driving voltages, good hole/electron ratio for charge balance, and confinement of excitons within the EML for maximum probability of radiative recombination. Many OLED materials can serve a number of functions. In a simple bi-layer device using Alq_3 and NPD, only a single layer of Alq_3 [20] performs the functions of all five (electron injection, electron transport, emissive host, emissive dopant, and hole blocking) materials that are used in more contemporary device structures. There exists the opportunity to independently

optimize the properties of each material based on the function it needs to perform; however, additional layers and interfaces also add complexity to device operation and performance.

Several device structures were investigated for use as a basis to begin testing of the novel emissive layers (EML) formed as a codeposited combination of host material and dopant molecules. Many literature reports exist with some commonality in device design with a characteristic example shown. Analysis of the function of each layer as well as empirical optimization lead to a baseline device structure shown in in Figure 14 that is suitable to evaluate novel emitting materials and adjusted optoelectronic architectures.

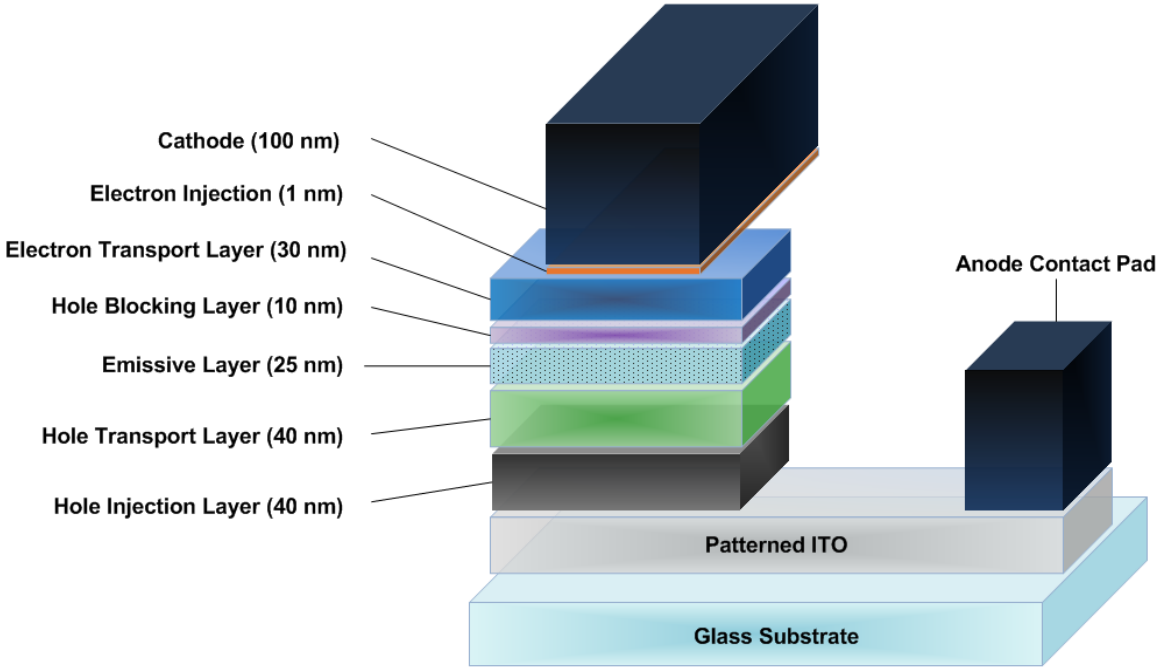

Figure 14. General scheme for a baseline phosphorescence OLED structure. The EML consists of a host matrix doped with emitter molecules.

OLED materials for use in thin film devices are typically fabricated to result in an amorphous structure with any relevant grain structure being small as compared to the film

thickness.[43-45] That is, a 40nm thick film should have grains much smaller than 40nm so that films can be largely isotropic and continuous. Each material layer has a particular structure and function that leads to desired device performance.

Anode: Indium Tin Oxide is a widely used for the anode materials. Indium-tin oxide (ITO) has excellent electrical conductivity, high transparency (~90%) and good chemical stability in the visible light region.[46,47] A number of materials have been studied as replacements for ITO and many treatments of these materials have been investigated with some prospect.[48,49] Still, ITO is very extensively used for device fabrication as it is deposited after solvent and UVO cleaning treatments.

Hole Transporting Layer (HTL): Holes are transported by radical cation hoping from molecules at the anode towards molecules near the EML. HTL materials must be electrically stable during repeated oxidation processes and readily donate electrons to facilitate hole injection from the anode.[43] Also, in the case that the HTL contacts the EML, it would be beneficial for it to be energetically unfavorable to create electron carriers in the HTL to improve confinement of electrons and excitons within the EML where they are there is an ideal path for radiative decay.[50]

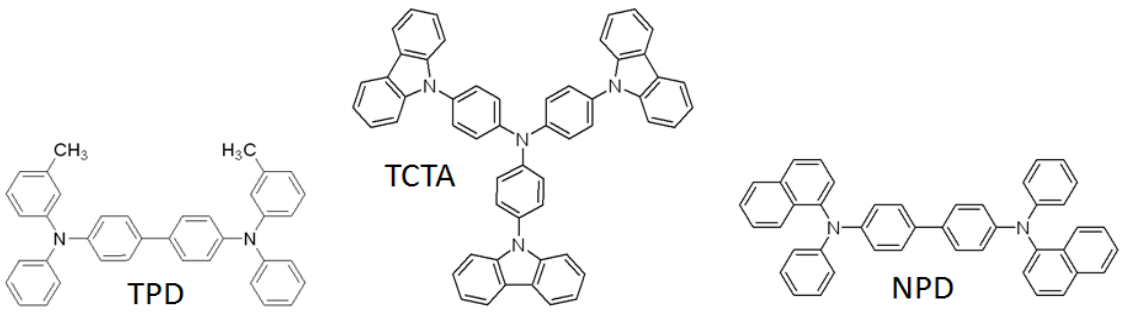

Figure 15. Chemical structures of selected hole transport layer HTL materials.[21]

Electron Blocking Layer (EBL): The EBL prevents electrons from escaping into the anode; however, most devices are naturally 'hole heavy' because of the typically lower electron mobility as compared to hole mobility in organic semiconductors. Another observed function of the EBL is to prevent exciplexes at the HTL/EML interface. It has been observed that adding as little as 3nm of TCTA (EBL) between the HTL and EML significantly changed the observed EL spectrum to suggest significantly reduction in NPD (HTL) and exciplex emission.[51]

Emissive Layer (EML): Most phosphorescent molecules would be very inefficient emitters if deposited as pure layers because of severe concentration quenching.[42,52,41] Thus, the emissive layer for phosphorescent devices typically consists of a dopant molecule contained by a host matrix material commonly fabricated from materials like those in Figure 16. Successful integration of a two materials matrix requires efficient energy transfer from host to dopant while minimizing non-radiative decay mechanisms. Efficient energy transfer can be accomplished by enabling Förster, Dexter, or direct exciton transfer to the dopant molecule. Limiting non-radiative mechanisms occurs by proper energy band alignment at the EML interfaces, exciton confinement, and large d-d band splitting within the dopant molecule.[39]

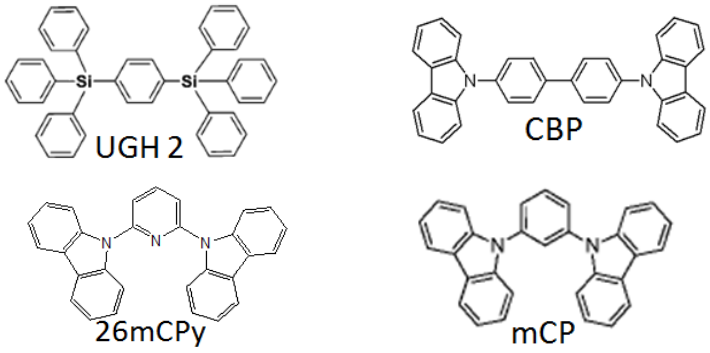

Figure 16. Chemical structures of selected host materials used in the emissive layer (EML).[21]

Electron Transporting Layer (ETL): This layer is responsible for radical anion hoping that results in electron carrier transport from the cathode towards desired recombination centers at the emissive portion of the device. The electron affinity of the ETL should be similar to the work function of the cathode to eliminate significant barriers to injection.[53] Injection from metal anode into the ETL has also been demonstrated to be highly dependent on defect states present at the metal-to-organic interface.[29,30,54] ETL materials shown in Figure 17 typically have lower charge carrier mobility than HTL materials making them the limiting component in high current devices that aim to maintain charge balance. Thus, the conductivity of a balanced device is often limited by the mobility of the ETL making this a contemporary area of interest for researchers.[39]

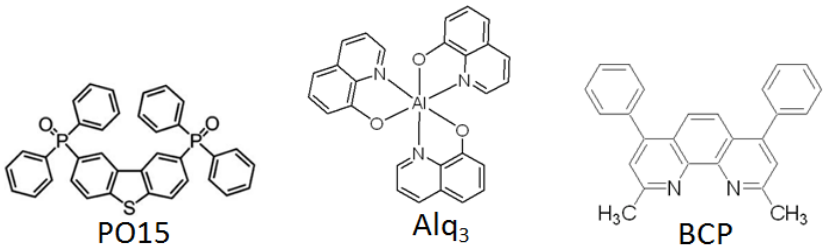

Figure 17. Chemical structures of selected ETL materials[21]

Metal Cathode: The cathode must make good electrical contact with the device and provide macroscopic contacts to the outside world. A material with low work function that will readily give up electrons will increase the rate of carrier injection into the ETL. Codeposited alloys like Mg/Ag can be used to construct the cathode. Aluminum is widely used and tends to minimize damage to underlying organic layers during physical vapor deposition (PVD) processes as compared to other metals because of its lower atomic weight and relatively low melting point. A small amount of Lithium Fluoride (LiF) can also be added to the metal organic interface to increase the number of defect states in the organic with energy appropriate for fast electron injection.[55]

1.6 Thin Film Mechanical Characterization using Buckling

Traditional mechanical characterization techniques have had limited application to organic electronic materials characterization. The first challenge facing traditional stress/strain and related test methods is the impracticality of bulk testing methods due to limited quantities and very high cost of organic electronic materials. Even if sufficient quantities of bulk material could be acquired, traditional load cells, strain gauges, and associated mechanical testing equipment are not easily applied to the bulk form of organic electronic materials as large crystals of OLED materials could be prohibitively difficult to

fabricate. Most suppliers and the results of common synthesis and purification techniques result in powders or small flakes. The second major challenge facing relevant mechanical measurements of organic electronic devices is due to difference in the behavior of thin film structures at confined length scale that does not correlate well with bulk behavior. It has been shown that the growth kinetics and resulting materials structure are dependent on film thickness. These surface effects could suggest that mechanical testing simply scaled from macroscopic observations to predict the behavior of submicron films could have very large error and another characterization technique that could be applied to the confined scale relevant to thin film organic electronics is needed.

When a stiff material is placed in homogeneous plane compression it can become energetically favorable for the material to bend instead of observing the lateral compliance required by the substrate deformation. Figure 18 shows two conditions where changing the geometry of the system can reduce the strain energy associated with plane compressive displacements.

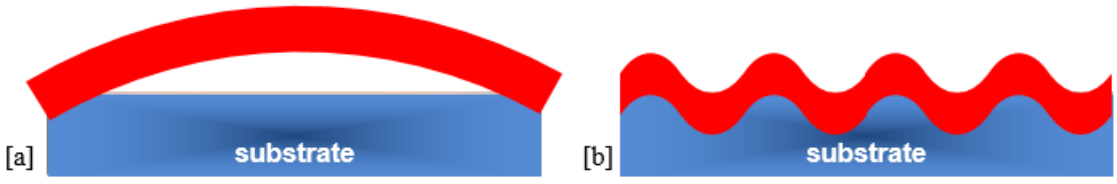

Figure 18. Deformation mechanisms observed for rigid thin film for [a] delamination and [b] wrinkling

Here the relatively large amount of energy required to strain the stiff material is avoided by realizing much smaller strains at the surface of the thin film. This phenomena commonly labeled bending or buckling is observed frequently for thin rigid materials. An everyday example of buckling can be observed in nature when the volume of a fruit changes. Figure 19 shows that it is energetically favorable for the stiff thin walls of grape to deform by buckling in response to compression in plane with the skin of the grape.

Figure 19. A shriveled grape skin demonstrates the response of the more rigid skin to a compressive strain as the volume of the fruit decreases. It becomes energetically favorable to wrinkle the skin in the case that delamination from the more compliant pulp does not occur.

In 2004 the Nature Publishing Group released an article by Stafford et al. that demonstrated carefully controlled buckling conditions in addition to carefully quantifying the resulting minimum energy configuration can successfully determine mechanical properties of an unknown thin film polymer material.[56] This method coined strain-induced elastic buckling instability for mechanical measurements (SIEBIMM) will be applied to

study the mechanical properties of thin films that are relevant to small molecule organic optoelectronic devices and it will become evident that SIEBIMM wrinkling can be applied to measure the mechanical properties of thin films used in organic electronic devices.

1.6.1 Single Layer Film Method

SIEBIMM wrinkling can be used to determine the modulus of thin films. Indentation, surface acoustic wave spectroscopy, Brillouin light scattering, and other traditional methods that can also be used to characterize mechanical properties are limited when attempting to characterize ultrathin organic materials due to the soft characteristic of these glassy films leading to substrate interferences especially for films below 50nm thicknesses.[56] The wrinkling is induced by the minimization of the total strain energy in a system composed of a pre-strained and relatively soft substrate adjacent to the thin film of interest. Upon release of the pre-strained substrate the adjacent film of interest will either undergo periodic buckling or delamination in order to minimize compressive strain energy that would otherwise dominate the system.[57,58] The buckling mechanism that dominates will be determined by the substrate modulus and the energy required to delaminate the film. Films on very rigid substrates and/or with poor adhesion will delaminate while films on compliant substrates ($E_s << E_f$) and/or with very good adhesion will buckle without delamination.[58] As a condition to apply a buckling based metrology to the measurement of thin films, the pre-strain (ε) of the substrate needs to be greater than a critical strain (ε_c) dependent on the ratio of the plane strain moduli of the substrate to the plane strain moduli of the film, $\bar{E}_s/\bar{E}_f$, as shown in Equation 5.

$$\varepsilon_c = -\frac{1}{4}\left(\frac{3\bar{E}_s}{\bar{E}_f}\right)^{2/3} \tag{5}$$

The negative sign in equation 1 denotes compression. A reduced modulus, $\bar{E}$, that is related to Young's elastic modulus, E, is defined as $\bar{E} = E/(1-\nu^2)$ to simplify equations. The amount of strain applied will be discussed in detail in subsequent experimental sections and will always be greater than or equal to the critical value. When $\varepsilon > \varepsilon_c$, a stable equilibrium state is observed where the film on a substrate is wrinkled in a uniform sinusoidal form. When the relative substrate thickness and pliability approach infinite ($h_f << h_s$) and ($\bar{E}_f >> \bar{E}_s$), any increase in the strain in addition to the critical strain results in increased amplitude of the wrinkles, but it does not result in any change to the wavelength of the wrinkles. It is a key observation that the wavelength of the wrinkles remains independent of any excess strain as long as the substrate deformation is limited enough to remain well approximated by a simple linear elastic model.[59] This strain invariance of the equilibrium wavelength results in an elegant relationship between the thin film modulus, $\bar{E}_f$, the modulus of the substrate, $\bar{E}_s$, and the film thickness, h_f that can be exploited to measure unknown properties.

A number of authors have derived the underlying mechanics that govern the wrinkling behavior of a rigid film adhered to a soft elastic substrate.[60-63] It is widely agreed (when a strain in excess of the critical strain is applied) that the modulus of a thin film will be related to a characteristic wrinkle wavelength, λ, according to the relationship shown in equation 6.

$$\frac{E_f}{1-\nu_f^2} = \bar{E}_f = 3\bar{E}_s\left(\frac{\lambda}{2\pi h_f}\right)^3 \qquad (6)$$

Accurate metrologies for determining both the film thickness, h_f, and the reduced modulus of the substrate, $\bar{E}_s$, are well established and will be discussed in at length within

experimental details sections. Poisson's ratio for a glassy film and rubbery substrate are well reported to have typical values $\nu_f = 0.33$ and $\nu_s = 0.5$ respectively. It is therefore, possible to determine the unknown film modulus by measuring the equilibrium wavelength, λ.[56]

1.6.2 Double Layer Film Method

Application of the buckling metrology to small molecule organic electronic films has shown time dependent measurements as a result of instability at room temperature. The observation (that will be discussed in a later section) was first noted as a result of color change of the wrinkled samples and further quantified by collecting variable angle spectroscopic elipsometry (VASE) data vs. time for several materials systems. A number of methods were applied to reduce diffusion of the deposited film into the substrate that included: storage of deposited samples at low temperature, different choice of substrate material, and inclusion of a diffusion barrier. All methods demonstrated some reduction in time dependent behavior of the materials system. The most stable results were achieved with the addition of a polystyrene (PS) diffusion barrier; however, the additional barrier film must then be accounted for when using the buckling method to determine the modulus of new organic electronic materials. Figure 20 shows the proposed film stack to include a diffusion barrier that will contribute to the characteristic wavelength observed in the deformed sample. To enable SIEBIMM for materials that demonstrate substrate incompatibility requiring a diffusion barrier, it will be necessary to deconvolute the mechanical contributions from the additional barrier film.

Figure 20. Schematic of film stack used to determine the unknown modulus of a thin film when the film of interest is not stable when directly deposited on the substrate material.

When the multilayer stack deforms, both the film of interest as well as the diffusion barrier will contribute to the wrinkling behavior. The sum of the individual film flexural rigidities has been shown to accurately describe the total resistance to buckling from the film stack according to equation 7.

$$\bar{E}_{total} I_{total} = \bar{E}_f I_f + \bar{E}_{barrier} I_{barrier} = \frac{\bar{E}_s h_{total}}{4} \left(\frac{\lambda}{2\pi}\right)^3 \qquad (7)$$

The product of the reduced modulus, $\bar{E}_{total}$, and the second moment of area, I_{total}, on the left side of equation 7 define the flexural rigidity of the film stack. The flexural rigidity describes a material's resistance to bending due to its mechanical properties in addition to the material's distribution in space. In the special case of a single homogenous film, the neutral axis is exactly the middle of the film and the symmetry of the second moment reduces to equation 6. The terms in the far right of equation 7 do agree with equation 6 in the special single film case where $I_{barrier}$ vanishes and $\bar{E}_{total} I_{total} = \bar{E}_f I_f$. In the more general case, the second moments of area from a multi film stack will not be symmetrical and will have a complex dependence on the thicknesses of both film layers. That is, the flexural rigidity as a result of the heterogeneous material distribution in space will require $\bar{E}_{total} I_{total}$

to be a complex function of the component second moments of area (I_f and $I_{barrier}$) that will be defined by the film thicknesses (h_f and $h_{barrier}$).

The general form mathematical description of a two plate composite solved for the reduced modulus of the unknown film is shown in equations 8 with the nested definitions of: κ, $\bar{E}_{eff}$, and ϕ shown in equation 9, equation 10, and equation 11 respectively. The relationship has been applied to a variety of materials systems and has been shown to correlate well with empirical data.[64]

$$\bar{E}_f = \frac{\frac{\bar{E}_{eff}}{4} - \bar{E}_{barrier}\left[\left(\phi_{barrier}-\frac{\kappa}{2}\right)^3+\left(\frac{\kappa}{2}\right)^3\right]}{\left(1-\frac{\kappa}{2}\right)^3-\left(\phi_{barrier}-\frac{\kappa}{2}\right)^3} \tag{8}$$

$$\kappa = \frac{1+\phi_{barrier}^2\left(\frac{\bar{E}_{barrier}}{\bar{E}_f}-1\right)}{1+\phi_{barrier}\left(\frac{\bar{E}_{barrier}}{\bar{E}_f}-1\right)} \tag{9}$$

$$\phi_{barrier} = \frac{h_{barrier}}{h_{total}} = \frac{h_{barrier}}{h_f+h_{barrier}} \tag{10}$$

$$\bar{E}_{eff} = 3\bar{E}_s\left(\frac{\lambda}{2\pi h_{total}}\right)^3 \tag{11}$$

Solving equation 8 requires an iterative numerical solution. An initial value for κ = 1 would only be correct for a homogeneous film where $\bar{E}_f = \bar{E}_{barrier}$. Recursive substitution of the film reduced modulus, $\bar{E}_f$, obtained from equation 8 to determine a new value for κ converges rapidly until the values predicted no longer change with additional iterations. A custom script written in MATLAB was used to iterate results to floating point precision; however, other authors have suggested that no more than four iterations should be necessary to achieve a modulus unchanging to at least the third decimal point.[64]

1.7 References

1. Chiang C, Fincher Jr C, Park Y, et al. Electrical conductivity in doped polyacetylene. *Phys Rev Lett*. 1977;39(17):1098-1101.

2. Furst M, Kallman H. High energy induced fluorescence in organic liquid solutions(energy transport in liquids). III. *Physical Review*. 1952;85(5):816-825.

3. Pope M, Kallmann H, Magnante P. Electroluminescence in organic crystals. *J Chem Phys*. 1963;38:2042-2043.

4. Chamberlain G. Organic solar cells: A review. *Solar Cells*. 1983;8(1):47-83.

5. Friend R, Gymer R, Holmes A, et al. Electroluminescence in conjugated polymers. *Nature*. 1999;397(6715):121-128.

6. Sony Corporation. Sony style USA. http://www.sonystyle.com/webapp/wcs/stores/servlet/CategoryDisplay?catalogId=10551&storeId=10151&langId=-1&categoryId=8198552921644539854.

7. Duggal A. Next generation lighting projects with DOE. http://ge.geglobalresearch.com/blog/next-generation-lighting-projects-with-doe/.

8. Galaxy S7 edge homepage. http://www.samsung.com/us/explore/galaxy-s7-features-and-specs/?cid=ppc-2016.

9. Forrest SR. The path to ubiquitous and low-cost organic electronic appliances on plastic. *Nature*. 2004;428(6986):911-918.

10. http://solutions.3m.com/wps/portal/3M/en_US/FlexibleCircuits/Home/ManufacturingFoundries/RolltoRollProcessing/2013.

11. Dresner J. Double injection electroluminescence in anthracene. *RCA Rev*. 1969;30(2):322.

12. Helfrich W, Schneider W. Recombination radiation in anthracene crystals. *Phys Rev Lett*. 1965;14(7):229-231.

13. Adachi C, Baldo MA, Thompson ME, Forrest SR. Nearly 100% internal phosphorescence efficiency in an organic light-emitting device. *J Appl Phys*. 2001;90:5048.

14. Forrest S, Bradley D, Thompson M. Measuring the efficiency of organic light-emitting devices. *Adv Mater*. 2003;15(13):1043-1048.

15. Hung HW, Yokoyama N, Yahiro M, Adachi C. Low driving voltage organic light emitting diode using phenanthrene oligomers as electron transport layer. *Thin Solid Films*. 2008;516(23):8717-8720.

16. Brooks J, Babayan Y, Lamansky S, et al. Synthesis and characterization of phosphorescent cyclometalated platinum complexes. *Inorg Chem*. 2002;41(12):3055-3066.

17. Chu TY, Lee YH, Song OK. Effects of interfacial stability between electron transporting layer and cathode on the degradation process of organic light-emitting diodes. *Appl Phys Lett*. 2007;91:223509.

18. Kondakov D, Lenhart W, Nichols W. Operational degradation of organic light-emitting diodes: Mechanism and identification of chemical products. *J Appl Phys*. 2007;101:024512.

19. Forrest SR, Thompson ME. Introduction: Organic electronics and optoelectronics. *Chem Rev*. 2007;107(4):923-925.

20. Tang C, VanSlyke S. Organic electroluminescent diodes. *Appl Phys Lett*. 1987;51(12):913.

21. Sigma-Aldrich. Organic and printed electronics. http://www.sigmaaldrich.com/materials-science/organic-electronics.html. Accessed 5/05, 2010.

22. Wang Z, Helander M, Greiner M, Qiu J, Lu Z. Carrier mobility of organic semiconductors based on current-voltage characteristics. *J Appl Phys*. 2010;107:034506.

23. Shirota Y, Kageyama H. Charge carrier transporting molecular materials and their applications in devices. *Chem Rev*. 2007;107(4):953-1010.

24. Karl N, Kraft KH, Marktanner J, et al. Fast electronic transport in organic molecular solids? *Journal of Vacuum Science & Technology A: Vacuum, Surfaces, and Films*. 1999;17:2318.

25. Schein L. Temperature independent drift mobility along the molecular direction of as_ {2} s_ {3}. *Physical Review B*. 1977;15(2):1024-1034.

26. Kiy M, Losio P, Biaggio I, Koehler M, Tapponnier A, Günter P. Observation of the Mott–Gurney law in tris (8-hydroxyquinoline) aluminum films. *Appl Phys Lett*. 2002;80:1198.

27. Schein L. Comparison of charge transport models in molecularly doped polymers. *Philosophical Magazine Part B*. 1992;65(4):795-810.

28. Murgatroyd P. Theory of space-charge-limited current enhanced by frenkel effect. *J Phys D*. 1970;3:151-156.

29. Scott JC, Malliaras GG. Charge injection and recombination at the metal-organic interface. *Chemical Physics Letters*. 1999;299(2):115-119.

30. Scott JC. Metal–organic interface and charge injection in organic electronic devices. *Journal of Vacuum Science & Technology A: Vacuum, Surfaces, and Films*. 2003;21:521.

31. Burrows P, Shen Z, Bulovic V, et al. Relationship between electroluminescence and current transport in organic heterojunction light-emitting devices. *J Appl Phys*. 1996;79:7991.

32. Probst K, Karl N. Energy levels of electron and hole traps in the band gap of doped anthracene crystals. *physica status solidi (a)*. 2006;27(2):499-508.

33. Blom P, De Jong M, Breedijk S. Temperature dependent electron-hole recombination in polymer light-emitting diodes. *Appl Phys Lett*. 1997;71(7):930-932.

34. Karl N, Marktanner J, Stehle R, Warta W. High-field saturation of charge carrier drift velocities in ultrapurified organic photoconductors. *Synth Met*. 1991;42(3):2473-2481.

35. Davids P, Campbell I, Smith D. Device model for single carrier organic diodes. *J Appl Phys*. 1997;82:6319.

36. Koehler M, Hümmelgen I. Regional approximation approach to space charge limited tunneling injection in polymeric devices. *J Appl Phys*. 2000;87:3074.

37. Bakken N, Torres JM, Li J, Vogt BD. Thickness dependent modulus of vacuum deposited organic molecular glasses for organic electronics applications. *Soft Matter*. 2011;7(16):7269.

38. Baldo M, O'brien D, You Y, et al. Highly efficient phosphorescent emission from organic electroluminescent devices. *Nature*. 1998;395(6698):151-154.

39. Yeh SJ, Wu MF, Chen CT, et al. New dopant and host materials for blue-light-emitting phosphorescent organic electroluminescent devices. *Adv Mater*. 2005;17(3):285-289.

40. Baldo M, Thompson M, Forrest S. Phosphorescent materials for application to organic light omitting devices. *Pure and Applied Chemistry*. 1999;71(11):2095-2106.

41. Baldo M, Lamansky S, Burrows P, Thompson M, Forrest S. Very high-efficiency green organic light-emitting devices based on electrophosphorescence. *Appl Phys Lett*. 1999;75:4.

42. K. Mullen, S. Ullrich, eds. *Organic light-emitting devices*. Darmstadt, Germany: Wiley-VCH; 2006.

43. Adachi C, Nagai K, Tamoto N. Molecular design of hole transport materials for obtaining high durability in organic electroluminescent diodes. *Appl Phys Lett*. 1995;66:2679.

44. Adachi C, Tsutsui T, Saito S. Blue light-emitting organic electroluminescent devices. *Appl Phys Lett*. 1990;56:799.

45. Adachi C, Tsutsui T, Saito S. Confinement of charge carriers and molecular excitons within 5-nm-thick emitter layer in organic electroluminescent devices with a double heterostructure. *Appl Phys Lett*. 1990;57:531.

46. Vossen J. Physics of thin films. *New York: Academic*. 1977.

47. You Y, Kim Y, Choi D, Jang H, Lee J, Kim D. Electrical and optical study of ITO films on glass and polymer substrates prepared by DC magnetron sputtering type negative metal ion beam deposition. *Mater Chem Phys*. 2008;107(2-3):444-448.

48. Fenenko L, Adachi C. Influence of heat treatment on indium-tin-oxide anodes and copper phthalocyanine hole injection layers in organic light-emitting diodes. *Thin Solid Films*. 2007;515(11):4812-4818.

49. Ho JJ, Chen CY, Hsiao RY, Ho OL. The work function improvement on indium− tin− oxide epitaxial layers by doping treatment for organic light-emitting device applications. . 2007.

50. Shirota Y. Photo-and electroactive amorphous molecular materials—molecular design, syntheses, reactions, properties, and applications. *Journal of Materials Chemistry*. 2005;15(1):75-93.

51. Lee JH, Huang CL, Hsiao CH, Leung MK, Yang CC, Chao CC. Blue phosphorescent organic light-emitting device with double emitting layer. *Appl Phys Lett*. 2009;94:223301.

52. Wang Y, Herron N, Grushin V, LeCloux D, Petrov V. Highly efficient electroluminescent materials based on fluorinated organometallic iridium compounds. *Appl Phys Lett*. 2001;79:449.

53. Hughes G, Bryce MR. Electron-transporting materials for organic electroluminescent and electrophosphorescent devices. *Journal of Materials Chemistry*. 2005;15(1):94-107.

54. Zahn D, Salvan G, Gavrila G, Paez B. Chemistry and morphological properties of metal interfaces to organic semiconductors. *Advances in Solid State Physics*. :313-324.

55. Hung L, Tang C, Mason M. Enhanced electron injection in organic electroluminescence devices using an al/LiF electrode. *Appl Phys Lett*. 1997;70:152.

56. Stafford CM, Guo S, Harrison C, Chiang MYM. Combinatorial and high-throughput measurements of the modulus of thin polymer films. *Rev Sci Instrum*. 2005;76:062207.

57. Wilder EA, Guo S, Lin-Gibson S, Fasolka MJ, Stafford CM. Measuring the modulus of soft polymer networks via a buckling-based metrology. *Macromolecules*. 2006;39(12):4138-4143.

58. Huang R, Stafford CM, Vogt BD. Effect of surface properties on wrinkling of ultrathin films. *J Aerospace Eng*. 2007;20(1):38-44.

59. Duan H, Wang J, Huang Z, Karihaloo B. Size-dependent effective elastic constants of solids containing nano-inhomogeneities with interface stress. *J Mech Phys Solids*. 2005;53(7):1574-1596.

60. Biot M. Bending of an infinite beam on an elastic foundation. *Zeitschrift fiir Angewandte Maihematik und Mechanik*. 1922;2(3):165-184.

61. Allen HG. *Analysis and design of structural sandwich panels: The commonwealth and international library: Structures and solid body mechanics division.* Elsevier; 2013.

62. Volynskii A, Bazhenov S, Lebedeva O, Bakeev N. Mechanical buckling instability of thin coatings deposited on soft polymer substrates. *J Mater Sci*. 2000;35(3):547-554.

63. Groenewold J. Wrinkling of plates coupled with soft elastic media. *Physica A: Statistical Mechanics and its Applications*. 2001;298(1):32-45.

64. Nolte AJ, Cohen RE, Rubner MF. A two-plate buckling technique for thin film modulus measurements: Applications to polyelectrolyte multilayers. *Macromolecules*. 2006;39(14):4841-4847.

CHAPTER 2

MONOMER AND EXCIMER EMISSION FOR WHITE ORGANIC LIGHT EMITTING DEVICES USING A SINGLE EMITTER

2.1 Introduction

White organic light emitting diodes (WOLEDs) with high power efficiency are candidates for the next generation of illumination devices.[65,66] To date, however, the electroluminescent (EL) spectrum of WOLEDs is generated using multiple emitters embedded in a complex device structure.[67-71] In this research, efficient WOLEDs with high quality white light are fabricated using a single emitter. The ideal broad EL spectrum was realized by combining monomer and excimer emission in a 4-layer WOLED. A forward power efficiency of η_p=37.8 lm/W was achieved with an EL spectrum yielding CIE coordinates of (0.37, 0.40) and CRI of 80. The demonstration of efficient single-doped WOLEDs with high illumination quality presents a unique opportunity to simplify the device architecture and eliminate the problems of color aging and color instability for WOLEDs using multiple emitters. All of these improvements will help to enable future commercialization of WOLEDs for lighting applications.

Unlike rapidly maturing monochromatic OLEDs, one of greatest challenges for WOLEDs is the absence of a single organic emitter (fluorescent or phosphorescent material) that covers the entire visible spectrum.[72] The broad spectrum required for white light in organic devices has previously been obtained from the combined emission of multiple emissive dopants shown in the relatively complex structures illustrated in Figure 21.

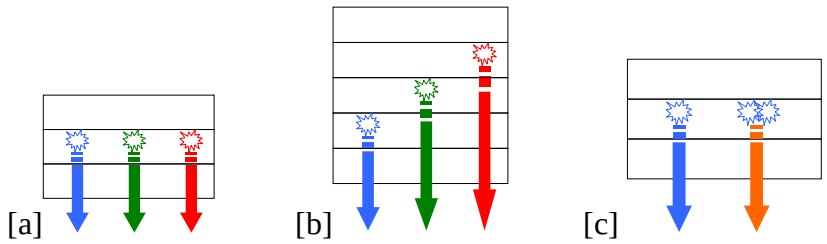

Figure 21. Schemes for three typical WOLEDs architectures: [a] triple-doped emissive layer, [b] multiple emissive layers, [c] emissive layer with a single dopant species with both monomer and excimer emission.

These structures include: a multiple-doped emissive layer (EML),[68,73-75] a multilayer of emitters (doped films or neat films),[70,71,76] multiple emissions from monomer and excimers or exciplexes,[77-80] hybrid polymers/inorganics,[81] etc. The development of WOLEDs has progressed rapidly during the last decade. The efficacy has reached over 100 lm/W with enhanced outcoupling effect.[65,66] The limited operational lifetime, which has previously handicapped OLED technology, has now been demonstrated to exceed 10,000 hours.[66] However, such high efficacy and long operational lifetime are achieved using multiple emissive dopants, which require relatively complex device structures. More complex device structures then create new challenges to achieve consistent and low cost manufacturing processes. The use of multiple emissive dopants also generates an unstable emission color for WOLEDs due to the energy transfer process between different emitters. It is common that the electroluminescent (EL) spectrum of WOLEDs varies with different driving voltages (or driving current) due to the change of ratio in blue, green, and red emission.[82] Moreover, the different degradation rates for each emissive dopant in

WOLEDs could create a problem of "color aging", i.e. the color of lighting changes significantly in the degradation process, resulting in a premature device failure. In order to prevent the color aging and enhance the color stability, the device structures will become inevitably more complex and expect an increase in the manufacturing cost. Towards overcoming these problems, this report will demonstrate WOLEDs using a single emitter with good color quality and illumination efficiency which can be realized by coupling blue-green like monomer emission and orange like excimer emission for reported square planar Platinum complexes.[77-79]

WOLEDs using a single emitter realized by coupling blue-green like monomer emission and orange like excimer emission have been reported for square planar Pt complexes, i.e. FPt and their analogs.[77-79] In contrast to most of organic emitters, Pt complexes can form a broadly emitting excimer. The strong Pt···Pt interaction can destabilize the highest occupied molecular orbital (HOMO), resulting in a red-shifted emission spectrum for excimers shown in Figure 22. If the excimer emission adequately complements monomer emission, the EL spectrum of excimer-based WOLEDs can include all visible wavelengths. The ratio of monomer/excimer emission can be controlled by varying the dopant concentration, the morphology of host materials or the relative balance of hole/electron injection, providing methods to control the color of WOLEDs.[77,78] Additionally, because an excimer does not have a bound ground state, the cascade of energy from the "blue" (higher energy) emitter to the excimer can be prevented, leading to a stable emission color that is independent of the driving voltage. Moreover, the problem of "color aging" can be resolved due to the use of a single emitter. The combination of

monomer and excimer emission provides a simple and elegant solution to achieve voltage-independent, stable and broad spectrum WOLEDs.

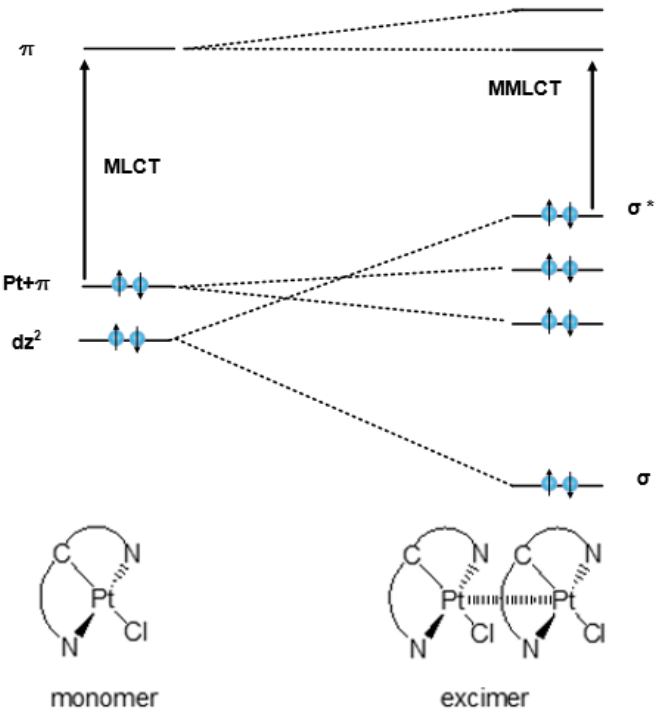

Figure 22. Illustration of excimer formation for square planar Pt complexes like Pt(N^C^N)Cl and their analogs. The newly formed Pt--Pt bond destabilized the highest occupied molecular orbital (HOMO), resulting in a red-shifted emission spectrum for excimer of Pt complexes.

2.2 Experimental

Synthesis of Pt-17: A mixture of bis(methyl-imidazolyl)toluene diiodide (1 mmol) and 0.5 mmol silver oxide was stirred in a solution of 100 ml acetonitrile for 5 h at room temperature before 1 equiv. platinum chloride and 1 equiv. potassium carbonate were added. The reaction mixture was heated to reflux for additional 24 h. Then the mixture

was cooled to room temperature before 100 ml water was added. The resulting yellow precipitate was filtered off and washed with excessive methanol, water and ether and dried under vacuum. The light yellowish product (in 20% yield) was obtained after thermal evaporation under high vacuum. Nuclear magnetic resonance spectroscopy (NMR) (500 MHz, DMSO): δ9.88 (s, 2H), 8.36 (d, 2H), 8.02 (d, 2H), 3.99 (s, 6H), 2.53 (s, 3H).

The layer sequence for WOLEDs on top of ITO substrate is: 30nm NPD as a hole-transporting layer/10nm TAPC as an electron-blocking layer/25nm emissive layer/20-80nm PO15 as an electron transporting layer and a hole-blocking layer/1nm LiF/90nm Al cathode. The emissive layer consists of ether 26mCPy as a host or TAPC:PO15(1:1) as co-host materials with Pt-17 as a phosphorescent emitter. Prior to organic depositions, the ITO substrates were cleaned by subsequent sonication in water, acetone, and isopropanol, followed by a 15 min UV−ozone treatment. PEDOT:PSS was filtered through a 0.2 μm filter and spin-coated on the prepared substrates, giving a 40- nm-thick film. All small molecular organic materials were deposited by thermal evaporation at rates of 1 +/- 0.5 Å/s with a working pressure of less than 10−7 Torr. A thin 1 nm LiF layer was deposited at a rate of < 0.2 Å/s and aluminum cathodes were deposited at 1−2 Å/s through a shadow mask without breaking the vacuum. Individual devices have areas of 0.04 cm^2 . I−V−L characteristics were taken with a Keithley 2400 Source-Meter and a Newport 818 Si photodiode inside a nitrogen-filled glovebox. Electroluminescence (EL) spectra were taken using a Jobin Yvon Fluorolog spectrofluorometer. Agreement between luminance, optical power, and EL spectra was verified with a calibrated Photo Research PR-670 spectroradiometer with all devices assumed to be Lambertian emitters.

2.3 Results

In order to meet the requirement for solid state lighting, several factors have to be considered for excimer-based WOLEDs including: the emission efficiency of monomer/excimer, the emission colors of monomer/excimer, and the optimization of charge injection and recombination inside of emissive layers. The ability to create high quality illumination that mimics natural light sources is particularly critical for lighting applications. Two important parameters are used to define the color quality of white light source: the Commission Internationale de L'Éclairage (CIE) chromaticity coordinates and the color rendering index (CRI). The highest quality white illumination requires sources with CIE coordinates close to (0.33, 0.33) and a CRI value over 80.[83] The phenomenon of excimer formation has been observed for a long time,[84] but the photophysical properties of excimers remain poorly understood. For this reason, progress on phosphorescent excimers has depended almost entirely on the synthesis and characterization of new materials.

2.3.1 Spectral Tuning Correlated to Dopant Concentration

To evaluate the electroluminescent properties of Pt-17, a series of WOLEDs were fabricated in a 4-layer device structure: NPD/TAPC/Pt-17:26mCy/PO15, with the dopant concentration ranging from 2-26%.[85] Forward viewing external quantum efficiency is plotted versus current density for these devices in Figure 23, with the corresponding EL spectra and CIE coordinates displayed in Figure 24.

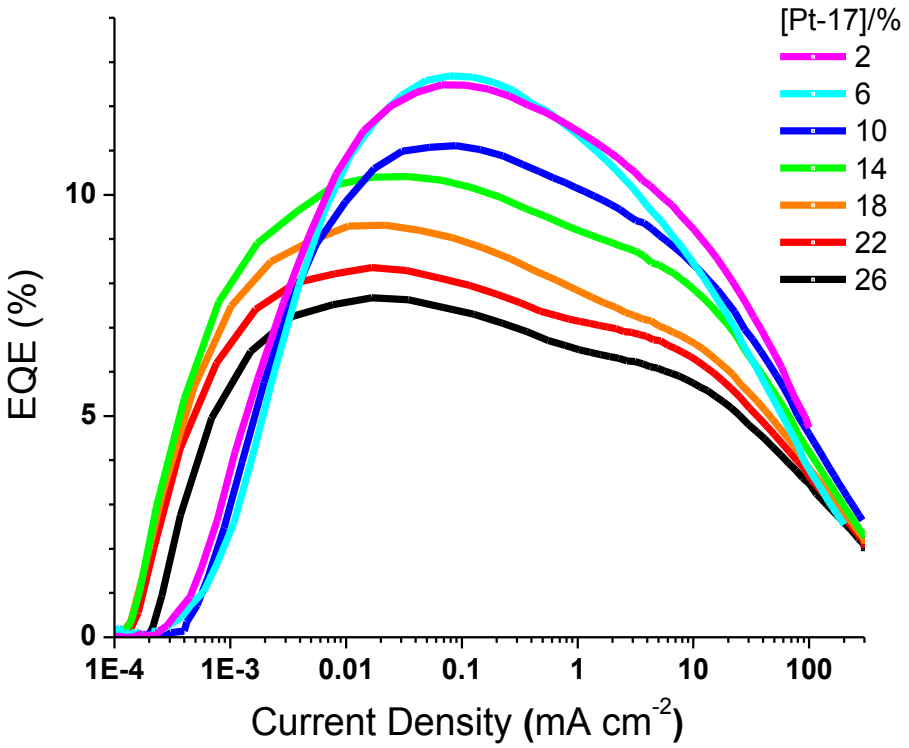

Figure 23. Forward viewing external quantum efficiency versus current density of the WOLEDs with structure (where x ranges from 2 to 26) is:

ITO/PEDOT/NPD(30nm)/TAPC(10nm)/x%Pt17:26mCPy(25nm)/PO15(20nm)/LiF/Al

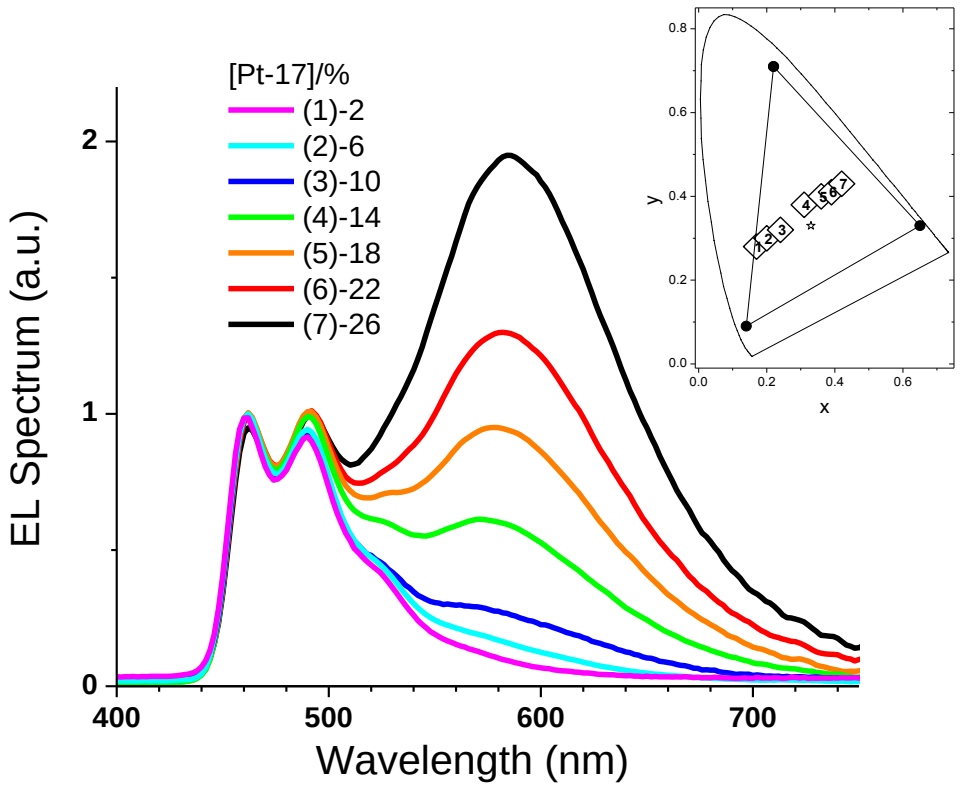

Figure 24. Normalized electroluminescent spectra and the CIE coordinates (inset) of the WOLEDs with structure (where x ranges from 2 to 26) is:

ITO/PEDOT/NPD(30nm)/TAPC(10nm)/x%Pt17:26mCPy(25nm)/PO15(20nm)/LiF/Al

Similar to the previously reported phosphorescent excimers, the gradual increase of dopant concentration raises the contribution from Pt-17 excimers, tuning the color of OLEDs from blue (exclusive monomer emission for 2% Pt-17 device) to broad and whiter emission. In contrast to both FPt and Pt-4 reported previously, all of Pt-17 devices have demonstrated reasonably high device efficiencies with peak values ranging from 8-13%, indicating that both monomer and excimer of Pt-17 are efficient phosphorescent emitters. This presents a great opportunity to fabricate an efficient WOLED in addition to having ideal color

combination of monomer and excimer emission. Figure 24 illustrates how a simple variation in the dopant concentration will allow to tuning the color of WOLEDs from cool white (CIEx=0.31, CIEy=0.38 for 14% Pt-17 device) to warm white (CIEx=0.42, CIEy=0.43 for 26% Pt-17 device) while maintaining a high CRI value (>75).

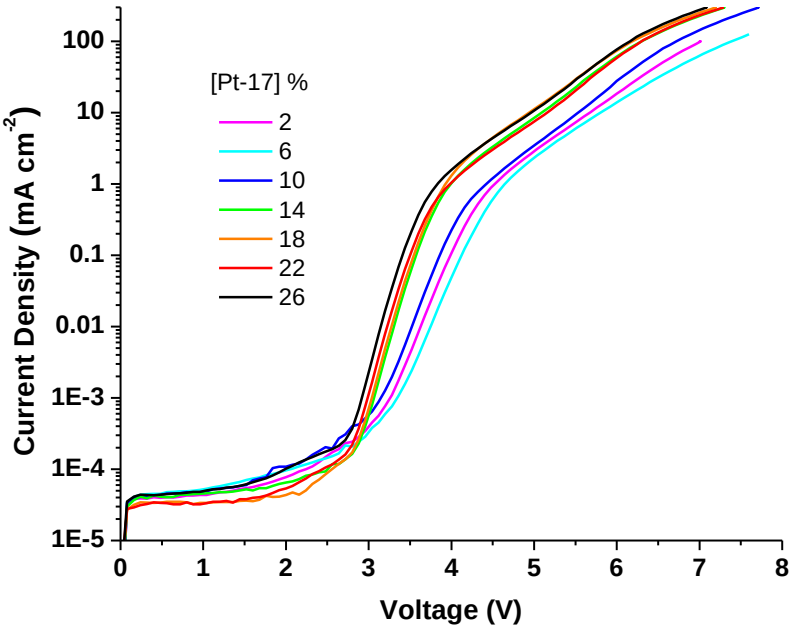

Figure 25. Plot of current density versus voltage for Pt 17 based WOLEDs using 26mCPy as a host material. The device structure (where x ranges from 2 to 26) is: ITO/PEDOT/NPD(30nm)/TAPC(10nm)/x%Pt17:26mCPy(25nm)/PO15(20nm)/LiF/Al

2.3.2 Improved Power Efficiency by Increasing Host Carrier Mobility

Increasing the dopant concentration slightly lowers the driving voltage; however, it also decreases the device efficiency. Charge carrier imbalance internal to the emissive layer could account for this behavior and might be resolved by employing a co-host system

with more balanced hole/electron transporting capabilities. A mixed layer of TAPC:PO15 is documented as one example, which can replace 26mCPy as host materials in a similar device setting.[85] The energy diagram for both device structures is shown in figure 25.

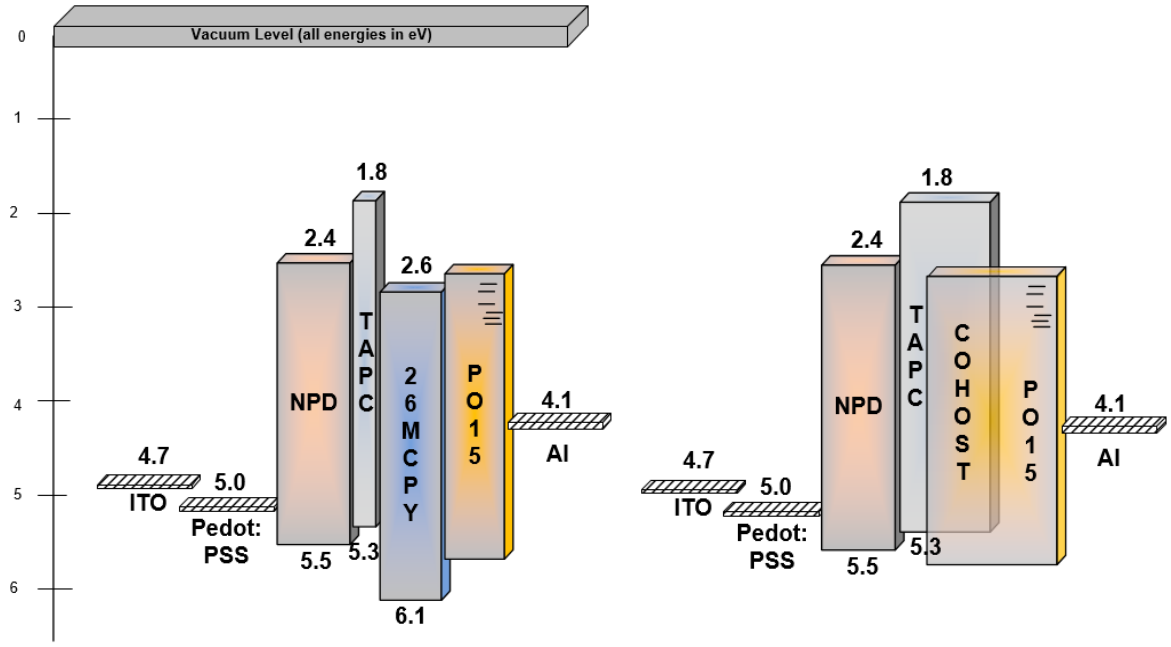

Figure 26. Energy diagrams for [a] device created with discrete codeposited emissive structure and [b] device fabricated with cohost structure

Electrical and optical performance characteristics for device structure NPD/TAPC/18% Pt-17:TAPC:PO15/PO15 are shown in Figure 27 and Figure 28. Forward viewing external quantum efficiency and power efficiency are plotted versus luminance in Figure 29. The thickness of electron transporting layer - PO15 was also optimized to 40nm in order to control the charge balance and maximize the device efficiencies (Figure 28). A maximum forward viewing EQE of η_{ext}=15.9% was achieved

at a current density of J=0.3 mA/cm^2, and only decreases slightly to η_{ext}=15.6% at a high forward viewing luminance of 500 cd/m^2. This device also gives a maximum forward power efficiency of η_p=37.8 lm/W and remains at a high η_p=25.2 lm/W at a practical luminance (500 cd/m^2). The electroluminescent spectrum of the device has a slight change due to the variation in a host system, yielding highly desirable CIE coordinates of (0.37, 0.40) and CRI of 80, which also demonstrates an independence of current density. The illumination quality of this WOLED is comparable or even superior to WOLEDs previously reported that require comparatively more complex structures.

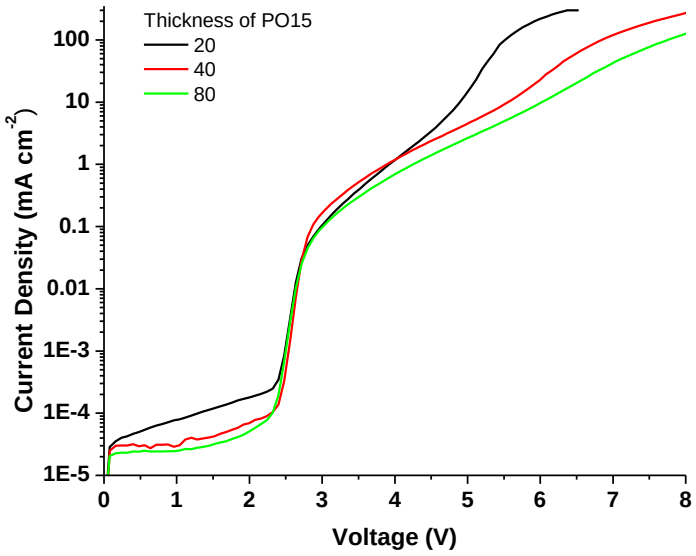

[a]

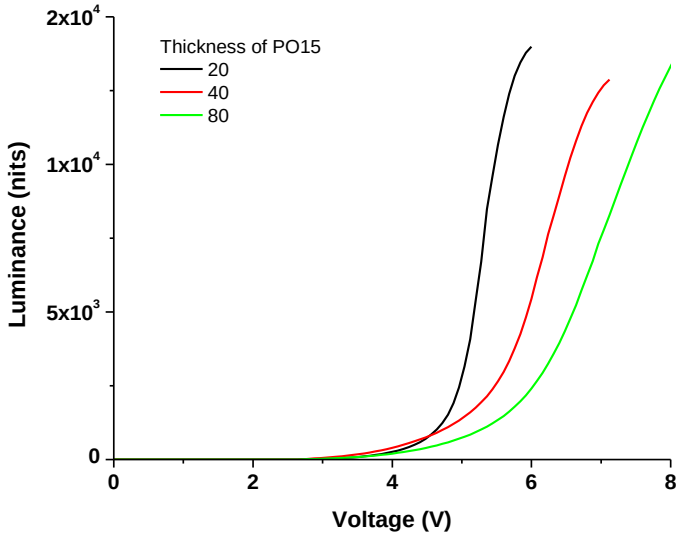

[b]

Figure 27. Performance characteristics of Pt 17 based WOLEDs using TAPC:PO15 as co-host materials. [a] current density versus voltage, [b] luminance versus voltage. The device structure is ITO/PEDOT/NPD(30nm)/TAPC(10nm)/18%Pt17:TAPC:PO15(25nm) /PO15(x nm)/LiF/Al. PO15 thickness ranges from 20nm to 80nm.

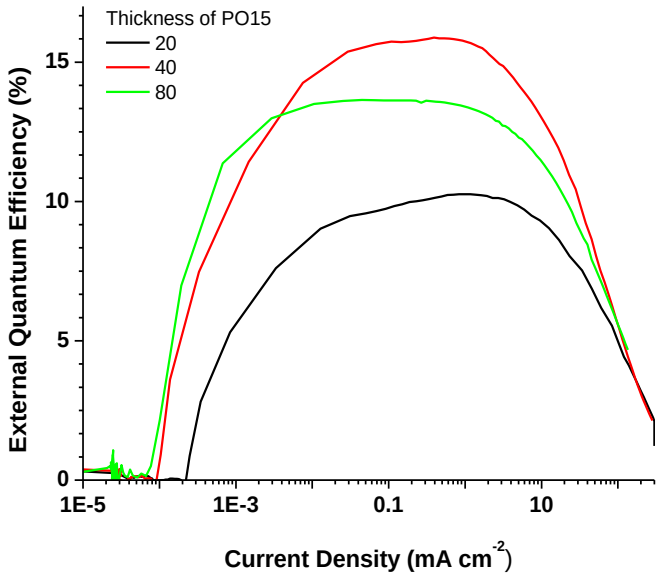

[a]

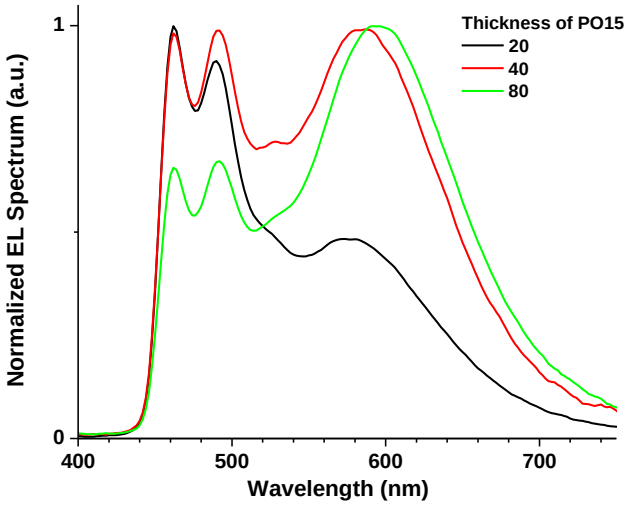

[b]

Figure 28. [a] Forward viewing external quantum efficiency versus current density, [b] electroluminescent spectra of WOLEDs. The device structure is ITO/PEDOT/NPD(30nm)/TAPC(10nm)/18%Pt17:TAPC:PO15(25nm) /PO15(x nm)/LiF/Al. PO15 thickness ranges from 20nm to 80nm.

The efficiency of the present co-host device can be further improved by using state-of-the-art charge-injection materials and charge-blockers, resulting in a higher forward viewing EQE (20% or higher) and a higher forward power efficiency (46 lm/W or higher).[86] The employment of higher-refractive-index substrate could extract more photons out of the device, leading to a two-fold increase in power efficiency according to demonstrated methods.[65,87] Thus, a single-doped WOLED with η_p of 100 lm/W can be realized by integrating Pt-17 monomer plus excimer emission with established outcoupling enhancement technologies.

[a]

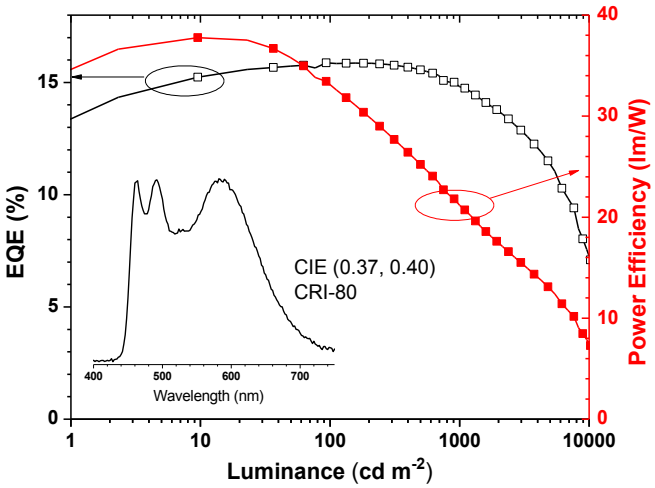

[b]

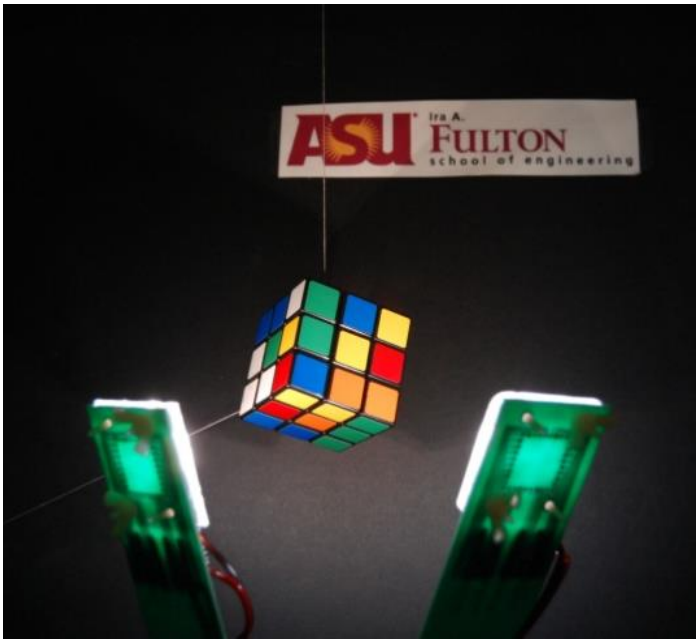

Figure 29. Performance characteristics of Pt 17 based WOLEDs using TAPC:PO15 as co-host materials. [a] Forward viewing external quantum efficiency (open squares) and power efficiency (filled squares) versus luminance of the WOLED. The device structure is ITO/PEDOT/NPD(30nm)/TAPC(10nm)/18%Pt-17:TAPC:PO15(25nm) /PO15(40nm)/LiF/Al. [b] An image of a magic cube illuminated by the WOLED demonstrating white color and high color rendering index value.

Moreover, Pt-17 is a fluorine-free blue phosphorescent emitter indicating that its design is aligned with molecules that have demonstrated stability for long operational lifetime.[88] Continued characterization and development should provide a viable route to develop stable and efficient phosphorescent excimers for lighting applications. Demonstration of single-doped WOLEDs with high efficiency and high illumination quality does present a unique opportunity to significantly simplify the device architecture and eliminate the problems of color aging and color instability for WOLEDs using multiple emitters. This will help to expedite the commercialization of WOLEDs for lighting applications.

2.4 Conclusion

To the Author's knowledge, the device based on Pt-17 demonstrated the world's first efficient single-doped WOLEDs with high quality of white light using a novel Pt complex. As illustrated in Figure 30, FPt and Pt-4 cannot produce a satisfactory white EL spectra due to ether inefficient monomer emission (FPt)[78] or unsuitable excimer emission color (Pt-4).[79]

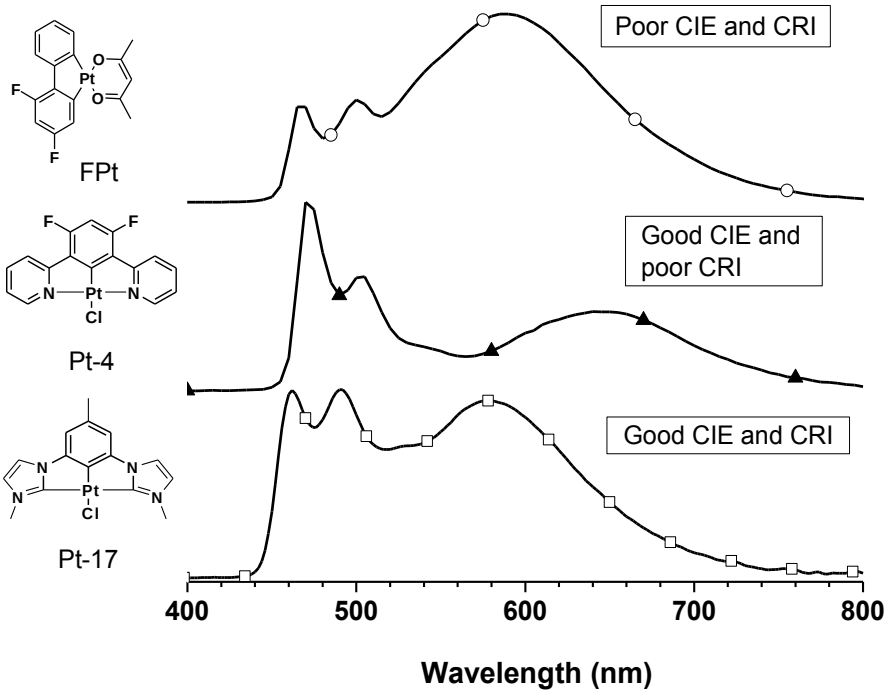

Figure 30. Electroluminescent spectra of OLEDs using FPt, Pt 4 and Pt 17, the chemical structures of which are shown in the left side of graph.

Compared with FPt, both Pt-17 and Pt-4 are more efficient blue phosphorescent emitters due to the specific choice of the metal complex system, i.e. Pt(N^C^N)Cl, where N^C^N are dipyridinyl bezene and their analogs.[89] Replacing pyridinyl group with methyl-imidazolyl group could potentially weaken the intermolecular interaction, resulting in a blue-shifted excimer emission for Pt-17. Thus, an ideal white EL spectrum can be accomplished by combining the appropriate proportion of monomer and excimer emission of Pt-17.

2.5 References

65. Reineke S, Lindner F, Schwartz G, et al. White organic light-emitting diodes with fluorescent tube efficiency. *Nature*. 2009;459(7244):234-238.

66. D'Andrade B.W. et al. Realizing white phosphorescent 100 lm/W OLED efficacy. *Proc SPIE*. 2008;70510Q:7051.

67. D'Andrade BW, Forrest SR. White organic light-emitting devices for solid-state lighting. *Adv Mater*. 2004;16(18):1585-1595.

68. Gather MC, Köhnen A, Meerholz K. White organic light-emitting diodes. *Adv Mater*. 2011;23(2):233-248.

69. D'Andrade B, Holmes R, Forrest S. Efficient organic electrophosphorescent white-light-emitting device with a triple doped emissive layer. *Adv Mater*. 2004;16(7):624-628.

70. Kido J, Kimura M, Nagai K. Multilayer white light-emitting organic electroluminescent device. *Science*. 1995;267(5202):1332.

71. Sun Y, Giebink NC, Kanno H, Ma B, Thompson ME, Forrest SR. Management of singlet and triplet excitons for efficient white organic light-emitting devices. *Nature*. 2006;440(7086):908-912.

72. Koehler A, Wilson JS, Friend RH. Fluorescence and phosphorescence in organic materials. *Advanced Engineering Materials*. 2002;4(7):453.

73. Eom SH, Zheng Y, Wrzesniewski E, et al. White phosphorescent organic light-emitting devices with dual triple-doped emissive layers. *Appl Phys Lett*. 2009;94:153303.

74. Wu FI, Yang XH, Neher D, Dodda R, Tseng YH, Shu CF. Efficient White-Electrophosphorescent devices based on a single polyfluorene copolymer. *Advanced Functional Materials*. 2007;17(7):1085-1092.

75. Huang J, Li G, Wu E, Xu Q, Yang Y. Achieving High-Efficiency polymer White-Light-Emitting devices. *Adv Mater*. 2006;18(1):114-117.

76. Schwartz G, Pfeiffer M, Reineke S, Walzer K, Leo K. Harvesting triplet excitons from fluorescent blue emitters in white organic Light-Emitting diodes. *Adv Mater*. 2007;19(21):3672-3676.

77. Adamovich V, Brooks J, Tamayo A, et al. High efficiency single dopant white electrophosphorescent light emitting diodes. *New journal of chemistry*. 2002;26(9):1171-1178.

78. Williams E, Haavisto K, Li J, Jabbour G. Excimer-based white phosphorescent organic light-emitting diodes with nearly 100% internal quantum efficiency. *Adv Mater*. 2007;19(2):197-202.

79. Yang X, Wang Z, Madakuni S, Li J, Jabbour GE. Efficient blue-and white-emitting electrophosphorescent devices based on platinum (II)[1, 3-difluoro-4, 6-di (2-pyridinyl) benzene] chloride. *Adv Mater*. 2008;20(12):2405-2409.

80. Feng J, Li F, Gao W, Liu S, Liu Y, Wang Y. White light emission from exciplex using tris-(8-hydroxyquinoline) aluminum as chromaticity-tuning layer. *Appl Phys Lett*. 2001;78:3947.

81. Hide F, Kozodoy P, DenBaars SP, Heeger AJ. White light from InGaN/conjugated polymer hybrid light-emitting diodes. *Appl Phys Lett*. 1997;70:2664.

82. Gather MC, Alle R, Becker H, Meerholz K. On the origin of the color shift in White-Emitting OLEDs. *Adv Mater*. 2007;19(24):4460-4465.

83. Rea MS, America Illuminating Engineering Society. *Lighting handbook.* Illuminating Engineering Society of North America USA; 1995.

84. Turro NJ. *Modern molecular photochemistry.* Univ Science Books; 1991.

85. Chopra N, Swensen JS, Polikarpov E, Cosimbescu L, So F, Padmaperuma AB. High efficiency and low roll-off blue phosphorescent organic light-emitting devices using mixed host architecture. *Appl Phys Lett*. 2010;97:033304.

86. Sasabe H, Takamatsu J, Motoyama T, et al. High-Efficiency blue and white organic Light-Emitting devices incorporating a blue iridium carbene complex. *Adv Mater*.

87. Sun Y, Forrest SR. Enhanced light out-coupling of organic light-emitting devices using embedded low-index grids. *Nature Photonics*. 2008;2(8):483-487.

88. Giebink N, D'Andrade B, Weaver M, et al. Intrinsic luminance loss in phosphorescent small-molecule organic light emitting devices due to bimolecular annihilation reactions. *J Appl Phys*. 2008;103:044509.

89. Wang Z, Turner E, Mahoney V, Madakuni S, Groy T, Li J. Facile synthesis and characterization of phosphorescent pt (N∧ C∧ N) X complexes. *Inorg Chem*. 2010.

CHAPTER 3

SQUARE PLANAR CYCLOMETALATED PLATINUM COMPLEXES FOR STABLE DEEP BLUE EMISSION

3.1 Introduction

The success of OLED technology for full color displays will require emitting materials that can produce high energy light to fulfill the blue component, while maintaining good efficiency and stability. The current NTSC standard CIE coordinates for blue are x=0.14, y=0.09. The increased band gap necessary for high energy emission can be accomplished by reduction of the HOMO energy or increase of the LUMO energy. A number of studies have applied halogens to delocalize electron density with respect to the metal core atom.[39,90-93,69] The delocalization increases the LUMO level because of the halogen atom's ability to shift molecular triplet energies. Unfortunately, device structures that have employed this blue shifting mechanism have proven to show significantly degraded luminance performance over timescales that would interfere with application to displays. The potentially short operational lifetimes are attributed to the electrochemical reactivity of the halogen atoms.[94] Irreversible oxidation or reduction behavior leading to device degradation cannot be tolerated in commercial application; therefore, the addition of fluorine or chlorine to ligand structures might not be an ideal blue shifting mechanism.

Another method to increase to the energy gap of phosphorescent emitters could be to lower the HOMO energy level. Iridium based emitters have demonstrated that substitution of a five-member ring in place of a larger six-member ring can blue shift emitting molecules. Specifically, substitution of methyl-benzimidazolyl (five-member group) in place of pyridine has been reported to shift triplet energy. PL peak wavelengths

below 400 nm have been observed for blue phosphors such as fac- and mer-Ir(pmb), FIrpic, and Fir6.[91-93,95] These molecules have been added to suitable high energy band gap host to demonstrate external quantum efficiencies approaching 6% with the first emission peak below 400 nm without the presence of halogen atoms. Substitution of smaller five-member methyl-benzimidazolyl groups has been demonstrated to shift the emission of phosphorescent emitters towards the blue regions of interest without specifically impacting operational lifetime by addition of Halogens. Here, a novel halogen-free emitter will be used to fabricate devices to demonstrate stable and efficient blue organic light emitting devices.

3.2 Experimental

Devices employing Pt-002 and fac-Ir(ppy)3 as emitters were fabricated on glass substrates pre-coated with a patterned transparent indium tin oxide (ITO) anode using a device architecture of ITO/PEDOT:PSS/20nm TAPC/25nm 8% emitter:26mCPy/10nm PO15/30nm BmPyPB/LiF/Al, where PEDOT:PSS = poly(3,4-ethylenedioxythiophene) poly- (styrenesulfonate), TAPC = 1,1-bis[4-[N,N′-di(p-tolyl)amino]- phenyl] cyclohexane, 26mCPy = 2,6-bis(N-carbazolyl)pyridine, PO15 = 2,8-bis(diphenylphosphoryl)-dibenzothiophene, and BmPyPB57 = 1, 3-bis[3, 5-di(pyridin-3-yl)phenyl]benzene). Prior to organic depositions, the ITO substrates were cleaned by subsequent sonication in water, acetone, and isopropanol followed by a 15 min UV−ozone treatment. PEDOT:PSS was filtered through a 0.2 μm filter and spin-coated on the prepared substrates, giving a 40- nm-thick film. All small molecular organic materials were deposited by thermal evaporation at rates of 1 +/- 0.5 Å/s with a working pressure of less than 10−7 Torr. A thin 1nm LiF layer was deposited at a rate of < 0.2 Å/s and aluminum cathodes were deposited at 1−2 Å/s

through a shadow mask without breaking the vacuum. Individual devices that have areas of 0.04 cm^2 . I−V−L characteristics were taken with a Keithley 2400 Source-Meter and a Newport 818 Si photodiode inside a nitrogen-filled glovebox. Electroluminescence (EL) spectra were taken using the Jobin Yvon Fluorolog spectrofluorometer. Agreement between luminance, optical power, and EL spectra was verified with a calibrated Photo Research PR-670 spectroradiometer with all devices assumed to be Lambertian emitters.

3.3 Results

3.3.1 Stability of Fluorine-Free Blue Phosphorescent Emitters

Figure 31 shows the accelerated aging of resulting stability of the blue emitter. A number of procedures to project OLED lifetime by utilizing accelerated aging methods across a statistically relevant number of devices have been documented. This data can be used to tune charge balance, select stable supporting device layers, and achieve device lifetime that approaches the degradation rate fundamental to the stability of the emitter. In the absence of these resources and quantity of units, a direct comparison using identical device structures and materials will be employed to compare halogen-free Pt-002 to a known stable emitter Ir(ppy)3. This will provide a relative quantification to measure the stability of an unknown emitter when the resources for statistical descriptions and characterization of accelerated aging mechanisms are not available.

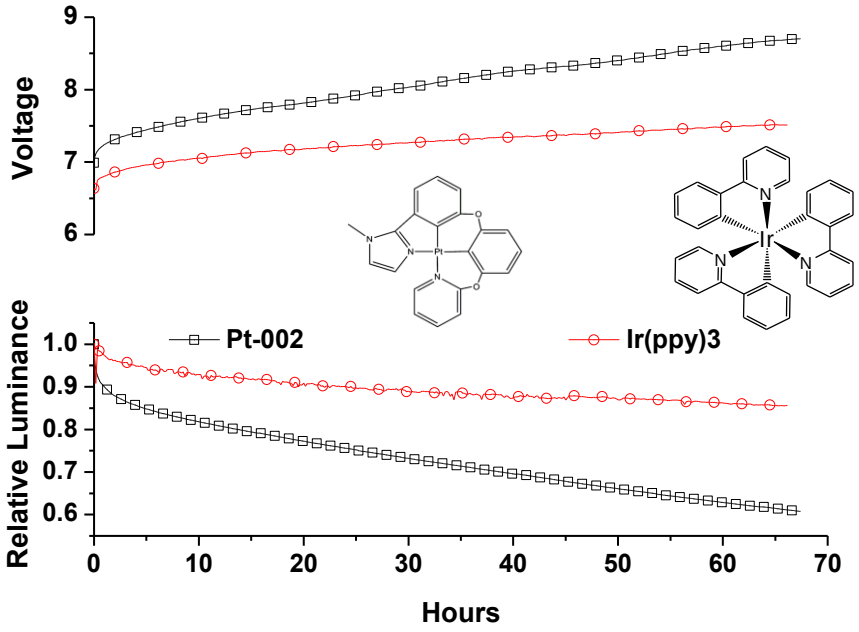

Figure 31. Plots of (a) drive voltage vs. time and (b) initial luminance vs. time for Ir(ppy)3 (red) and Pt-002 (black) devices operating at constant of 10mA cm-2 inside of glove box (oxygen<0.1ppm, water<0.1ppm). The device structure is: ITO/NPD 40nm/CBP:Dopant/BAlq 10nm/Alq_3 30nm/LiF 1nm/Al

Some theoretical and empirical evidence supporting stability makes it interesting to consider adopting the substitution of five member groups to increase triplet energies in a whole range of novel Pt based emitters. The intensely studied Cyclometalated Ir complexes are typically bulky due to the 3-dimensional geometry resulting from octahedral coordination. Also, Ir molecular design is somewhat limited by the constraints applied by the octahedral structure requiring three paired coordinating ligands. In contrast, Pt complexes are typically more planar in nature due to their four independent coordination points. The square structure is beneficial to allow more latitude in molecular design;

however, it represents a hurdle to achieve exclusive high energy emission without a significant excimer component. Morphology studies have revealed that molecules with high aspect ratios tend to deposit with preferred orientation parallel to the substrate surface.[96,97] This geometry tends to align multiple z-axis as well as to maximize Pi-Pi interactions from electrons localized above and below aromatic rings. The result is an increased propensity for excimer emission in platinum as compared to octahedral iridium complexes that do not have such pronounced intermolecular alignment tendencies. Figure 32 demonstrates that Pt-002 is capable of exclusive high energy emission without a significant excimer component.

3.3.2 High Energy Organic Light Emitters for Blue Display Component

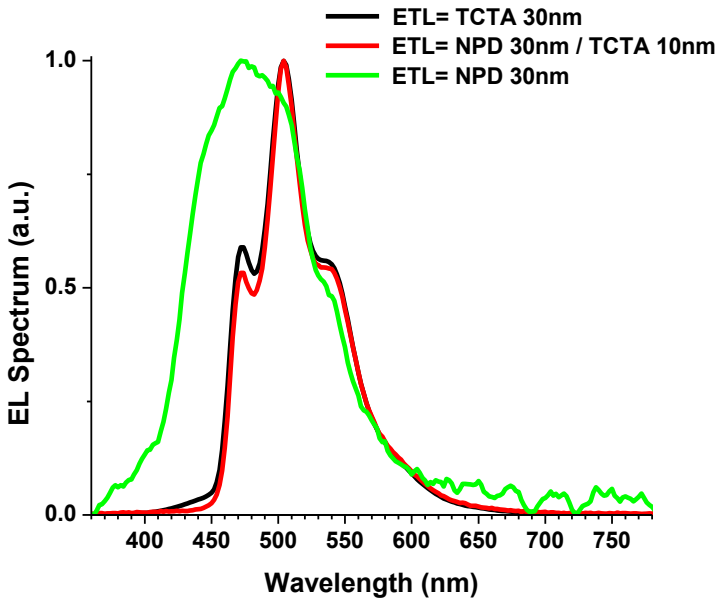

Figure 32. EL spectrum for device: (a) ITO/Pedot:PSS 45nm/TCTA 30nm/26mCPy:Pt-002 (2wt%)/BCP 30nm/LiF 1nm/Al; (b) ITO/Pedot:PSS 45nm/NPD 30nm/TCTA 10nm/26mCPy:Pt-002 (2wt%)/BCP 30nm/LiF 1nm/Al; (c) ITO/NPD 40nm/CBP:Pt-002 (2wt%)/BAlq 10nm/Alq3 30nm/LiF 1nm/Al

Energy minimization routines suggest a structure for Pt-002 that is deviated from planar as shown in Figure 33. It is reasonable to associate the deviation with planarity with a reduced propensity for excimer emission. Z-axis alignment of the metal atom as well as pi-pi overlap between aromatic rings of adjacent molecules are less geometrically favorable for a molecule that deviates from the most ideal stacking in a planar structure. Devices fabricated with as high as 15 mass percent Pt-002 in the EML still do not show significant excimer emission.

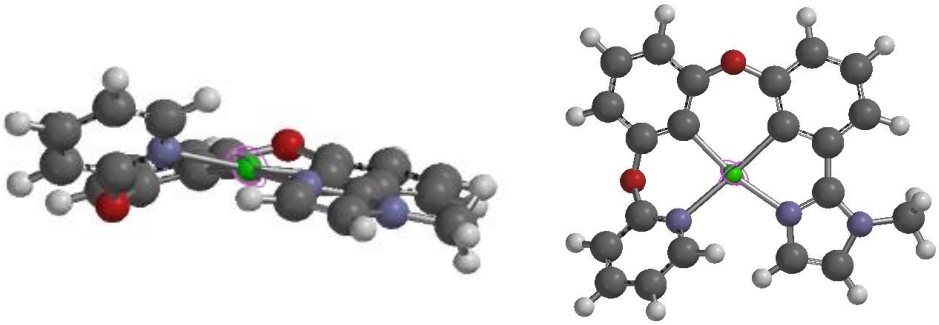

Figure 33. Side view (left) and top view (right) of molecular structure of Pt-002. The geometry is approximated by perturbing bond orientations to minimize configurational energy.

Many iterations of device fabrication and performance optimization lead to a device structure based on a codeposited EML comprised of only 2% Pt-002. TCTA provides an effective blocking layer to prevent charge or exciton transfer into the NPD as is demonstrated by the exclusive emission shown in Figure 32. Devices that do not employ the TCTA blocking layer show higher energy EL emission corresponding to the larger HOMO-LUMO gap for the hole transporting layer, NPD. Thus, TCTA prevents inefficient fluorescence in NPD and enables increased Pt-002 efficiency for application to display

technology. Device performance as reported by [a] current density vs voltage and [b] external quantum efficiency (EQE) and luminance vs current density is shown in Figure 34.

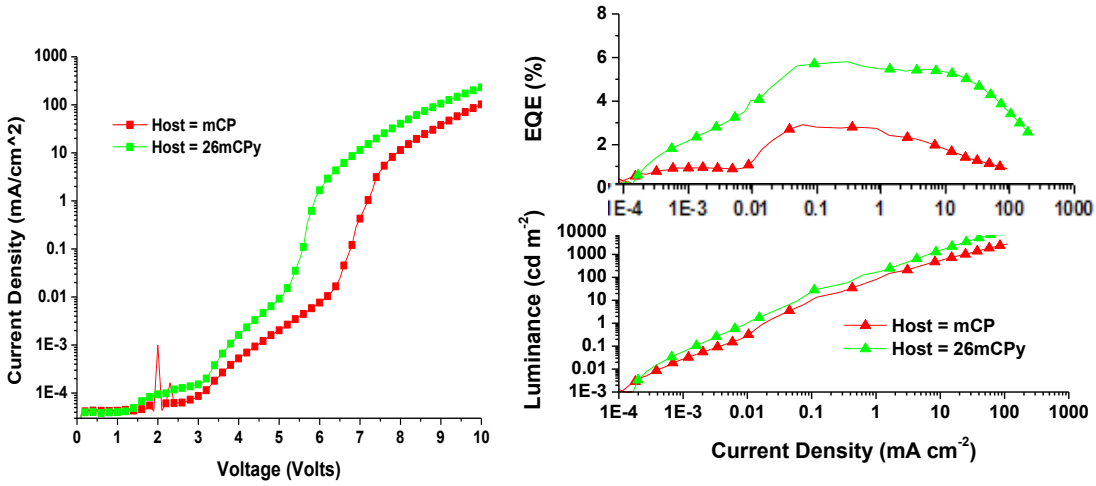

Figure 34. Plots of (a) current density vs. voltage (b) EQE vs current density and (c) luminance vs current density for devices: ITO/Pedot:PSS 45nm/NPD 30nm/TCTA 10nm/Host:Pt-002 (2wt%)/BCP 30nm/LiF 1nm/Al. The hosts are mCP (red) and 26mCPy (green) accordingly

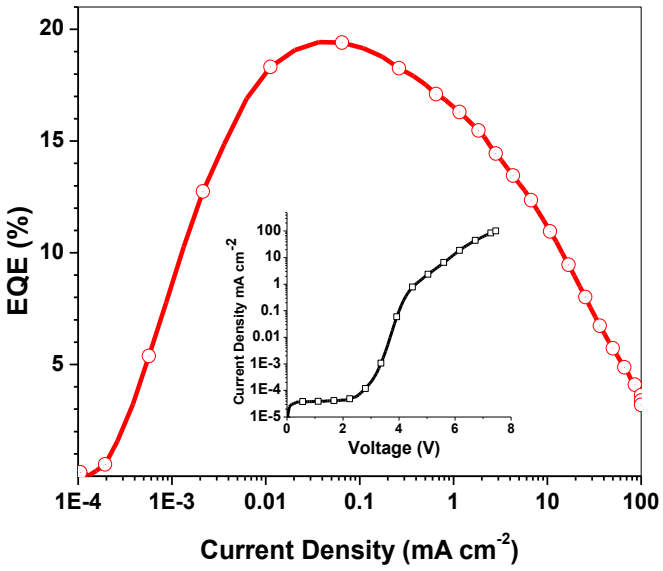

Figure 35. Plot of EQE vs. current density for device ITO/Pedot:PSS 45nm/NPD 30nm/TAPC 10nm/26mCPy:Pt-002 (2wt%)/PO15 40nm/LiF 1nm/Al. Inset shows the plot of current density vs voltage for the device.

3.4 Conclusion

In summary, Pt-002 shows promise for stability in preliminary lifetime testing. In addition to reasonable stability and efficiency, Pt-002 does not indicate a particular affinity for the formation of aggregates and excimer emission. This is ideal for display applications where a "pure deep blue" emitter could benefit from an emissive architecture that maximized efficiency without concern for limiting unwanted lower energy emission. Additional development of molecules like Pt-002 to improve CIE coordinates and EL efficiency could certainly hope to achieve a stable, efficient, and deep blue emitter suitable for new display technology.

3.5 References

39. Yeh SJ, Wu MF, Chen CT, et al. New dopant and host materials for blue-light-emitting phosphorescent organic electroluminescent devices. *Adv Mater*. 2005;17(3):285-289.

69. D'Andrade B, Holmes R, Forrest S. Efficient organic electrophosphorescent white-light-emitting device with a triple doped emissive layer. *Adv Mater*. 2004;16(7):624-628.

90. Li J, Djurovich PI, Alleyne BD, et al. Synthetic control of excited-state properties in cyclometalated ir (III) complexes using ancillary ligands. *Inorg Chem*. 2005;44(6):1713-1727.

91. Tokito S, Iijima T, Suzuri Y, Kita H, Tsuzuki T, Sato F. Confinement of triplet energy on phosphorescent molecules for highly-efficient organic blue-light-emitting devices. *Appl Phys Lett*. 2003;83:569.

92. Lo SC, Richards G, Markham J, et al. A light-blue phosphorescent dendrimer for efficient solution-processed light-emitting diodes. *Advanced Functional Materials*. 2005;15(9):1451-1458.

93. Holmes R, Forrest S, Tung YJ, et al. Blue organic electrophosphorescence using exothermic host–guest energy transfer. *Appl Phys Lett*. 2003;82:2422.

94. Holmes R, Forrest S, Sajoto T, et al. Saturated deep blue organic electrophosphorescence using a fluorine-free emitter. *Appl Phys Lett*. 2005;87(24):243507-243507.

95. Sajoto T, Djurovich PI, Tamayo A, et al. Blue and near-UV phosphorescence from iridium complexes with cyclometalated pyrazolyl or N-heterocyclic carbene ligands. *Inorg Chem*. 2005;44(22):7992-8003.

96. Yokoyama D, Sakaguchi A, Suzuki M, Adachi C. Horizontal molecular orientation in vacuum-deposited organic amorphous films of hole and electron transport materials. *Appl Phys Lett*. 2008;93:173302.

97. Yokoyama D, Sakaguchi A, Suzuki M, Adachi C. Horizontal orientation of linear-shaped organic molecules having bulky substituents in neat and doped vacuum-deposited amorphous films. *Organic Electronics*. 2009;10(1):127-137.

CHAPTER 4

THICKNESS DEPENDENT PROPERTIES OF SMALL MOLECULE ORGANIC ELECTRONIC THIN FILMS.

4.1 Introduction

The unique amorphous nature of organic electronics can be leveraged to enable fabrication without the need for high vacuum, ultra clean, and high temperature environments. Solution based processing, roll-to-roll processing, organic vapor phase deposition (OVPD), and even inkjet printing methods using non-rigid substrates have all been proposed as potentially feasible low-cost manufacturing methods for organic electronics.[9] Also, the long term operational stability of flexible electronics requires mechanical robustness of the active materials under operationally induced strain. A direct fabrication of electronics on plastic substrates using inorganic active materials usually leads to a limited flexibility where bending can create catastrophic device failure.[98] Compared with their inorganic counterpart, it is intuitive that polymers and organic materials are more compliant and intrinsically compatible with flexible substrates; however, little is known about their specific mechanical properties.[99] The lack of knowledge regarding mechanical properties for organic semiconductor materials results from their high cost and limited quantities that makes traditional tensile testing infeasible. Other common methods like nanoindentation have been attempted to measure the mechanical properties of Alq_3, but the results showed a strong dependence on the substrate choice.[100,101] This dependence is likely from convolution of the measurement with the underlying substrate that is commonly observed when using nanoindentation on thin compliant films.[102] Thus, a better mechanism to measure and a better understanding of the

mechanical properties of organic thin films at the confined length scale can be critical to characterize mechanical strain within organic flexible electronics and potentially enable low cost manufacturing without the need for rigid substrates. Here the mechanical properties of selected organic electronic materials will be investigated using a wrinkling based metrology.

4.2 Experimental

Alq_3, CBP, TPD, and NPD were purchased from Sigma Aldrich. These materials were then purified by sublimation in a four-zone thermal gradient furnace under a pressure of 10^{-6} Torr. The structure for each of these molecules is shown in Figure 36**.** For an elastic substrate, Dow Corning Sylgard 184 polydimethylsiloxane (PDMS) was cast at either 10:1 or 20:1 base:cure agent onto float glass and allowed to degass and gel at ambient for 3 prior to curing at 100C for 2 h. After cooling to ambient temperature, the PDMS sheet was cut into approximately 75 mm × 25 mm × 1.5 mm slabs, which function as the elastic substrates for the films to be evaluated.

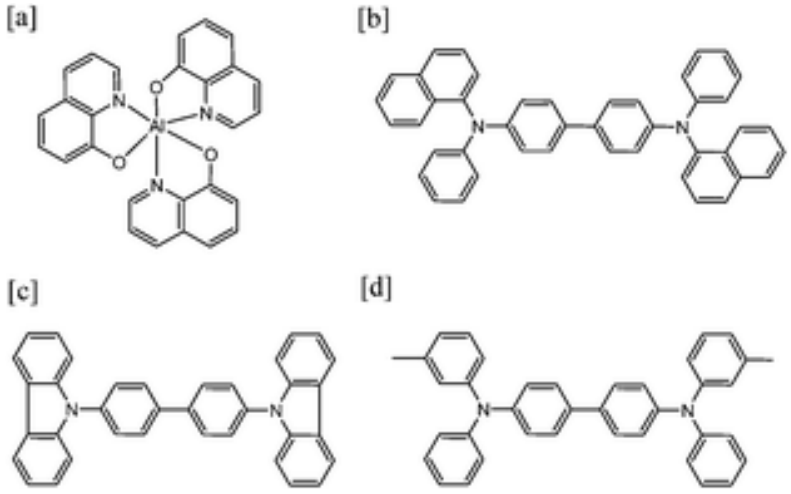

Figure 36. The chemical structures for [a] Alq3 [b] NPD [c] CBP and [d] TPD

The modulus of the PDMS from each batch was determined using a Texture Technologies model TA.XT Plus Texture Analyzer (TA). The optical constants for PDMS were determined using a Cauchy model to fit to data from J. A. Woollam Co. Variable Angle Spectroscopic Ellipsometer (VASE) over a wavelength range from 250nm to 1700nm measured at three incident angles (67, 70, 73). Variation in the formulation ratio or cure temperature can impact the mechanical properties of the PDMS, but characterization of each batch was performed to mitigate variation in the calculated moduli for the organic glass films. The PDMS slabs where then pre-strained 3% in preparation for wrinkling.[56] Polystyrene (PS, M_n = 9.4 kg mol^{-1}, Polymer Laboratories) or addition polynorbornene (Add PENb)[103] films were utilized as barrier coatings to inhibit the diffusion of the small molecules into PDMS.[104] These polymers were spin cast onto cleaned silicon wafers, annealed under nitrogen at T = T_g + 20 °C and transferred to the pre-strained PDMS.[64] The thickness of the PS or Add PENb film was determined using VASE over a wavelength range from 250nm to 1700nm measured at three incident angles (65°, 70°, and 75°) both on the silicon wafer and once transferred onto the PDMS. The thickness of these barrier films ranged from 24nm–26nm.

Alq_3, NPD, CBP, and TPD were deposited from a resistively heated tantalum boat in a vacuum deposition system from Trovato Mfg. with pressure at or below 10^{-7} Torr. A 16 mm diameter shadow mask was used to define the deposition area. Deposition rate was controlled between 1–1.5 Å/s onto the pre-strained polymer-PDMS using crystal growth monitors. Growth rate calibrations used to report absolute thin film thicknesses ranging from 8nm to 100nm on elastic and silicon substrates were accomplished through agreement between three sources of measurement. First, direct measurements from the film(s) on

Silicon and PDMS were collected before small molecule deposition using VASE. Second, identical depositions for thicknesses representing the full range of experimental data were also performed with silicon substrates loaded in place of the PDMS, and their thickness was measured by both VASE and a KLA-Tencore P-6 profilometer. Profile scans were collected across shadow masked edges as well as ledges exposed by post-deposition removal of Kapton tape to enable sampling at the center of the film. The third measurement was taken after small molecule depositions were complete but prior to releasing the strained substrates. The thicknesses of the barrier and organic glass thin films were again modeled on the PDMS using VASE. All methods to characterize variation in deposition rate and associated error in film thickness were shown in agreement within the bounds of reported experimental error.

Surface wrinkling was induced by releasing the pre-strain at approximately 0.1 mm s^{-1} under ambient conditions (T = 21 °C +/- +/-2 °C). The wavelength of the wrinkled surface was determined using Park XE-150 atomic force microscopy (AFM) in intermittent contact mode using a constant scan size of 10 μm by 10 μm, and Mititoyo Ultraplan FS-110 optical microscopy (OM). Images were analyzed using 1D Fast Fourier Transform (FFT).

4.3 Results

4.3.1 Diffusion of Small Molecule Organic Electronic Films into PDMS

It was observed that Alq_3 films deposited onto PDMS would change color as compared to the as-deposited film over the course of several hours. To quantify the changes in the films, the ellipsometric angles for the film are obtained at an incident angle of 55 degrees for about 3 hours. Figure 37 shows that Alq_3 thickness on a PDMS substrate

as determined from VASE shows a significant reduction in the film thickness as the film ages at ambient conditions. Alq_3 is known to be marginally unstable in air[105]; however, the change in thickness is too great to be attributed to degradation. PDMS formulated with 20 : 1 base to curing agent forms a network with a modulus of 0.7 MPa. This low modulus resulting from a loose polymer network enables Alq_3 to diffuse into the PDMS substrate. After 150 min, the thickness of the Alq_3 layer decreased by about 40%. If the base to curing agent ratio is doubled to 10 : 1, the crosslink density of the PDMS increases leading to a much higher modulus of 2 MPa. Alq_3 deposited onto the higher modulus 10 : 1 PDMS exhibited a decrease in film thickness of 23% after 150 min consistent with relatively slower diffusion into a more highly linked polymer network. Characterization of wrinkle wavelength from Alq3 on PDMS for SIEBIMM was not successful. In addition to poorly defined structures from the diffused samples, the effective film thickness and modulus would all be convoluted by the absence of a crisp interface. The low glass transition temperature of PDMS (Tg ~ 125 C) and large free volume of PDMS[106] appear to enable diffusion of Alq_3 and potentially other small molecules into the PDMS network; this may lead to a poorly defined system for wrinkling analysis[107]. Direct vapor deposition of small molecules on PDMS is likely problematic for determining their elastic moduli using wrinkling.

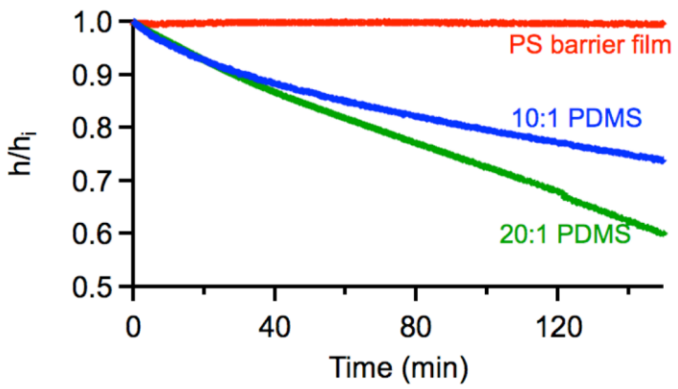

Figure 37. Measured Alq_3 film thickness as a function of time elapsed after deposition and sample loading and transfer.

4.3.2 Determination of the Elastic Modulus Using a Diffusion Barrier

It is possible to prevent diffusion of Alq_3 into the PDMS substrate by addition of a barrier film; in this case, a PS film appears to prevent diffusion of the Alq_3 into the PDMS substrate, as shown in Figure 37. The thickness of Alq_3 film remains constant for relevant time scales considered suggesting that PS has sufficiently reduced free volume to reduce diffusion rates and eliminate the impact of diffusion on SIEBIMM measurements. Diffusion of small molecule films also has implications in the fabrication of organic devices on flexible plastic substrates as charge transport is defined by the interfacial morphology. Diffusion of a small molecule film could play a significant role in the short or long term performance of optoelectronics. Figure 38 shows well defined wrinkles resulting from the deposition of a composite Alq_3/PS film stack. The addition of a PS barrier results in discrete interfaces at both of the PDMS/PS and the PS/Alq_3 film stack and alleviates the problem of diffusion of small molecule glassy films into a PDMS substrate. The wrinkles obtained were sufficient to determine a characteristic wavelength for

SIEBIMM, but the added PS layer must be included in the analysis of the wrinkling to deconvolute the elastic modulus of Alq_3.

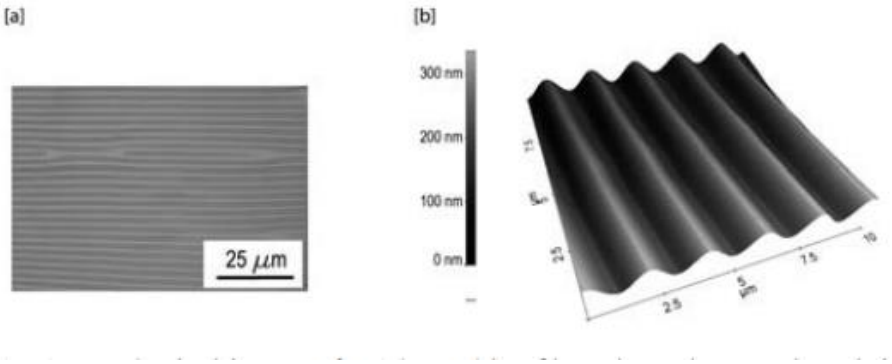

Figure 38. [a] Image of wrinkled 36nm thick Alq_3 film that corresponds to a wavelength 3.5 +/- 0.13um captured with an optical microscope [b] Image of a wrinkled 8nm thick Alq_3 film that corresponds to a wavelength 2.1um +/- 0.15um thick captured with an atomic force microscope.

The wrinkles in Figure 38 are formed by compression of the Alq_3/PS composite film on a pre-strained PDMS substrate. The elastic properties of the composite system of PS and Alq3 along with their thicknesses and elastic modulus of the PDMS are correlated to the wavelength of the wrinkle pattern. Thus, an effective plane-strain modulus of the Alq_3/PS composite film ($\bar{E}_{eff}$) can be determined from the wavelength, λ, as previously described in section 1.6.2 by equation 11.

$$\bar{E}_{eff} = 3\bar{E}_s \left(\frac{\lambda}{2\pi h_{total}}\right)^3 \qquad (11)$$

Where h_{total} is the total thickness of the Alq_3/PS composite film, and $\bar{E}_s$ is the plane-strain elastic modulus of the PDMS substrate. The sum of the flexural rigidity from both

contributing layers of PS and Alq_3 can be separated and solved iteratively to determine the elastic modulus for only the Alq_3 component. Modifying equations 8 through 11 (previously discussed in section 1.6.2) to describe the Alq_3/PS materials system results in equation 12-14 that are used to determine the mechanical properties of deposited small molecule Alq_3 thin films.

$$\bar{E}_{Alq_3} = \frac{\frac{\bar{E}_{eff}}{4} - \bar{E}_{PS}\left[\left(\phi_{PS}-\frac{\kappa}{2}\right)^3+\left(\frac{\kappa}{2}\right)^3\right]}{\left(1-\frac{\kappa}{2}\right)^3-\left(\phi_{PS}-\frac{\kappa}{2}\right)^3} \tag{12}$$

$$\kappa = \frac{1+\phi_{PS}^2\left(\frac{\bar{E}_{PS}}{\bar{E}_{Alq_3}}-1\right)}{1+\phi_{PS}\left(\frac{\bar{E}_{PS}}{\bar{E}_{Alq_3}}-1\right)} \tag{13}$$

$$\phi_{PS} = \frac{h_{PS}}{h_{total}} = \frac{h_{PS}}{h_{Alq_3}+h_{PS}} \tag{14}$$

The Alq_3 and PS film thicknesses and the moduli of the PS film and the PDMS need to be determined in order to calculate the unknown modulus of the Alq_3 film. A constant PS film thickness of 21nm +/- 2nm with a modulus of 3.61 GPa +/- 0.26 GPa was determined. The PDMS substrate had modulus vary between 0.6 MPa and 0.8 MPa as a result of batch-to-batch variation. Equation 12 can be iteratively solved to determine the modulus of the Alq_3 film. The Young's elastic modulus the Alq_3 films can be determined from the plane-strain relation shown in equation 15.

$$E_{Alq_3} = \bar{E}_{Alq_3}(1-\nu_{Alq_3}^2) \tag{15}$$

Poisson's ratio of the Alq_3 and other small molecule organic thin films is determined to be similar to most organic glassy materials where $\nu = 0.33$. This agrees with a recent study where the Poisson's ratio of vapor deposited molecular glass of indomethacin was

measured by BLS and determined to be 0.36.[108,109] The Poisson's ratio for small molecule glasses used in organic optoelectronics considered here will be approximated as $\nu = 0.33$. Based upon this assumption, the Young's modulus of the 36 nm thick Alq_3 film shown in Figure 38 is 0.94 GPa +/- 0.18 GPa. This is significantly less than the modulus for Alq_3 ~ 100 GPa determined using 100nm thick films on silicon wafers with Nano indentation (NI).[100] The modulus obtained from NI is extremely large for an organic molecule and much more likely to be related to the hard Silicon substrate with elastic modulus around 130 GPa. If a substantial structure difference resulting in orders of magnitude difference mechanical properties exists, one would expect optical and/or surface morphology to vary between the samples. However, neither of optical constants for Alq_3 as determined by VASE or surface morphology as determined by AFM between films deposited on PS/PDMS or silicon showed any meaningful differences. So, it appears that the substrate acts to convolute the measurement rather than modify properties of the thin film. The elastic modulus of the Alq_3 film reported by SIEBIMM appears to be reasonable based upon comparison to other organic molecular glasses. Other studies have concluded that thin polymer films show a decrease in elastic modulus when thickness is less than about 50nm.[110,111] It might then be possible to expect an even lower modulus for the 8nm thick Alq_3 film if organic small molecules and polymers behave similarly at the nanoscale. However, the Young's modulus of the 8nm thick Alq_3 film is calculated to be 1.66 GPa +/- 0.21 GPa. This indicates that the modulus of Alq_3 increases at confined length scale. Figure 39 shows the plane-strain modulus dependence on film thickness. For films thicker than 20nm, the modulus is independent of film thickness at approximately 1.0 GPa. This behavior is similar to pentacene, which has been shown to have a modulus independent of

films greater than or equal to 25nm.[112] However, as the film thickness of Alq_3 is reduced from 20nm to 10nm, the plane-strain modulus appears to increase significantly. Decreasing the thickness from 20nm to10nm results in an increase in the plane strain modulus from 1.01 GPa +/- 0.27 GPa to 1.69 +/- 0.32 GPa. A nearly 70% increase in the elastic properties of Alq_3 is observed when the structure is confined to 10nm. This large increase in elastic modulus contradicts typical behavior for glassy polymers where 10nm films can exhibit a modulus that is on order 10% of the bulk.

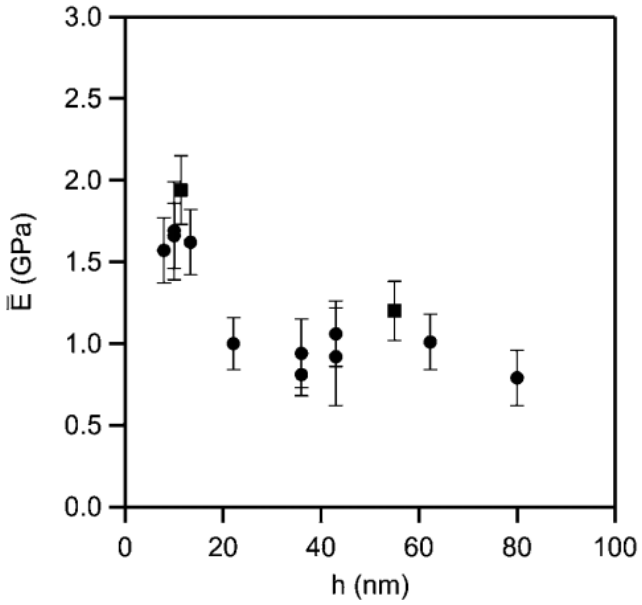

Figure 39. Thickness dependence of Alq3 determined using 2 plate buckling method with PS diffusion barrier. Circles indicate PS chains (9.4 kg/mol) while squares indicate (492 kg/mol)

In the same way that diffusion of a small molecule glassy film into the underlying substrate has convoluted Alq_3 on PDMS measurements, it is possible to suspect that

diffusion of Alq_3 into PS could be responsible for perceived increase in modulus especially at confined length scales. To investigate this possibility, two different molecular mass PS were applied as diffusion barriers for Alq_3 wrinkling experiments. If diffusion was a contributing factor, a difference between barrier films constructed from relatively short PS chains (9.4 kg/mol) and highly entangled PS chains (492 kg/mol) might be observed.[113] Figure 39 shows no such divergence in the calculated moduli as a result of the different barrier films for Alq_3. The behavior supports that interdiffusion might not be responsible for the observed increased moduli of Alq_3 for ultrathin films. In contrast to softened thin film polymers, some reports have shown that materials systems like metallic glasses can experience increased yield strength and ductility when confined to the nanoscale.[114] This shows that both enhanced and degraded mechanical properties upon confinement to the nanoscale could be expected. It is plausible that changes in the structure of Alq_3 near interfaces could be responsible for the deviations in mechanical properties, especially considering the very small length scales at which changes in the elastic moduli are observed. For example, it has been reported that changing the deposition conditions for indomethacin and trisnaphthylbenzene films can increase Young's modulus by 19% as a result of improved packing of the glass.[115] Pentacene films have also been reported to demonstrate a change in morphology as a function of thickness from a monolayer to bulk dimensions.[116,117] It is reported that the ordered film structure degrades to a less ordered structure away from the substrate interface and that optimized deposition conditions can extend the well-ordered structure to as thick as 19nm.[118] In summary, a number of reports have shown materials' properties that depend on thin film thickness. Data is available to show both enhanced and degraded mechanical properties and it is particularly interesting

that the behavior of Pentacene films show some similarities to Alq3 above and below ~19nm transition. Strain-induced elastic buckling instability for mechanical measurements SIEBIMM appears to be an elegant and accurate way to characterize the mechanical properties of small molecule thin films used to build organic optoelectronics.

4.3.3 Thickness Dependence of Mechanical Properties

Following the success of a buckling based metrology on Alq_3, the elastic moduli of a series of vacuum deposited triarylamines was determined using SIEBIMM.[56,64] Figure 40 illustrates a representative image of a wrinkled surface for a 64 nm thick TPD film and the corresponding FFT determination of λ.

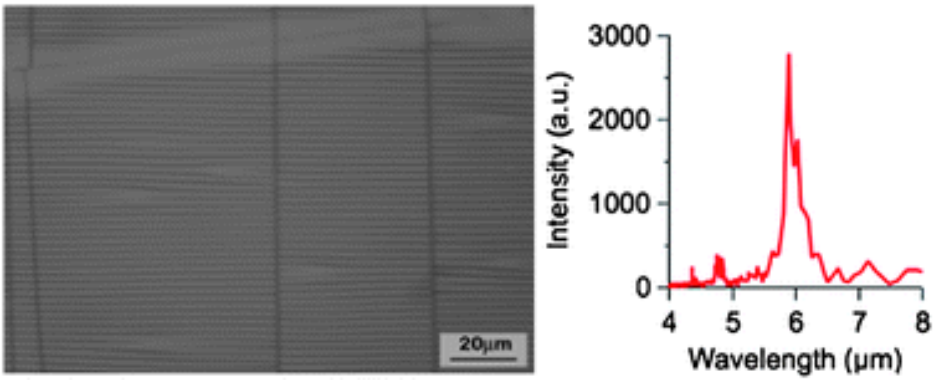

Figure 40. Optical micrograph of a mechanically wrinkled 64 nm thick TPD film on a PS barrier film and the corresponding FFT.

Periodic and well-aligned wrinkles observed occur due to the biaxial strain that is applied from the stretching of the PDMS. A wavelength of 5.85 +/- 1.3 μm is determined from a Gaussian fit of λ, which can be used to calculate the modulus ($\bar{E}_f$ of 1.53 +/- 0.17 GPa) for this film. These measurements are repeated for different triarylamines and film thicknesses to provide insight into the role of molecular structure on the thickness dependent moduli of small molecule glasses.

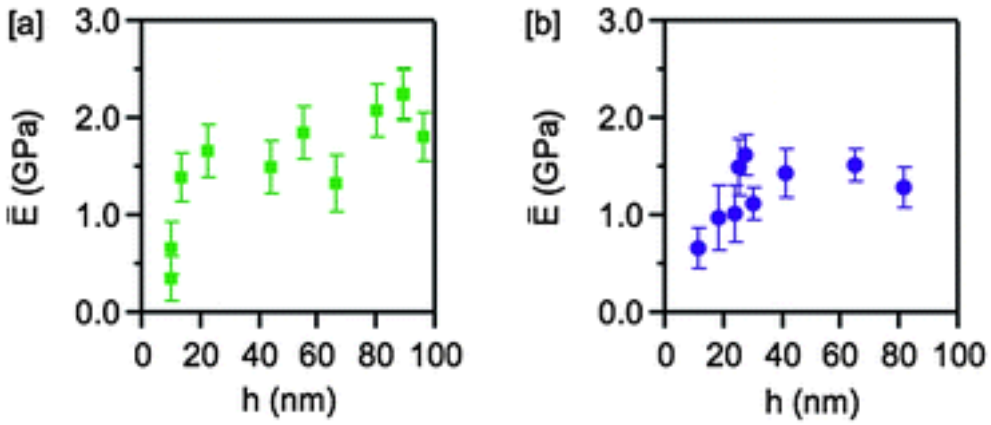

Figure 41. Moduli of vapor deposited (a) CBP and (b) TPD as a function of film thickness. The error bars represent one standard deviation from uncertainty propagation of the measurements.

Figure 41 illustrates the thickness dependencies in the moduli of CBP. The bulk-like modulus of CBP is 1.9 +/- 0.4 GPa, but films less than 20nm show a reduced value. This behavior contradicts results from the previously examined Alq_3 (Figure 42) where the modulus is found to increase at thicknesses below 20nm.[104] Modifications of the CBP structure (NPD and TPD as shown in Figure 36) that maintain molecular similarity were then considered in order to identify a systematic response of the modulus to decreasing thickness. TPD has a slightly higher T_g = 62 °C as compared to CBP (T_g = 60 °C), but both are less than NPD (T_g= 95 °C).

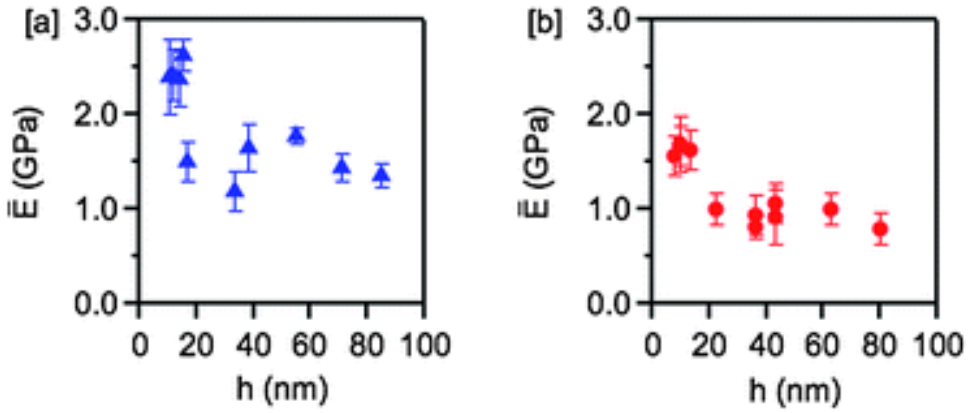

Figure 42. Moduli of vapor deposited (a) NPD and (b) Alq3 as a function of film thickness. The error bars represent one standard deviation of the data, which is taken as the experimental uncertainty of the measurements.

Figure 41 shows that CBP and TPD share the same dependence of moduli as a function of film thickness in addition to a similar T_g. The same behavior has been observed in polymers that have attributed a reduced modulus at the polymer–air interface[119] that can be measured *via* indentation.[120] Thus, a similar effect could be responsible for the decreased ultrathin modulus present in CBP and TPD; however, the mechanism for increased moduli of the Alq_3 and NPD must then still be explained. Figure 42 illustrates the thickness dependent moduli of Alq_3 and NPD. The modulus of NPD is independent of thickness for films greater than 20 nm thick (1.65 +/- 0.23 GPa), yet for a 10.3 nm thick film, the modulus of NPD increases by approximately 50% to 2.39 +/- 0.33GPa. This behavior is also observed in structurally dissimilar Alq_3.

For polymer thin films, it is understood that the proximity of the bulk T_g to the measurement temperature is a critical factor in determining the length scale at which deviations from the bulk modulus are observed.[110] The thin film behavior of polymers has

been shown to not only depend upon the free surface,[121] but also the substrate interface.[122] For the case of vacuum deposited small molecules, molecular packing and packing density has been shown to depend upon deposition conditions such as temperature and the characteristics of substrate surface.[115,123,124] Specifically, the proximity of the substrate temperature to bulk T_g has been found to be critical for the density, aging, and thermal properties of glasses with an optimal deposition temperature determined to be ~$0.85T_g$ (with T_g in Kelvin).[124] Temperatures close to T_g enable a monolayer of increased mobility that allows for configurational sampling of the molecule as it arrives at the substrate leading to increased molecular packing density.[123] The enhanced dynamics allow molecules to assemble in an efficient space-utilization layer-by-layer fashion. This mechanism is consistent with the 19% and 14% modulus increase reported for IMD and TNB films deposited at $0.85T_g$ as compared to the ordinary glass.[115]

The room temperature deposition of CBP and TPD with T_g's of 60 °C and 62 °C can be determined to be $0.89T_g$ and $0.88T_g$, which is closer to the optimum conditions of $0.85T_g$. Thus, one would expect significant rearrangement of the surface to improve molecular packing. The decrease of moduli for sub-20 nm CBP and TPD films can be attributed to the enhanced surface mobility. An increase in molecular mobility should lead to a decrease in the capacity of the material to store stress and hence a decrease in modulus. This enhanced surface mobility in the molecular glass is similar to what has been reported for PS surfaces[125] where a decrease in moduli for ultrathin films has been reported.[119] To explain the thin film moduli behavior of Alq_3 (T_g ~175 °C) and NPD (T_g ~95 °C), we can make a consistent argument. At deposition temperatures below T_g ($<0.85T_g$), molecules are deposited without significant surface mobility. This lack of rearrangement creates

glasses with lower packing densities, and high enthalpies. The surface should not be mobile as the deposition conditions correspond to $0.66T_g$ and $0.78T_g$ for Alq3 and NPD, respectively. Additionally, the deposition surface can impact the structure of the film for vacuum deposited molecules. For example, hole injection barrier for NPD and pentacene reveals an order of magnitude difference between the materials deposited on Au or electronic polymer layers, which is attributed to the impact of the substrate on molecular packing.[126] Moreover, an increase in mobility of the first monolayer of pentacene has been attributed to a unique packing of the first monolayer of pentacene.[127] Thus, the initial monolayer of Alq_3 and NPD may be more densely packed due to interactions with the substrate. As the film grows, the lack of surface mobility of the molecules leads to a decrease in packing efficiency. This proposed behavior is consistent with the thickness dependent moduli reported for Alq_3 and NPD. The bulk T_g of the molecule is shown to be a critical factor in assessing the thickness dependent behavior. Continued mechanical characterization of WOLED materials will be needed as devices are implemented in non-rigid substrate manufacturing processes and flexible devices.

4.3.4 Thickness Dependence of Optical Properties

The thickness dependent mechanical properties at confined length scale suggest that the molecular structure at the substrate surface could be different than in the bulk. If the growth kinetics leading to such behavior are evident in the mechanical film properties, it follows that the optical properties of the film would also change at confined length scale. Here, the interaction with light as measured by VASE is used to model the dielectric function by fitting a series of Lorentzian oscillators to match empirical results.[128] The behavior of individual molecules can be decoupled from the thin film

behavior so that some conclusion can be drawn from a systematic change in the aggregate optical response as the film thickness decreases. Comparing a thickness range from 80nm to 12nm will represent the transitions from bulk towards very thin (approaching confinement in two dimensions).

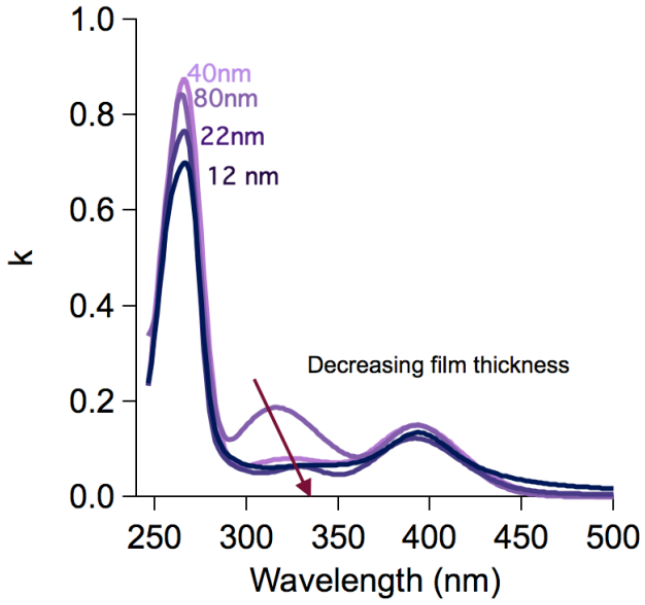

Figure 43. Absorption coefficient as modeled from Lorentz oscillators fit to VASE data for Alq_3 films 12nm, 22nm, 40nm, and 80nm demonstrating thickness dependence of optical properties.

Figure 43 shows the lossy coefficient, k, for a range of thin film thicknesses. Dilute solution of Alq_3 has been reported to have absorption peaks near at 4.77eV and 3.22eV.[129] These energies correlate well to the absorption peaks observed in thin film absorption at 260nm and 385nm respectively. Because the absorption in dilute solution is assumed to have very little molecule-to-molecule interaction, it is likely that the analogous absorption

in thin film can be attributed to the individual film molecules that would not have a strong dependence on film structure except for the case of preferential orientation of anisotropic molecules. In Figure 43 a third peak that is not well explained by the optical properties of the individual molecules exists between 310nm and 340nm. This absorption is then the likely result of aggregate interactions that would be expected to depend on the film structure and resulting molecule-to-molecule arrangement that has also been reported elsewhere.[130] This intermediate energy absorption from aggregates does show a dependence on film thickness. First, the behavior of the thinnest films becomes more like the behavior of individual molecules in solution which is consistent with reduced aggregation as the film approaches a monolayer. Second, the energy of the aggregate absorption shifts to longer wavelengths which is in agreement with the proposed change in molecular packing. Finally, a decrease in the molecular absorption peaks at 260 nm and 385 nm could be associated with interdiffusion of Alq_3 into the PS layer (diluting the absorption as PS is transparent in this wavelength range) as porous Alq_3 films show a similar trend in decreased k.[117] To better understand the substrate or substrate diffusion influence on the optical properties observed, spectra collected on both Si and PS/PDMS substrates were evaluated. Figure 44 shows very little substrate dependence on the substrate and suggests that the changes in the absorption spectra are likely related to the thin film morphology. A change in morphology would also be consistent with the observed variation in elastic modulus previously discussed. It is not well understood how different molecular packing influences the absorption energy and intensity, but the thin film structure appears to be influencing the observed optical properties of Alq_3 in this case. Future work could consider of a more diverse set of materials to continue quantifying

differences in morphology as a function of film thickness. It is evident from this data, however, that a thickness dependent morphology is supported by both of optical and mechanical materials properties.

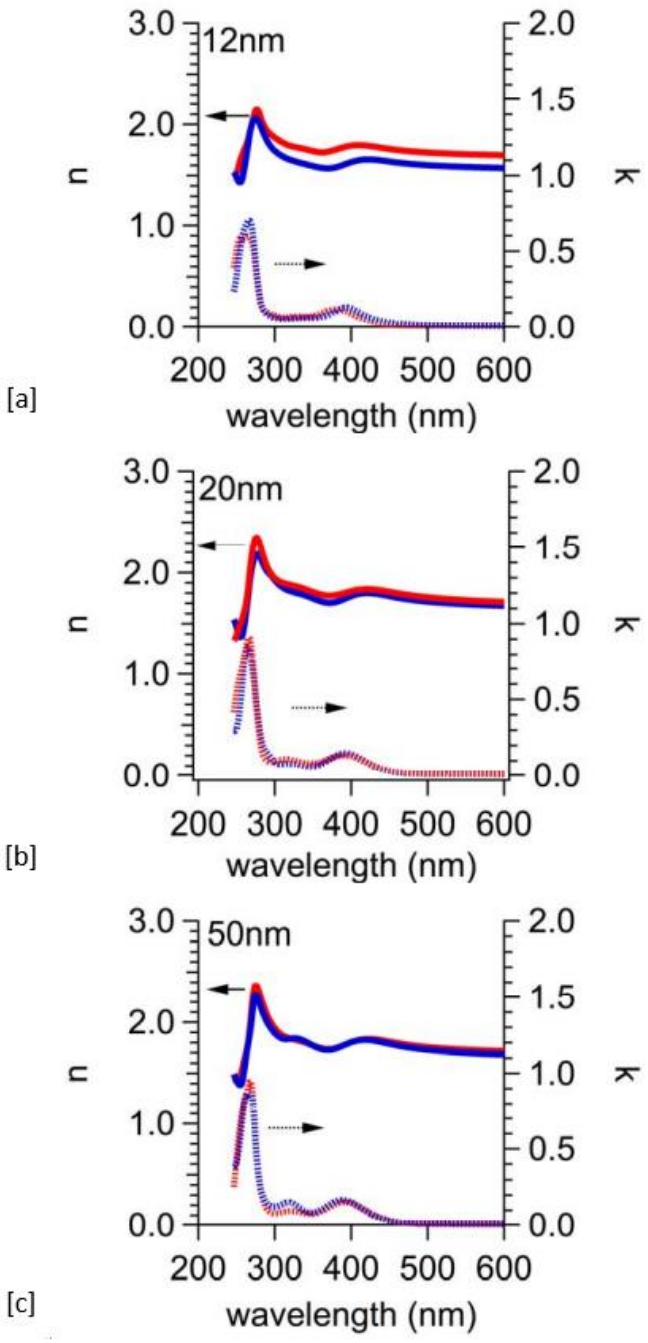

Figure 44. Optical properties of Alq3 thin films where the index of refraction n and extinction coefficient k are measured on Silicon substrates (red) and PS/PDMS substrates (blue) for film thicknesses equal to [a] Alq_3 = 12nm [b] Alq_3 = 20nm [c] Alq_3 = 50nm

4.4 Conclusion

The elastic moduli of a series of triarylamine films, *i.e.* NPD, CBP and TPD, were determined utilizing a two plate wrinkling instability as a function of film thickness. The moduli of sub-20 nm thick films tend to depend on the bulk T_g of the material. For materials with $T_{ambient} > 0.85T_g$, their sub-20 nm films are observed to have a systematic decrease from bulk modulus. This behavior is similar to that of polymeric thin films, which is attributed to the free surface effects. Materials with higher bulk T_g ($T_{ambient} < 0.85T_g$) exhibit an increase in sub-20nm moduli that is attributed to increased packing frustration due to initial surface directed packing and lower surface mobility of the material during film growth.

Surface wrinkling[131] has been successfully employed to determine the elastic moduli of pentacene[132] and Alq_3.[104] The low modulus of Alq_3 glass (~1 GPa) suggests that the material could be compatible with non-rigid substrate fabrication. Moreover, a recent report shows that the moduli of conjugated polymers can be well correlated with electronic properties such as mobility.[133] Annealing of polymeric semiconductor films results in a two-fold increase in modulus and a four-fold increase in hole mobility.[22] Both electrical and mechanical properties of organic electronics are strongly correlated with mass density.[134] This result suggests that the measurement of mechanical properties can provide indirect information regarding the nature of mechanisms that cause a dependence of device performance on processing conditions.[135]

The properties of organic glasses have also shown to be size dependent at the nanometer length scale.[112,125,136-139] Moreover, material properties can be influenced by both a complex interplay between interfacial interactions and a loss of entropy due to

confinement.[5] For example, the modulus of Alq_3 is significantly enhanced by almost a factor of two as the thickness of the film is decreased to less than 20nm.[104] However, this behavior is counter to the decrease of modulus in the order of magnitude that has been reported for ultrathin polymeric films.[110,140] These results show the possibility for complex behavior of organic thin films at such small length scales, which requires additional investigations on a wide range of organic semiconductor materials. In this section, several common hole transporting layers and host materials for OLEDs, CBP, TPD, and NPD were examined for their thickness dependent moduli behavior for the purpose of further understanding phenomena observed in Alq3. This information will help to describe the impact that structure has on molecular glasses at the nanoscale, potentially leading to improvements in design for non-rigid substrate manufacturing and flexible electronics.

4.5 References

9. Forrest SR. The path to ubiquitous and low-cost organic electronic appliances on plastic. *Nature*. 2004;428(6986):911-918.

56. Stafford CM, Guo S, Harrison C, Chiang MYM. Combinatorial and high-throughput measurements of the modulus of thin polymer films. *Rev Sci Instrum*. 2005;76:062207.

64. Nolte AJ, Cohen RE, Rubner MF. A two-plate buckling technique for thin film modulus measurements: Applications to polyelectrolyte multilayers. *Macromolecules*. 2006;39(14):4841-4847.

98. Gleskova H, Cheng I. Mechanics of thin-film transistors and solar cells on flexible substrates. *Solar Energy*. 2006;80(6):687-693.

99. Sirringhaus H, Kawase T, Friend R, et al. High-resolution inkjet printing of all-polymer transistor circuits. *Science*. 2000;290(5499):2123.

100. Chiang CJ, Bull S, Winscom C, Monkman A. A nano-indentation study of the reduced elastic modulus of Alq3 and NPB thin-film used in OLED devices. *Organic Electronics*. 2010;11(3):450-455.

101. Chiang CJ, Winscom C, Bull S, Monkman A. Mechanical modeling of flexible OLED devices. *Organic Electronics*. 2009;10(7):1268-1274.

102. VanLandingham MR, Villarrubia JS, Guthrie WF, Meyers GF. Nanoindentation of polymers: An overview. . 2001;167(1):15-44.

103. Bishop JP, Register RA. Poly (phenylethylnorbornene) s and their hydrogenated derivatives. *Macromolecular Rapid Communications*. 2008;29(9):713-718.

104. Torres JM, Bakken N, Stafford CM, Li J, Vogt BD. Thickness dependence of the elastic modulus of tris (8-hydroxyquinolinato) aluminium. *Soft Matter*. 2010;6(22):5783-5788.

105. Vivo P, Jukola J, Ojala M, Chukharev V, Lemmetyinen H. Influence of alq 3/au cathode on stability and efficiency of a layered organic solar cell in air. *Solar Energy Mater Solar Cells*. 2008;92(11):1416-1420.

106. Lötters J, Olthuis W, Veltink P, Bergveld P. The mechanical properties of the rubber elastic polymer polydimethylsiloxane for sensor applications. *J Micromech Microengineering*. 1997;7(3):145.

107. Göbel R, Krska R, Kellner R, Seitz R, Tomellini S. Investigation of different polymers as coating materials for IR/ATR spectroscopic trace analysis of chlorinated hydrocarbons in water. *Appl Spectrosc*. 1994;48(6):678-683.

108. Rodríguez-Tinoco C, Gonzalez-Silveira M, Ràfols-Ribé J, Lopeandía AF, Clavaguera-Mora MT, Rodríguez-Viejo J. Evaluation of growth front velocity in ultrastable glasses of indomethacin over a wide temperature interval. *The Journal of Physical Chemistry B*. 2014;118(36):10795-10801.

109. Perez-Castaneda T, Rodriguez-Tinoco C, Rodriguez-Viejo J, Ramos MA. Suppression of tunneling two-level systems in ultrastable glasses of indomethacin. *Proc Natl Acad Sci U S A*. 2014;111(31):11275-11280.

110. Torres JM, Stafford CM, Vogt BD. Elastic modulus of amorphous polymer thin films: Relationship to the glass transition temperature. *ACS nano*. 2009;3(9):2677-2685.

111. Zhao J, Kiene M, Hu C, Ho PS. Thermal stress and glass transition of ultrathin polystyrene films. *Appl Phys Lett*. 2000;77:2843.

112. Priestley RD, Ellison CJ, Broadbelt LJ, Torkelson JM. Structural relaxation of polymer glasses at surfaces, interfaces, and in between. *Science*. 2005;309(5733):456.

113. Jabbari E, Peppas NA. Molecular weight and polydispersity effects on interdiffusion at the interface between polystyrene and poly (vinyl methyl ether). *J Mater Sci*. 1994;29(15):3969-3978.

114. Jang D, Greer JR. Transition from a strong-yet-brittle to a stronger-and-ductile state by size reduction of metallic glasses. *Nature materials*. 2010;9(3):215-219.

115. Kearns KL, Still T, Fytas G, Ediger M. High-Modulus organic glasses prepared by physical vapor deposition. *Adv Mater*. 2010;22(1):39-42.

116. Fritz SE, Martin SM, Frisbie CD, Ward MD, Toney MF. Structural characterization of a pentacene monolayer on an amorphous SiO2 substrate with grazing incidence X-ray diffraction. *J Am Chem Soc*. 2004;126(13):4084-4085.

117. Bouchoms I, Schoonveld W, Vrijmoeth J, Klapwijk T. Morphology identification of the thin film phases of vacuum evaporated pentacene on SiO 2 substrates. *Synth Met*. 1999;104(3):175-178.

118. Ruiz R, Mayer AC, Malliaras GG, et al. Structure of pentacene thin films. *Appl Phys Lett*. 2004;85(21):4926-4928.

119. Torres JM, Stafford CM, Vogt BD. Impact of molecular mass on the elastic modulus of thin polystyrene films. *Polymer*. 2010.

120. Miyake K, Satomi N, Sasaki S. Elastic modulus of polystyrene film from near surface to bulk measured by nanoindentation using atomic force microscopy. *Appl Phys Lett*. 2006;89:031925.

121. Mundra MK, Donthu SK, Dravid VP, Torkelson JM. Effect of spatial confinement on the glass-transition temperature of patterned polymer nanostructures. *Nano letters*. 2007;7(3):713-718.

122. Tsui O, Russell T, Hawker C. Effect of interfacial interactions on the glass transition of polymer thin films. *Macromolecules*. 2001;34(16):5535-5539.

123. Dawson KJ, Kearns KL, Yu L, Steffen W, Ediger MD. Physical vapor deposition as a route to hidden amorphous states. *Proceedings of the National Academy of Sciences*. 2009;106(36):15165.

124. Swallen SF, Kearns KL, Mapes MK, et al. Organic glasses with exceptional thermodynamic and kinetic stability. *Science*. 2007;315(5810):353.

125. Fakhraai Z, Forrest J. Measuring the surface dynamics of glassy polymers. *Science*. 2008;319(5863):600.

126. Koch N, Elschner A, Schwartz J, Kahn A. Organic molecular films on gold versus conducting polymer: Influence of injection barrier height and morphology on current–voltage characteristics. *Appl Phys Lett*. 2003;82(14):2281-2283.

127. Mayer AC, Ruiz R, Headrick RL, Kazimirov A, Malliaras GG. Early stages of pentacene film growth on silicon oxide. *Organic electronics*. 2004;5(5):257-263.

128. Djurii A, Kwong C, Guo W, et al. Spectroscopic ellipsometry of the optical functions of tris (8-hydroxyquinoline) aluminum (Alq3). *Thin Solid Films*. 2002;416(1-2):233-241.

129. Aziz A, Narasimhan K. Optical absorption in AlQ. *Synth Met*. 2000;114(2):133-137.

130. Himcinschi C, Meyer N, Hartmann S, et al. Spectroscopic ellipsometric characterization of organic films obtained via organic vapor phase deposition. *Applied Physics A*. 2005;80(3):551-555.

131. Stafford CM, Harrison C, Beers KL, et al. A buckling-based metrology for measuring the elastic moduli of polymeric thin films. *Nature materials*. 2004;3(8):545-550.

132. Tahk D, Lee HH, Khang DY. Elastic moduli of organic electronic materials by the buckling method. *Macromolecules*. 2009;42(18):7079-7083.

133. O'Connor B, Chan EP, Chan C, et al. Correlations between mechanical and electrical properties of polythiophenes. *ACS nano*.

134. Al-Douri Y, Abid H, Aourag H. Correlation between the bulk modulus and the charge density in semiconductors. *Physica B: Condensed Matter*. 2001;305(2):186-190.

135. DeLongchamp DM, Vogel BM, Jung Y, et al. Variations in semiconducting polymer microstructure and hole mobility with spin-coating speed. *Chemistry of materials*. 2005;17(23):5610-5612.

136. Ellison CJ, Torkelson JM. Sensing the glass transition in thin and ultrathin polymer films via fluorescence probes and labels. *Journal of Polymer Science Part B: Polymer Physics*. 2002;40(24):2745-2758.

137. Jackson CL, McKenna GB. The glass transition of organic liquids confined to small pores. *J Non Cryst Solids*. 1991;131:221-224.

138. Yang Z, Fujii Y, Lee FK, Lam CH, Tsui OKC. Glass transition dynamics and surface layer mobility in unentangled polystyrene films. *Science*. 2010;328(5986):1676.

139. O'connell P, McKenna G. Rheological measurements of the thermoviscoelastic response of ultrathin polymer films. *Science*. 2005;307(5716):1760.

140. Stafford CM, Vogt BD, Harrison C, Julthongpiput D, Huang R. Elastic moduli of ultrathin amorphous polymer films. *Macromolecules*. 2006;39(15):5095-5099.

CHAPTER 5

DEPOSITION SUBSTRATE TEMPERATURE DEPENDENT STRUCTURE AND PROPERTIES OF SMALL MOLECULE THIN FILMS

5.1 Introduction

Organic light emitting devices based on small molecule thin film materials have been researched for many years with most investigations looking at new materials or alternative device architectures to improve the efficiency and performance of these devices for displays and lighting.[141,142] More recently, the kinetics of thin film growth is understood to impact the device performance as well due to varied structures achieved by either of preferential or random molecular orientations with in the film stacks.[97,143,144] Several methods have been reported to tune thin film structure to achieve more desirable charge transport or optical properties. In the case of physical vapor deposition (PVD) accomplished with line-of-site vacuum evaporation that is commonly used for device fabrication, the thickness of layers and the orientation of the molecules will have significant impact to the relevant optoelectronic materials properties.[97,143-145] Results have also demonstrated a surface effect where the elastic modulus of PVD thin films (< 20nm) is different in thicker films produced using the same deposition parameters.[37,104] The kinetics of film deposition, annealing procedures, and the resulting materials performance[146] are then dependent on both film thickness as well as the deposition parameters.[147,148]

The highest elastic modulus observed as a result of optimized thickness of NPD and/or deposition temperature of NPD is the same and we propose that the orientation of packed molecules is a result of both variables. The thickness dependent modulus could be explained as a result of increased mobility at the surface to enable lower energy

configurational states while subsequent layers observed in thicker films solidify in higher energy configurations because of reduced molecular mobility in the bulk glass as compared to the film surface.[37,104] The deposition temperature dependence could then be a result of substrate temperature contribution to the most energetically favorable film configuration. This theory is consistent with reports of ultrastable glass formed by slow vapor deposition near the glass transition temperature (T_g) where the increased stability is correlated to molecular exploration of multiple configurations to achieve a lower energy configuration.[149,150] Many studies have investigated the behavior of ultrastable glasses.[108,151-154] The increased density is shown to improve mechanical properties in comparison to ordinary glasses.[115] This is of particular interest for OLED because of: 1) correlations between mechanical, optical, and electrical properties[37,104]; 2) the desire for robust, flexible, and/or stretchable devices[155]; 3) the increased reliability from suppressed water uptake in higher density films.[156,157]

Other researchers have reported controlling substrate temperature to alter molecular orientation from edge-on to face-on and a strong correlation between kinetic stability and molecular orientation for small molecule OLED films.[146,158] In this chapter, the water uptake and mechanical properties of NPD as a function of both thickness and deposition temperature are reported to show that significant enhancements to the elastic moduli, thickness independent moduli, and significant reductions in water uptake can be obtained by carefully controlling the substrate temperature during deposition. Controlling substrate temperature is shown to be a valuable method to improve the thin film characteristics for materials common to small molecule organic electronic devices.

5.2 Experimental

N,N'-di-1-naphthyl-N,N'-diphenyl-1,1'-biphenyl-4,4'diamine (NPD) was purchased from (Sigma Aldrich) and purified in a four zone furnace as described previously.[37] Water uptake studies were conducted using a MHz chromium coated quartz crystals from (Maxtek). The substrate crystals were cleaned for 30 seconds in UV ozone cleaner (model 342, Jelight, Inc.).

Mechanical measurements of poly(dimethyl siloxane) (PDMS) from (Dow Corning) were taken using a Texture Analyzer (TA.XT Plus, Texture Technologies). PDMS was cast onto float glass at a 20:1 (volume: volume) base to curing agent ratio to an approximate thickness of 1.5 mm. Prior to curing, the material was degased under ambient conditions for 3 h. Curing was performed at 120 °C for 2 h. The PDMS was then cut into 75 mm x 25 mm x 1.5 mm pieces for modulus pre-characterization. The PDMS slabs were then placed onto a custom built strain stage[56] and pre-strained to approximately 3%. Polystyrene (PS, M_n = 9.4 kg/mol, Polymer Laboratories) was spin coated from toluene onto clean silicon wafers and the films were annealed under nitrogen at $T = T_g + 20$ °C. The polymer film was transferred onto the PDMS from the spin coated silicon wafer. The thickness of the polymer film was determined utilizing a UV-Vis-NIR (250 nm – 1700 nm) Variable Angle Spectroscopic Ellipsometer (VASE, M-2000, J.A. Woollam Co., Inc.). PS was employed as a diffusion barrier for NPD into the PDMS. The purified NPD was vacuum deposited (Trovato Mfg.) at pressures below 10^{-7} Torr and deposition rates between 1-1.5 Å/s through a 16 mm diameter circular shadow mask onto the chromium coated quartz crystals for water uptake studies or onto the polymer film on PDMS for

mechanical measurements. The thickness of the NPD film was confirmed by VASE. The substrate temperature during deposition was varied from approximately 21 °C to 95 °C.

The thickness of NPD film, h_{NPD}, on the polymer film on the PDMS substrates was determined using the UV-Vis-NIR VASE. Measurements were performed in the pre-strained state so that the ellipsometric angles could be fit to a three-layer model (NPD/polymer/PDMS) with fixed optical constants for the PDMS and polymer film. Although the optical properties of these vapor deposited films can be anisotropic,[159] the thickness of NPD obtained from the fit was observed to be invariant (within uncertainty) between isotropic and anisotropic models. Similarly, the thickness of the NPD on the quartz crystal was determined by VASE with the optical constants[160] for each chromium coated crystal determined prior to deposition of NPD.

Surface wrinkling metrology of the NPD/polymer layer on the PDMS was used to determine the elastic modulus of thin films.[131,161,162] Wrinkling was induced by releasing the pre-strain in the PDMS at approximately 0.1 mm/s under ambient conditions (T = 21 °C +/- 2 °C). The surface wrinkles were characterized by either optical microscopy (OM, Mitoyo Ultraplan FS-100) with an image resolution of 1024 pixels x 768 pixels or using atomic force microscopy (AFM, Park XE-150) in intermittent contact mode. The wrinkling wavelength was obtained by analyzing the images using 1D Fast Fourier Transforms. The wavelength, λ, was used to determine the plane-strain modulus of the NPD, $\bar{E}_{NPD}$, with a two-plate composite model previously described:[56,163]

$$\bar{E}_{NPD} = \frac{\frac{3\bar{E}_S\lambda^3}{32\pi^3(h_P+h_{NPD})} - \bar{E}_P\left[\left(\phi_P-\frac{\kappa}{2}\right)^3+\left(\frac{\kappa}{2}\right)^3\right]}{\left(1-\frac{\kappa}{2}\right)^3-\left(\phi_P-\frac{\kappa}{2}\right)^3} \qquad (16)$$

where $\bar{E}_S$ and $\bar{E}_P$ are the plane strain moduli of the PDMS substrate and polymer, respectively, ϕ_P is the height fraction of polymer for the two films ($= h_P/(h_P + h_{NPD})$, and κ is the deviation factor for the neutral axis of bending as:

$$\kappa = \frac{1+\phi_P^2\left(\frac{\bar{E}_P}{\bar{E}_{NPD}}-1\right)}{1+\phi_P\left(\frac{\bar{E}_P}{\bar{E}_{NPD}}-1\right)} \quad (17)$$

Water uptake into the thin films was measured using a Maxtek quartz crystal microbalance (QCM) with 5 MHz chromium coated quartz crystals. All measurements were performed at T = 21 °C +/- 2 °C with nearly saturated water vapor generated in a bubbler system. The amount of water absorbed was determined by previously described method according to the Sauerbrey equation:

$$\Delta f = -\frac{2 f_o^2 \Delta m}{nA(\mu_q p_q)^{0.5}} = -C_f \frac{\Delta m}{nA} \quad (18)$$

where Δf is the change in frequency, Δm is the change in mass, f is the measured resonant frequency, A is the electrode area (0.25 cm^2), n is the harmonic at which the crystal is driven, C_f is the sensitivity constant of the crystal (57 Hz/μg/cm^2), μ_q and ρ_q are the shear modulus (2.95×10^6 N cm^{-2}) and the density (2.65 g/cm^3) of the quartz. All measurements were repeated three times.

5.3 Results

5.3.1 Elastic Modulus Dependence on Deposition Temperature

The elastic modulus vs. deposition temperature are shown to be independent of the barrier film selected in Figure 45 for films that are 50 nm thick. The modulus increases by more than 50 % when increasing the substrate temperature from room temperature to 70 °C. The maximum elastic modulus is observed at about $0.93T/T_g$ and decreases at

temperatures above this value. This maximum is a little higher than the $0.85T/T_g$ that was reported as the optimum substrate temperature for stability of indomethacin (IMC) glass.[164] It was also a little higher than the temperature that resulted in highest density of ethylbenzene ($0.86\text{-}0.91T/T_g$).[150]

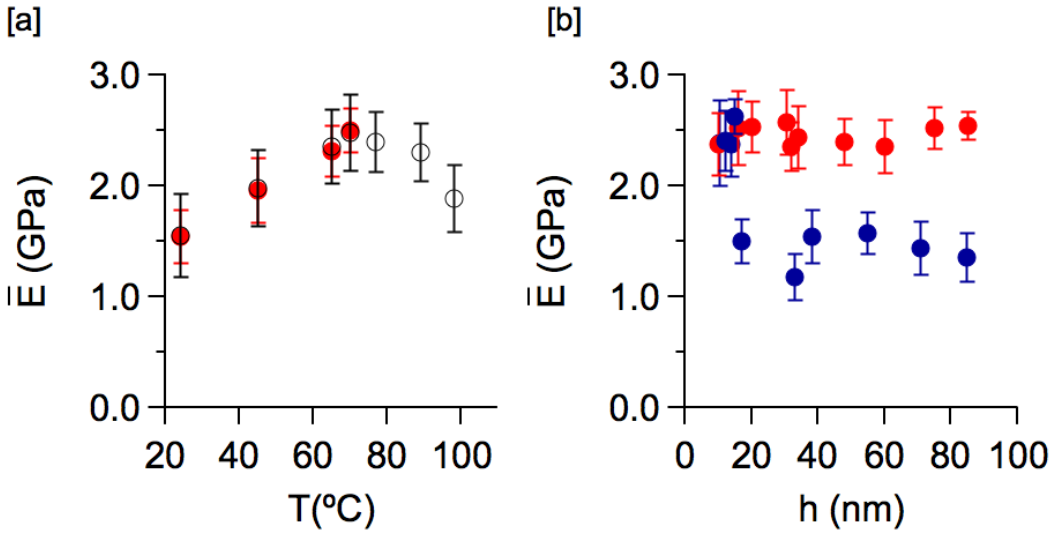

Figure 45. [a] Substrate temperature vs. elastic modulus for NPD (●) and AddPENb (○) [b] Thickness vs. elastic modulus for NPD deposited at 22 ºC (blue) and 70 ºC (red).

Figure 45b shows that the maximum modulus obtained at 70C for NPD is now thickness independent for the film thicknesses tested. In contrast, room temperature depositions show relatively high modulus of 2.4GPa for films less than 18nm, but observe about a 50% reduction in modulus for films above 20nm. This suggests a surface effect where the initial 18nm of deposited NPD leads to packing structure that is independent of temperature and results in the moduli that is the highest that we have been able to obtain for NPD. In contrast, the films deposited at 22 ºC predict an abrupt change in the structure around 20 nm that leads to reduced film stiffness. The same behavior has been reported for the

thickness dependence of other vapor deposited glass films at ambient temperature.[37,104] Controlling the deposition temperature to 70 ºC enables the maximum and thickness independent modulus of the thin film to be realized in organic electronic devices. This is important new information because the modulus correlated with device optoelectronic, mechanical, and reliability characteristics.

5.3.2 Water Uptake Dependence on Deposition Temperature

Water uptake for 50nm deposited films are shown in Figure 46 as compared against the control substrate only for deposition temperatures 22 ºC, 55 ºC and 70 ºC correlating to the range where maximum and minimum elastic moduli were observed. Environmental control to prevent device degradation from ambient moisture is well documented. The reduction in water uptake shown for films deposited correlates to enhanced mechanical properties and more ideal reduced absorption of water. These results are consistent with the decreased equilibrium water uptake in ultrastable glasses of IMC[157] previously reported. The accuracy of absorption using thin films on quartz crystals can be reduced because of the impact of the buried interface on total uptake[165,166] Accumulation of water at this interface [167-169] can contribute significantly to the total sorption. For the quartz crystals used here, the blank, uncoated crystal adsorbs more than 100 ng/cm^2. This represents 1/3 of the sorption in the NPD film deposited at 22 ºC, while this is > 65 % of the total sorption into the NPD film deposited at 80 ºC.

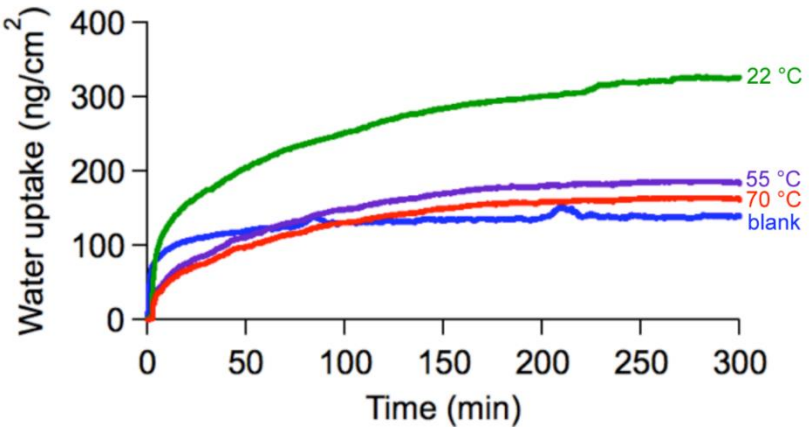

Figure 46. Water uptake for NPD films as measured by QCM at 22, 55, and 70 degrees Celsius

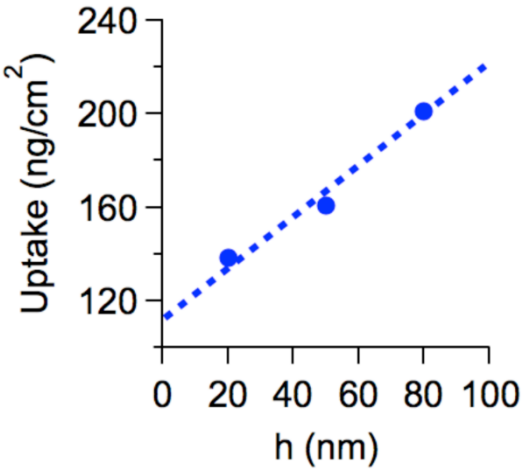

Figure 47. Thickness of NPD vs. water uptake

The difference in uptake of the crystal interface as compared to the deposited film would predict a non-linear response for water uptake as a function of deposited film thickness or a non-zero uptake for zero extrapolated thickness.[157] To measure this response, the sorption is measured for a series of film thicknesses. Figure 47 shows that this trend is indeed linear; however, a relatively large offset in the extrapolated zero thickness uptake

is noted. The offset of about 115 ng/cm^2 is similar to what would be expected from the blank sensor without film deposition and suggests that the water uptake is highly dependent on the interfaces and less dependent on the bulk response of the NPD film intended for measurement. Still, a demonstrated qualitative reduction of uptake in NPD deposited at an optimized temperature could indicate a potential to increase device reliability by slowing oxidation of device layers from ambient moisture.

5.4 Conclusion

It has been demonstrated that the moduli of 50 nm thick (NPD) films can be increased from 1.5 GPa to 2.5 GPa by increasing the temperature of the substrate during deposition with a maximum in moduli found at $T/T_g = 0.93$. This maximum in modulus is the same modulus obtained for very thin (<15 nm) NPD films deposited at 295 K ($T/T_g = 0.80$). However, the modulus of films deposited at this lower temperature abruptly decreases to approximately 1.5 GPa for thicker films; the modulus from deposition at $T/T_g = 0.94$ is thickness independent. In addition to the thin film moduli, the substrate temperature significantly impacts the water uptake in NPD films. From QCM, the water volume fraction at equilibrium with nearly saturated water vapor decreases from nearly 10 % to less than 2 % as the substrate temperature increases from $T/T_g = 0.82$ to $T/T_g = 0.93$

The properties of physical vapor deposited films of NPD are strongly dependent on the substrate temperature during deposition. The elastic modulus increases with temperature to a maximum at $0.93T/T_g$ for NPD films showing a 50% increase as compared to room temperature. In addition to a substantial change in mechanical properties, measurements of water uptake show a factor of 5 reduction in water solubility for films deposited at 0.93T/Tg as compared to room temperature. Substrate temperature control

has demonstrated the potential to optimize the properties of organic electronic devices for higher performance, integration with flexible electronics, and increased lifetime.

5.5 References

37. Bakken N, Torres JM, Li J, Vogt BD. Thickness dependent modulus of vacuum deposited organic molecular glasses for organic electronics applications. *Soft Matter*. 2011;7(16):7269.

56. Stafford CM, Guo S, Harrison C, Chiang MYM. Combinatorial and high-throughput measurements of the modulus of thin polymer films. *Rev Sci Instrum*. 2005;76:062207.

97. Yokoyama D, Sakaguchi A, Suzuki M, Adachi C. Horizontal orientation of linear-shaped organic molecules having bulky substituents in neat and doped vacuum-deposited amorphous films. *Organic Electronics*. 2009;10(1):127-137.

104. Torres JM, Bakken N, Stafford CM, Li J, Vogt BD. Thickness dependence of the elastic modulus of tris (8-hydroxyquinolinato) aluminium. *Soft Matter*. 2010;6(22):5783-5788.

108. Rodríguez-Tinoco C, Gonzalez-Silveira M, Ràfols-Ribé J, Lopeandía AF, Clavaguera-Mora MT, Rodríguez-Viejo J. Evaluation of growth front velocity in ultrastable glasses of indomethacin over a wide temperature interval. *The Journal of Physical Chemistry B*. 2014;118(36):10795-10801.

115. Kearns KL, Still T, Fytas G, Ediger M. High-Modulus organic glasses prepared by physical vapor deposition. *Adv Mater*. 2010;22(1):39-42.

141. Sasabe H, Kido J. Development of high performance OLED for general lighting. *Journal of Materials Chemistry C*. 2013.

142. Sasabe H, Kido J. Multifunctional materials in high-performance OLEDs: Challenges for solid-state lighting†. *Chemistry of Materials*. 2010;23(3):621-630.

143. Yokoyama D. Molecular orientation in small-molecule organic light-emitting diodes. *Journal of Materials Chemistry*. 2011;21(48):19187-19202.

144. Lin H, Lin C, Chang H, et al. Anisotropic optical properties and molecular orientation in vacuum-deposited ter (9, 9-diarylfluorene) s thin films using spectroscopic ellipsometry. *J Appl Phys*. 2004;95(3):881-886.

145. Ko YW, Chung C, Lee JH, et al. Efficient white organic light emission by single emitting layer. *Thin Solid Films*. 2003;426(1):246-249.

146. Komino T, Tanaka H, Adachi C. Selectively controlled orientational order in linear-shaped thermally activated delayed fluorescent dopants. *Chemistry of Materials*. 2014;26(12):3665-3671.

147. Flämmich M, Frischeisen J, Setz DS, et al. Oriented phosphorescent emitters boost OLED efficiency. *Organic Electronics*. 2011;12(10):1663-1668.

148. Kim K, Moon C, Lee J, Kim S, Kim J. Highly efficient organic Light-Emitting diodes with phosphorescent emitters having high quantum yield and horizontal orientation of transition dipole moments. *Adv Mater*. 2014;26(23):3844-3847.

149. Kearns KL, Swallen SF, Ediger M, Wu T, Sun Y, Yu L. Hiking down the energy landscape: Progress toward the kauzmann temperature via vapor deposition. *The Journal of Physical Chemistry B*. 2008;112(16):4934-4942.

150. Ishii K, Nakayama H, Hirabayashi S, Moriyama R. Anomalously high-density glass of ethylbenzene prepared by vapor deposition at temperatures close to the glass-transition temperature. *Chemical Physics Letters*. 2008;459(1):109-112.

151. Sepúlveda A, Leon-Gutierrez E, Gonzalez-Silveira M, Clavaguera-Mora M, Rodríguez-Viejo J. Anomalous transformation of vapor-deposited highly stable glasses of toluene into mixed glassy states by annealing above T g. *The journal of physical chemistry letters*. 2012;3(7):919-923.

152. Chen Z, Sepúlveda A, Ediger M, Richert R. Dynamics of glass-forming liquids. XVI. observation of ultrastable glass transformation via dielectric spectroscopy. *J Chem Phys*. 2013;138(12):12A519.

153. Whitaker KR, Scifo DJ, Ediger M, Ahrenberg M, Schick C. Highly stable glasses of cis-decalin and cis/trans-decalin mixtures. *The Journal of Physical Chemistry B*. 2013;117(42):12724-12733.

154. Léonard S, Harrowell P. Macroscopic facilitation of glassy relaxation kinetics: Ultrastable glass films with frontlike thermal response. *J Chem Phys*. 2010;133(24):244502.

155. Wu J, Liu Z, Song J, et al. Stretchability of encapsulated electronics. *Appl Phys Lett*. 2011;99(6):061911.

156. Chabinyc ML, Endicott F, Vogt BD, et al. Effects of humidity on unencapsulated poly (thiophene) thin-film transistors. *Appl Phys Lett*. 2006;88(11):113514.

157. Dawson KJ, Kearns KL, Ediger M, Sacchetti MJ, Zografi GD. Highly stable indomethacin glasses resist uptake of water vapor. *The Journal of Physical Chemistry B*. 2009;113(8):2422-2427.

158. Komino T, Nomura H, Koyanagi T, Adachi C. Suppression of efficiency roll-off characteristics in thermally activated delayed fluorescence based organic light-emitting diodes using randomly oriented host molecules. *Chemistry of Materials*. 2013;25(15):3038-3047.

159. Dalal SS, Fakhraai Z, Ediger M. High-throughput ellipsometric characterization of vapor-deposited indomethacin glasses. *The Journal of Physical Chemistry B*. 2013;117(49):15415-15425.

160. Herzinger C, Johs B, McGahan W, Woollam JA, Paulson W. Ellipsometric determination of optical constants for silicon and thermally grown silicon dioxide via a multi-sample, multi-wavelength, multi-angle investigation. *J Appl Phys*. 1998;83(6):3323-3336.

161. Harrison C, Stafford CM, Zhang W, Karim A. Sinusoidal phase grating created by a tunably buckled surface. *Appl Phys Lett*. 2004;85(18):4016-4018.

162. Howarter JA, Stafford CM. Instabilities as a measurement tool for soft materials. *Soft Matter*. 2010;6(22):5661-5666.

163. Nolte AJ, Rubner MF, Cohen RE. Determining the young's modulus of polyelectrolyte multilayer films via stress-induced mechanical buckling instabilities. *Macromolecules*. 2005;38(13):5367-5370.

164. Kearns KL, Swallen SF, Ediger M, Wu T, Yu L. Influence of substrate temperature on the stability of glasses prepared by vapor deposition. *J Chem Phys*. 2007;127(15):154702-154702.

165. Vogt BD, Soles CL, Jones RL, et al. Interfacial effects on moisture absorption in thin polymer films. *Langmuir*. 2004;20(13):5285-5290.

166. Karul A, Tan KT, White CC, et al. Impact of polymer modulus/chain mobility on water accumulation at polymer/metal oxide interfaces. *Polymer*. 2009;50(14):3234-3239.

167. Wu W, Orts WJ, Hunston DL, Majkrzak CJ. Water adsorption at a polyimide/silicon wafer interface. *Polymer Engineering & Science*. 1995;35(12):1000-1004.

168. Nguyen HK, Labardi M, Lucchesi M, Rolla P, Prevosto D. Plasticization in ultrathin polymer films: The role of supporting substrate and annealing. *Macromolecules*. 2013;46(2):555-561.

169. Galvin CJ, Dimitriou MD, Satija SK, Genzer J. Swelling of polyelectrolyte and polyzwitterion brushes by humid vapors. *J Am Chem Soc*. 2014;136(36):12737-12745.

REFERENCES

1. Chiang C, Fincher Jr C, Park Y, et al. Electrical conductivity in doped polyacetylene. *Phys Rev Lett*. 1977;39(17):1098-1101.

2. Furst M, Kallman H. High energy induced fluorescence in organic liquid solutions(energy transport in liquids). III. *Physical Review*. 1952;85(5):816-825.

3. Pope M, Kallmann H, Magnante P. Electroluminescence in organic crystals. *J Chem Phys*. 1963;38:2042-2043.

4. Chamberlain G. Organic solar cells: A review. *Solar Cells*. 1983;8(1):47-83.

5. Friend R, Gymer R, Holmes A, et al. Electroluminescence in conjugated polymers. *Nature*. 1999;397(6715):121-128.

6. Sony Corporation. Sony style USA. http://www.sonystyle.com/webapp/wcs/stores/servlet/CategoryDisplay?catalogId=10551&storeId=10151&langId=-1&categoryId=8198552921644539854.

7. Duggal A. Next generation lighting projects with DOE. http://ge.geglobalresearch.com/blog/next-generation-lighting-projects-with-doe/.

8. Galaxy S7 edge homepage. http://www.samsung.com/us/explore/galaxy-s7-features-and-specs/?cid=ppc-2016.

9. Forrest SR. The path to ubiquitous and low-cost organic electronic appliances on plastic. *Nature*. 2004;428(6986):911-918.

10. http://solutions.3m.com/wps/portal/3M/en_US/FlexibleCircuits/Home/ManufacturingFoundries/RolltoRollProcessing/2013.

11. Dresner J. Double injection electroluminescence in anthracene. *RCA Rev*. 1969;30(2):322.

12. Helfrich W, Schneider W. Recombination radiation in anthracene crystals. *Phys Rev Lett*. 1965;14(7):229-231.

13. Adachi C, Baldo MA, Thompson ME, Forrest SR. Nearly 100% internal phosphorescence efficiency in an organic light-emitting device. *J Appl Phys*. 2001;90:5048.

14. Forrest S, Bradley D, Thompson M. Measuring the efficiency of organic light-emitting devices. *Adv Mater*. 2003;15(13):1043-1048.

15. Hung HW, Yokoyama N, Yahiro M, Adachi C. Low driving voltage organic light emitting diode using phenanthrene oligomers as electron transport layer. *Thin Solid Films*. 2008;516(23):8717-8720.

16. Brooks J, Babayan Y, Lamansky S, et al. Synthesis and characterization of phosphorescent cyclometalated platinum complexes. *Inorg Chem*. 2002;41(12):3055-3066.

17. Chu TY, Lee YH, Song OK. Effects of interfacial stability between electron transporting layer and cathode on the degradation process of organic light-emitting diodes. *Appl Phys Lett*. 2007;91:223509.

18. Kondakov D, Lenhart W, Nichols W. Operational degradation of organic light-emitting diodes: Mechanism and identification of chemical products. *J Appl Phys*. 2007;101:024512.

19. Forrest SR, Thompson ME. Introduction: Organic electronics and optoelectronics. *Chem Rev*. 2007;107(4):923-925.

20. Tang C, VanSlyke S. Organic electroluminescent diodes. *Appl Phys Lett*. 1987;51(12):913.

21. Sigma-Aldrich. Organic and printed electronics. http://www.sigmaaldrich.com/materials-science/organic-electronics.html. Accessed 5/05, 2010.

22. Wang Z, Helander M, Greiner M, Qiu J, Lu Z. Carrier mobility of organic semiconductors based on current-voltage characteristics. *J Appl Phys*. 2010;107:034506.

23. Shirota Y, Kageyama H. Charge carrier transporting molecular materials and their applications in devices. *Chem Rev*. 2007;107(4):953-1010.

24. Karl N, Kraft KH, Marktanner J, et al. Fast electronic transport in organic molecular solids? *Journal of Vacuum Science & Technology A: Vacuum, Surfaces, and Films*. 1999;17:2318.

25. Schein L. Temperature independent drift mobility along the molecular direction of as_ {2} s_ {3}. *Physical Review B*. 1977;15(2):1024-1034.

26. Kiy M, Losio P, Biaggio I, Koehler M, Tapponnier A, Günter P. Observation of the Mott–Gurney law in tris (8-hydroxyquinoline) aluminum films. *Appl Phys Lett*. 2002;80:1198.

27. Schein L. Comparison of charge transport models in molecularly doped polymers. *Philosophical Magazine Part B*. 1992;65(4):795-810.

28. Murgatroyd P. Theory of space-charge-limited current enhanced by frenkel effect. *J Phys D*. 1970;3:151-156.

29. Scott JC, Malliaras GG. Charge injection and recombination at the metal-organic interface. *Chemical Physics Letters*. 1999;299(2):115-119.

30. Scott JC. Metal–organic interface and charge injection in organic electronic devices. *Journal of Vacuum Science & Technology A: Vacuum, Surfaces, and Films*. 2003;21:521.

31. Burrows P, Shen Z, Bulovic V, et al. Relationship between electroluminescence and current transport in organic heterojunction light-emitting devices. *J Appl Phys*. 1996;79:7991.

32. Probst K, Karl N. Energy levels of electron and hole traps in the band gap of doped anthracene crystals. *physica status solidi (a)*. 2006;27(2):499-508.

33. Blom P, De Jong M, Breedijk S. Temperature dependent electron-hole recombination in polymer light-emitting diodes. *Appl Phys Lett*. 1997;71(7):930-932.

34. Karl N, Marktanner J, Stehle R, Warta W. High-field saturation of charge carrier drift velocities in ultrapurified organic photoconductors. *Synth Met*. 1991;42(3):2473-2481.

35. Davids P, Campbell I, Smith D. Device model for single carrier organic diodes. *J Appl Phys*. 1997;82:6319.

36. Koehler M, Hümmelgen I. Regional approximation approach to space charge limited tunneling injection in polymeric devices. *J Appl Phys*. 2000;87:3074.

37. Bakken N, Torres JM, Li J, Vogt BD. Thickness dependent modulus of vacuum deposited organic molecular glasses for organic electronics applications. *Soft Matter*. 2011;7(16):7269.

38. Baldo M, O'brien D, You Y, et al. Highly efficient phosphorescent emission from organic electroluminescent devices. *Nature*. 1998;395(6698):151-154.

39. Yeh SJ, Wu MF, Chen CT, et al. New dopant and host materials for blue-light-emitting phosphorescent organic electroluminescent devices. *Adv Mater*. 2005;17(3):285-289.

40. Baldo M, Thompson M, Forrest S. Phosphorescent materials for application to organic light omitting devices. *Pure and Applied Chemistry*. 1999;71(11):2095-2106.

41. Baldo M, Lamansky S, Burrows P, Thompson M, Forrest S. Very high-efficiency green organic light-emitting devices based on electrophosphorescence. *Appl Phys Lett*. 1999;75:4.

42. K. Mullen, S. Ullrich, eds. *Organic light-emitting devices*. Darmstadt, Germany: Wiley-VCH; 2006.

43. Adachi C, Nagai K, Tamoto N. Molecular design of hole transport materials for obtaining high durability in organic electroluminescent diodes. *Appl Phys Lett*. 1995;66:2679.

44. Adachi C, Tsutsui T, Saito S. Blue light-emitting organic electroluminescent devices. *Appl Phys Lett*. 1990;56:799.

45. Adachi C, Tsutsui T, Saito S. Confinement of charge carriers and molecular excitons within 5-nm-thick emitter layer in organic electroluminescent devices with a double heterostructure. *Appl Phys Lett*. 1990;57:531.

46. Vossen J. Physics of thin films. *New York: Academic*. 1977.

47. You Y, Kim Y, Choi D, Jang H, Lee J, Kim D. Electrical and optical study of ITO films on glass and polymer substrates prepared by DC magnetron sputtering type negative metal ion beam deposition. *Mater Chem Phys*. 2008;107(2-3):444-448.

48. Fenenko L, Adachi C. Influence of heat treatment on indium-tin-oxide anodes and copper phthalocyanine hole injection layers in organic light-emitting diodes. *Thin Solid Films*. 2007;515(11):4812-4818.

49. Ho JJ, Chen CY, Hsiao RY, Ho OL. The work function improvement on indium− tin− oxide epitaxial layers by doping treatment for organic light-emitting device applications. . 2007.

50. Shirota Y. Photo-and electroactive amorphous molecular materials—molecular design, syntheses, reactions, properties, and applications. *Journal of Materials Chemistry*. 2005;15(1):75-93.

51. Lee JH, Huang CL, Hsiao CH, Leung MK, Yang CC, Chao CC. Blue phosphorescent organic light-emitting device with double emitting layer. *Appl Phys Lett*. 2009;94:223301.

52. Wang Y, Herron N, Grushin V, LeCloux D, Petrov V. Highly efficient electroluminescent materials based on fluorinated organometallic iridium compounds. *Appl Phys Lett*. 2001;79:449.

53. Hughes G, Bryce MR. Electron-transporting materials for organic electroluminescent and electrophosphorescent devices. *Journal of Materials Chemistry*. 2005;15(1):94-107.

54. Zahn D, Salvan G, Gavrila G, Paez B. Chemistry and morphological properties of metal interfaces to organic semiconductors. *Advances in Solid State Physics*. :313-324.

55. Hung L, Tang C, Mason M. Enhanced electron injection in organic electroluminescence devices using an al/LiF electrode. *Appl Phys Lett*. 1997;70:152.

56. Stafford CM, Guo S, Harrison C, Chiang MYM. Combinatorial and high-throughput measurements of the modulus of thin polymer films. *Rev Sci Instrum*. 2005;76:062207.

57. Wilder EA, Guo S, Lin-Gibson S, Fasolka MJ, Stafford CM. Measuring the modulus of soft polymer networks via a buckling-based metrology. *Macromolecules*. 2006;39(12):4138-4143.

58. Huang R, Stafford CM, Vogt BD. Effect of surface properties on wrinkling of ultrathin films. *J Aerospace Eng*. 2007;20(1):38-44.

59. Duan H, Wang J, Huang Z, Karihaloo B. Size-dependent effective elastic constants of solids containing nano-inhomogeneities with interface stress. *J Mech Phys Solids*. 2005;53(7):1574-1596.

60. Biot M. Bending of an infinite beam on an elastic foundation. *Zeitschrift fiir Angewandte Maihematik und Mechanik*. 1922;2(3):165-184.

61. Allen HG. *Analysis and design of structural sandwich panels: The commonwealth and international library: Structures and solid body mechanics division.* Elsevier; 2013.

62. Volynskii A, Bazhenov S, Lebedeva O, Bakeev N. Mechanical buckling instability of thin coatings deposited on soft polymer substrates. *J Mater Sci*. 2000;35(3):547-554.

63. Groenewold J. Wrinkling of plates coupled with soft elastic media. *Physica A: Statistical Mechanics and its Applications*. 2001;298(1):32-45.

64. Nolte AJ, Cohen RE, Rubner MF. A two-plate buckling technique for thin film modulus measurements: Applications to polyelectrolyte multilayers. *Macromolecules*. 2006;39(14):4841-4847.

65. Reineke S, Lindner F, Schwartz G, et al. White organic light-emitting diodes with fluorescent tube efficiency. *Nature*. 2009;459(7244):234-238.

66. D'Andrade B.W. et al. Realizing white phosphorescent 100 lm/W OLED efficacy. *Proc SPIE*. 2008;70510Q:7051.

67. D'Andrade BW, Forrest SR. White organic light-emitting devices for solid-state lighting. *Adv Mater*. 2004;16(18):1585-1595.

68. Gather MC, Köhnen A, Meerholz K. White organic light-emitting diodes. *Adv Mater*. 2011;23(2):233-248.

69. D'Andrade B, Holmes R, Forrest S. Efficient organic electrophosphorescent white-light-emitting device with a triple doped emissive layer. *Adv Mater*. 2004;16(7):624-628.

70. Kido J, Kimura M, Nagai K. Multilayer white light-emitting organic electroluminescent device. *Science*. 1995;267(5202):1332.

71. Sun Y, Giebink NC, Kanno H, Ma B, Thompson ME, Forrest SR. Management of singlet and triplet excitons for efficient white organic light-emitting devices. *Nature*. 2006;440(7086):908-912.

72. Koehler A, Wilson JS, Friend RH. Fluorescence and phosphorescence in organic materials. *Advanced Engineering Materials*. 2002;4(7):453.

73. Eom SH, Zheng Y, Wrzesniewski E, et al. White phosphorescent organic light-emitting devices with dual triple-doped emissive layers. *Appl Phys Lett*. 2009;94:153303.

74. Wu FI, Yang XH, Neher D, Dodda R, Tseng YH, Shu CF. Efficient White-Electrophosphorescent devices based on a single polyfluorene copolymer. *Advanced Functional Materials*. 2007;17(7):1085-1092.

75. Huang J, Li G, Wu E, Xu Q, Yang Y. Achieving High-Efficiency polymer White-Light-Emitting devices. *Adv Mater*. 2006;18(1):114-117.

76. Schwartz G, Pfeiffer M, Reineke S, Walzer K, Leo K. Harvesting triplet excitons from fluorescent blue emitters in white organic Light-Emitting diodes. *Adv Mater*. 2007;19(21):3672-3676.

77. Adamovich V, Brooks J, Tamayo A, et al. High efficiency single dopant white electrophosphorescent light emitting diodes. *New journal of chemistry*. 2002;26(9):1171-1178.

78. Williams E, Haavisto K, Li J, Jabbour G. Excimer-based white phosphorescent organic light-emitting diodes with nearly 100% internal quantum efficiency. *Adv Mater*. 2007;19(2):197-202.

79. Yang X, Wang Z, Madakuni S, Li J, Jabbour GE. Efficient blue-and white-emitting electrophosphorescent devices based on platinum (II)[1, 3-difluoro-4, 6-di (2-pyridinyl) benzene] chloride. *Adv Mater*. 2008;20(12):2405-2409.

80. Feng J, Li F, Gao W, Liu S, Liu Y, Wang Y. White light emission from exciplex using tris-(8-hydroxyquinoline) aluminum as chromaticity-tuning layer. *Appl Phys Lett*. 2001;78:3947.

81. Hide F, Kozodoy P, DenBaars SP, Heeger AJ. White light from InGaN/conjugated polymer hybrid light-emitting diodes. *Appl Phys Lett*. 1997;70:2664.

82. Gather MC, Alle R, Becker H, Meerholz K. On the origin of the color shift in White-Emitting OLEDs. *Adv Mater*. 2007;19(24):4460-4465.

83. Rea MS, America Illuminating Engineering Society. *Lighting handbook.* Illuminating Engineering Society of North America USA; 1995.

84. Turro NJ. *Modern molecular photochemistry.* Univ Science Books; 1991.

85. Chopra N, Swensen JS, Polikarpov E, Cosimbescu L, So F, Padmaperuma AB. High efficiency and low roll-off blue phosphorescent organic light-emitting devices using mixed host architecture. *Appl Phys Lett*. 2010;97:033304.

86. Sasabe H, Takamatsu J, Motoyama T, et al. High-Efficiency blue and white organic Light-Emitting devices incorporating a blue iridium carbene complex. *Adv Mater*.

87. Sun Y, Forrest SR. Enhanced light out-coupling of organic light-emitting devices using embedded low-index grids. *Nature Photonics*. 2008;2(8):483-487.

88. Giebink N, D'Andrade B, Weaver M, et al. Intrinsic luminance loss in phosphorescent small-molecule organic light emitting devices due to bimolecular annihilation reactions. *J Appl Phys*. 2008;103:044509.

89. Wang Z, Turner E, Mahoney V, Madakuni S, Groy T, Li J. Facile synthesis and characterization of phosphorescent pt (N∧ C∧ N) X complexes. *Inorg Chem*. 2010.

90. Li J, Djurovich PI, Alleyne BD, et al. Synthetic control of excited-state properties in cyclometalated ir (III) complexes using ancillary ligands. *Inorg Chem*. 2005;44(6):1713-1727.

91. Tokito S, Iijima T, Suzuri Y, Kita H, Tsuzuki T, Sato F. Confinement of triplet energy on phosphorescent molecules for highly-efficient organic blue-light-emitting devices. *Appl Phys Lett*. 2003;83:569.

92. Lo SC, Richards G, Markham J, et al. A light-blue phosphorescent dendrimer for efficient solution-processed light-emitting diodes. *Advanced Functional Materials*. 2005;15(9):1451-1458.

93. Holmes R, Forrest S, Tung YJ, et al. Blue organic electrophosphorescence using exothermic host–guest energy transfer. *Appl Phys Lett*. 2003;82:2422.

94. Holmes R, Forrest S, Sajoto T, et al. Saturated deep blue organic electrophosphorescence using a fluorine-free emitter. *Appl Phys Lett*. 2005;87(24):243507-243507.

95. Sajoto T, Djurovich PI, Tamayo A, et al. Blue and near-UV phosphorescence from iridium complexes with cyclometalated pyrazolyl or N-heterocyclic carbene ligands. *Inorg Chem*. 2005;44(22):7992-8003.

96. Yokoyama D, Sakaguchi A, Suzuki M, Adachi C. Horizontal molecular orientation in vacuum-deposited organic amorphous films of hole and electron transport materials. *Appl Phys Lett*. 2008;93:173302.

97. Yokoyama D, Sakaguchi A, Suzuki M, Adachi C. Horizontal orientation of linear-shaped organic molecules having bulky substituents in neat and doped vacuum-deposited amorphous films. *Organic Electronics*. 2009;10(1):127-137.

98. Gleskova H, Cheng I. Mechanics of thin-film transistors and solar cells on flexible substrates. *Solar Energy*. 2006;80(6):687-693.

99. Sirringhaus H, Kawase T, Friend R, et al. High-resolution inkjet printing of all-polymer transistor circuits. *Science*. 2000;290(5499):2123.

100. Chiang CJ, Bull S, Winscom C, Monkman A. A nano-indentation study of the reduced elastic modulus of Alq3 and NPB thin-film used in OLED devices. *Organic Electronics*. 2010;11(3):450-455.

101. Chiang CJ, Winscom C, Bull S, Monkman A. Mechanical modeling of flexible OLED devices. *Organic Electronics*. 2009;10(7):1268-1274.

102. VanLandingham MR, Villarrubia JS, Guthrie WF, Meyers GF. Nanoindentation of polymers: An overview. . 2001;167(1):15-44.

103. Bishop JP, Register RA. Poly (phenylethylnorbornene) s and their hydrogenated derivatives. *Macromolecular Rapid Communications*. 2008;29(9):713-718.

104. Torres JM, Bakken N, Stafford CM, Li J, Vogt BD. Thickness dependence of the elastic modulus of tris (8-hydroxyquinolinato) aluminium. *Soft Matter*. 2010;6(22):5783-5788.

105. Vivo P, Jukola J, Ojala M, Chukharev V, Lemmetyinen H. Influence of alq 3/au cathode on stability and efficiency of a layered organic solar cell in air. *Solar Energy Mater Solar Cells*. 2008;92(11):1416-1420.

106. Lötters J, Olthuis W, Veltink P, Bergveld P. The mechanical properties of the rubber elastic polymer polydimethylsiloxane for sensor applications. *J Micromech Microengineering*. 1997;7(3):145.

107. Göbel R, Krska R, Kellner R, Seitz R, Tomellini S. Investigation of different polymers as coating materials for IR/ATR spectroscopic trace analysis of chlorinated hydrocarbons in water. *Appl Spectrosc*. 1994;48(6):678-683.

108. Rodríguez-Tinoco C, Gonzalez-Silveira M, Ràfols-Ribé J, Lopeandía AF, Clavaguera-Mora MT, Rodríguez-Viejo J. Evaluation of growth front velocity in ultrastable glasses of indomethacin over a wide temperature interval. *The Journal of Physical Chemistry B*. 2014;118(36):10795-10801.

109. Perez-Castaneda T, Rodriguez-Tinoco C, Rodriguez-Viejo J, Ramos MA. Suppression of tunneling two-level systems in ultrastable glasses of indomethacin. *Proc Natl Acad Sci U S A*. 2014;111(31):11275-11280.

110. Torres JM, Stafford CM, Vogt BD. Elastic modulus of amorphous polymer thin films: Relationship to the glass transition temperature. *ACS nano*. 2009;3(9):2677-2685.

111. Zhao J, Kiene M, Hu C, Ho PS. Thermal stress and glass transition of ultrathin polystyrene films. *Appl Phys Lett*. 2000;77:2843.

112. Priestley RD, Ellison CJ, Broadbelt LJ, Torkelson JM. Structural relaxation of polymer glasses at surfaces, interfaces, and in between. *Science*. 2005;309(5733):456.

113. Jabbari E, Peppas NA. Molecular weight and polydispersity effects on interdiffusion at the interface between polystyrene and poly (vinyl methyl ether). *J Mater Sci*. 1994;29(15):3969-3978.

114. Jang D, Greer JR. Transition from a strong-yet-brittle to a stronger-and-ductile state by size reduction of metallic glasses. *Nature materials*. 2010;9(3):215-219.

115. Kearns KL, Still T, Fytas G, Ediger M. High-Modulus organic glasses prepared by physical vapor deposition. *Adv Mater*. 2010;22(1):39-42.

116. Fritz SE, Martin SM, Frisbie CD, Ward MD, Toney MF. Structural characterization of a pentacene monolayer on an amorphous SiO2 substrate with grazing incidence X-ray diffraction. *J Am Chem Soc*. 2004;126(13):4084-4085.

117. Bouchoms I, Schoonveld W, Vrijmoeth J, Klapwijk T. Morphology identification of the thin film phases of vacuum evaporated pentacene on SiO 2 substrates. *Synth Met*. 1999;104(3):175-178.

118. Ruiz R, Mayer AC, Malliaras GG, et al. Structure of pentacene thin films. *Appl Phys Lett*. 2004;85(21):4926-4928.

119. Torres JM, Stafford CM, Vogt BD. Impact of molecular mass on the elastic modulus of thin polystyrene films. *Polymer*. 2010.

120. Miyake K, Satomi N, Sasaki S. Elastic modulus of polystyrene film from near surface to bulk measured by nanoindentation using atomic force microscopy. *Appl Phys Lett*. 2006;89:031925.

121. Mundra MK, Donthu SK, Dravid VP, Torkelson JM. Effect of spatial confinement on the glass-transition temperature of patterned polymer nanostructures. *Nano letters*. 2007;7(3):713-718.

122. Tsui O, Russell T, Hawker C. Effect of interfacial interactions on the glass transition of polymer thin films. *Macromolecules*. 2001;34(16):5535-5539.

123. Dawson KJ, Kearns KL, Yu L, Steffen W, Ediger MD. Physical vapor deposition as a route to hidden amorphous states. *Proceedings of the National Academy of Sciences*. 2009;106(36):15165.

124. Swallen SF, Kearns KL, Mapes MK, et al. Organic glasses with exceptional thermodynamic and kinetic stability. *Science*. 2007;315(5810):353.

125. Fakhraai Z, Forrest J. Measuring the surface dynamics of glassy polymers. *Science*. 2008;319(5863):600.

126. Koch N, Elschner A, Schwartz J, Kahn A. Organic molecular films on gold versus conducting polymer: Influence of injection barrier height and morphology on current–voltage characteristics. *Appl Phys Lett*. 2003;82(14):2281-2283.

127. Mayer AC, Ruiz R, Headrick RL, Kazimirov A, Malliaras GG. Early stages of pentacene film growth on silicon oxide. *Organic electronics*. 2004;5(5):257-263.

128. Djurii A, Kwong C, Guo W, et al. Spectroscopic ellipsometry of the optical functions of tris (8-hydroxyquinoline) aluminum (Alq3). *Thin Solid Films*. 2002;416(1-2):233-241.

129. Aziz A, Narasimhan K. Optical absorption in AlQ. *Synth Met*. 2000;114(2):133-137.

130. Himcinschi C, Meyer N, Hartmann S, et al. Spectroscopic ellipsometric characterization of organic films obtained via organic vapor phase deposition. *Applied Physics A*. 2005;80(3):551-555.

131. Stafford CM, Harrison C, Beers KL, et al. A buckling-based metrology for measuring the elastic moduli of polymeric thin films. *Nature materials*. 2004;3(8):545-550.

132. Tahk D, Lee HH, Khang DY. Elastic moduli of organic electronic materials by the buckling method. *Macromolecules*. 2009;42(18):7079-7083.

133. O'Connor B, Chan EP, Chan C, et al. Correlations between mechanical and electrical properties of polythiophenes. *ACS nano*.

134. Al-Douri Y, Abid H, Aourag H. Correlation between the bulk modulus and the charge density in semiconductors. *Physica B: Condensed Matter*. 2001;305(2):186-190.

135. DeLongchamp DM, Vogel BM, Jung Y, et al. Variations in semiconducting polymer microstructure and hole mobility with spin-coating speed. *Chemistry of materials*. 2005;17(23):5610-5612.

136. Ellison CJ, Torkelson JM. Sensing the glass transition in thin and ultrathin polymer films via fluorescence probes and labels. *Journal of Polymer Science Part B: Polymer Physics*. 2002;40(24):2745-2758.

137. Jackson CL, McKenna GB. The glass transition of organic liquids confined to small pores. *J Non Cryst Solids*. 1991;131:221-224.

138. Yang Z, Fujii Y, Lee FK, Lam CH, Tsui OKC. Glass transition dynamics and surface layer mobility in unentangled polystyrene films. *Science*. 2010;328(5986):1676.

139. O'connell P, McKenna G. Rheological measurements of the thermoviscoelastic response of ultrathin polymer films. *Science*. 2005;307(5716):1760.

140. Stafford CM, Vogt BD, Harrison C, Julthongpiput D, Huang R. Elastic moduli of ultrathin amorphous polymer films. *Macromolecules*. 2006;39(15):5095-5099.

141. Sasabe H, Kido J. Development of high performance OLED for general lighting. *Journal of Materials Chemistry C*. 2013.

142. Sasabe H, Kido J. Multifunctional materials in high-performance OLEDs: Challenges for solid-state lighting†. *Chemistry of Materials*. 2010;23(3):621-630.

143. Yokoyama D. Molecular orientation in small-molecule organic light-emitting diodes. *Journal of Materials Chemistry*. 2011;21(48):19187-19202.

144. Lin H, Lin C, Chang H, et al. Anisotropic optical properties and molecular orientation in vacuum-deposited ter (9, 9-diarylfluorene) s thin films using spectroscopic ellipsometry. *J Appl Phys*. 2004;95(3):881-886.

145. Ko YW, Chung C, Lee JH, et al. Efficient white organic light emission by single emitting layer. *Thin Solid Films*. 2003;426(1):246-249.

146. Komino T, Tanaka H, Adachi C. Selectively controlled orientational order in linear-shaped thermally activated delayed fluorescent dopants. *Chemistry of Materials*. 2014;26(12):3665-3671.

147. Flämmich M, Frischeisen J, Setz DS, et al. Oriented phosphorescent emitters boost OLED efficiency. *Organic Electronics*. 2011;12(10):1663-1668.

148. Kim K, Moon C, Lee J, Kim S, Kim J. Highly efficient organic Light-Emitting diodes with phosphorescent emitters having high quantum yield and horizontal orientation of transition dipole moments. *Adv Mater*. 2014;26(23):3844-3847.

149. Kearns KL, Swallen SF, Ediger M, Wu T, Sun Y, Yu L. Hiking down the energy landscape: Progress toward the kauzmann temperature via vapor deposition. *The Journal of Physical Chemistry B*. 2008;112(16):4934-4942.

150. Ishii K, Nakayama H, Hirabayashi S, Moriyama R. Anomalously high-density glass of ethylbenzene prepared by vapor deposition at temperatures close to the glass-transition temperature. *Chemical Physics Letters*. 2008;459(1):109-112.

151. Sepúlveda A, Leon-Gutierrez E, Gonzalez-Silveira M, Clavaguera-Mora M, Rodríguez-Viejo J. Anomalous transformation of vapor-deposited highly stable glasses of toluene into mixed glassy states by annealing above T g. *The journal of physical chemistry letters*. 2012;3(7):919-923.

152. Chen Z, Sepúlveda A, Ediger M, Richert R. Dynamics of glass-forming liquids. XVI. observation of ultrastable glass transformation via dielectric spectroscopy. *J Chem Phys*. 2013;138(12):12A519.

153. Whitaker KR, Scifo DJ, Ediger M, Ahrenberg M, Schick C. Highly stable glasses of cis-decalin and cis/trans-decalin mixtures. *The Journal of Physical Chemistry B*. 2013;117(42):12724-12733.

154. Léonard S, Harrowell P. Macroscopic facilitation of glassy relaxation kinetics: Ultrastable glass films with frontlike thermal response. *J Chem Phys*. 2010;133(24):244502.

155. Wu J, Liu Z, Song J, et al. Stretchability of encapsulated electronics. *Appl Phys Lett*. 2011;99(6):061911.

156. Chabinyc ML, Endicott F, Vogt BD, et al. Effects of humidity on unencapsulated poly (thiophene) thin-film transistors. *Appl Phys Lett*. 2006;88(11):113514.

157. Dawson KJ, Kearns KL, Ediger M, Sacchetti MJ, Zografi GD. Highly stable indomethacin glasses resist uptake of water vapor. *The Journal of Physical Chemistry B*. 2009;113(8):2422-2427.

158. Komino T, Nomura H, Koyanagi T, Adachi C. Suppression of efficiency roll-off characteristics in thermally activated delayed fluorescence based organic light-emitting diodes using randomly oriented host molecules. *Chemistry of Materials*. 2013;25(15):3038-3047.

159. Dalal SS, Fakhraai Z, Ediger M. High-throughput ellipsometric characterization of vapor-deposited indomethacin glasses. *The Journal of Physical Chemistry B*. 2013;117(49):15415-15425.

160. Herzinger C, Johs B, McGahan W, Woollam JA, Paulson W. Ellipsometric determination of optical constants for silicon and thermally grown silicon dioxide via a multi-sample, multi-wavelength, multi-angle investigation. *J Appl Phys*. 1998;83(6):3323-3336.

161. Harrison C, Stafford CM, Zhang W, Karim A. Sinusoidal phase grating created by a tunably buckled surface. *Appl Phys Lett*. 2004;85(18):4016-4018.

162. Howarter JA, Stafford CM. Instabilities as a measurement tool for soft materials. *Soft Matter*. 2010;6(22):5661-5666.

163. Nolte AJ, Rubner MF, Cohen RE. Determining the young's modulus of polyelectrolyte multilayer films via stress-induced mechanical buckling instabilities. *Macromolecules*. 2005;38(13):5367-5370.

164. Kearns KL, Swallen SF, Ediger M, Wu T, Yu L. Influence of substrate temperature on the stability of glasses prepared by vapor deposition. *J Chem Phys*. 2007;127(15):154702-154702.

165. Vogt BD, Soles CL, Jones RL, et al. Interfacial effects on moisture absorption in thin polymer films. *Langmuir*. 2004;20(13):5285-5290.

166. Karul A, Tan KT, White CC, et al. Impact of polymer modulus/chain mobility on water accumulation at polymer/metal oxide interfaces. *Polymer*. 2009;50(14):3234-3239.

167. Wu W, Orts WJ, Hunston DL, Majkrzak CJ. Water adsorption at a polyimide/silicon wafer interface. *Polymer Engineering & Science*. 1995;35(12):1000-1004.

168. Nguyen HK, Labardi M, Lucchesi M, Rolla P, Prevosto D. Plasticization in ultrathin polymer films: The role of supporting substrate and annealing. *Macromolecules*. 2013;46(2):555-561.

169. Galvin CJ, Dimitriou MD, Satija SK, Genzer J. Swelling of polyelectrolyte and polyzwitterion brushes by humid vapors. *J Am Chem Soc*. 2014;136(36):12737-12745.

170. Environmental health & safety manual. http://www.asu.edu.ezproxy1.lib.asu.edu/aad/manuals/ehs/. Updated 2013.

171. Culture of safety. https://www.osha.gov/SLTC/laboratories/safetyculture.html. Updated 2013. Accessed 8/1/2014.

172. Chemical hygiene plan. http://www.asu.edu/ehs/documents/asu_chp.pdf. Updated 2013.

173. Ott R. Working on contaminated lab vacuum pumps and systems. https://cfo.asu.edu/node/2666. Updated 2013.

174. Vacuum pump and vacuum system safety. http://mmrc.caltech.edu/Vacuum/Edwards/VACUUM%20Pump%20Safety.pdf. Updated 2005.

APPENDIX A

LABORATORY SAFETY

The work described in this document as well as future research will require attention to safety during a variety of lab activities. Core competency operations will include synthesis, refining, storage, handling, thin film deposition, characterization, and disposal of OLED materials and/or related chemicals. The equipment used in these processes require careful navigation of hazards due to electrically energized systems, compressed fluids, mechanical pinch points, burn hazards/hot surfaces, freeze hazards/cryogenic equipment, flammable and/or reactive systems. Mitigating each of these hazards specific to the proposed research and enforcing a safe general laboratory environment will be accomplished by strict adherence to ASU's environmental health and safety (EHS) programs.[170] The requirements include required in-person and web based training, documentation of policy/procedures, assignment of a lab compliance officer, and periodic safety inspections. Most importantly, each researcher should make a personal commitment to place their own safety and the safety of adjacent lab occupants as priority one.[171]

Chemical safety is documented in the ASU Chemical Hygiene Plan.[172] The points that are most directly applicable to the proposed research are:

- Standard operating procedures for working with hazardous chemicals
- Criteria for the use of personal protective equipment and other engineering controls when working with extremely hazardous substances
- A program to ensure proper functioning of fume hoods
- A program to ensure employee training and access to information
- Procedures for waste disposal
- Criteria and procedures for reviewing laboratory process hazards

- Chemical inventory lists and material safety data sheets
- Provisions for medical consultations and examinations
- Personnel responsibilities and designation of a Chemical Hygiene Officer, a safety coordinator and safety committees
- Extra provisions for the safe use of select carcinogens and substances with high acute toxicity
- Procedures for annual review, evaluation, and updating
- Procedures for emergencies, evacuations, and first aid
- Methods used to document and preserve records required by the standard

Vacuum safety is addressed in the chemical hygiene plan. Because of the substantial use of and modification to vacuum equipment required for device fabrication research in addition to the requirement for in-house repair and preventative maintenance of these systems, additional considerations are pertinent. Working on contaminated vacuum equipment will require use of additional purge/exhaust ventilation systems, PPE, and notification to surrounding workers as compared to the requirements for general lab operations.[173] Manufacture's guidelines for vacuum pump should also be studied and observed.[174] Users participating in device fabrication should have individual equipment specific training in addition to completion of a restricted apprenticeship period before unsupervised operation is permitted to ensure safe equipment operation. Electrical safety is specific to OLED fabrication due to the high current and/or high voltages present in deposition and characterization systems. In most cases, equipment has sufficient interlocks in place to protect users and maintenance/repairs can be performed in a de-energized state. Cases where exposure to energized sources is necessary will only be handled by qualified

persons as described by ASU's EHS section 118.[170] All procedures for approved research activities will be completed in a safe and responsible manner in accordance to ASU laboratory rules and regulations.

The proposed research will collect electrical and optical data from devices fabricated on glass substrates with an active area 0.04 cm^2 for each of four devices. Shadow masks replicate each device condition four times on a single substrate to reduce the impact of random variation (defects) on collected data. The instruments used for optoelectronic measurements are included in table 1.

Table 1. Equipment used to characterize electroluminescence of optoelectronics.

Instrument	**Measurement type**
Keithley 2400 source meter	Voltage (V)
Keithley 2400 source meter	Current (A)
Keithley 6485 picoammeter	Photocurrent (A)
Keithly 4200	Voltage (V)
Keithly 4200	Current (A)
Ocean Optics USB2000	EL spectrum
Ocean Optics USB2000	Radiant power (W=J/s)
Ocean Optics HR4000	EL spectrum
Ocean Optics HR4000	Radiant power (W=J/s)
Photo Research PR670	EL spectrum
Photo Research PR670	Luminance (cd/m^2)
Konica luminance meter	Radiant power (W=J/s)
Newport 818 Si photodiode	Radiant power (W=J/s)
Hamamatsu Si photodiode	Radiant power (W=J/s)